

Scuola di Scienze
Dipartimento di Fisica e Astronomia
Corso di Laurea in Fisica

**Rheology-based sea ice dynamics: from the
fluid-like to the state-of-the-art solid-like brittle
approach**

Supervisor:
Prof. Natale Alberto Carrassi

Submitted by:
Niccolò Zanotti

Co-supervisor:
Dr. Ivo Pasmans

Academic year 2022/2023

“Nature uses only the longest threads to weave her patterns, so that each small piece of her fabric reveals the organization of the entire tapestry.”

Richard P. Feynman

Abstract

The increasing interest in the climate in general and, in particular, in the role that Arctic processes play within it has led to an increasing demand for accurate predictions for sea ice motion. However, the problem of finding suitable equations to accurately describe the drift and deformation of the sea ice cover has challenged the sea ice dynamics community for many years. This thesis presents the developments in sea ice modeling research, from its origins to the current state focusing on models based on a continuum mechanics framework. To do so, we will first describe the relevant sea ice state parameters: sea ice velocity, sea ice thickness, sea ice concentration, internal sea ice stresses and sea ice properties like cohesion as well as the equations describing their time evolution. Special attention will be devoted to the formulation of the internal stress as function of the (rate of) deformation, i.e. the rheology. This relation changed from being absent, as the earliest models did not include internal stresses, via a simple linear relation, similar to the one found in a viscous fluid, to rheologies in which ice can exhibit different relations below and above a critical stress threshold given by a yield curve. The Mohr-Coulomb curve and elliptic yield curves will be discussed. Subcritical ice behavior is either elastic, viscous or a combination of the two. Supercritical ice deforms plastically. Discussed examples of such rheologies are the elastic-plastic (EP) and viscous-plastic (VP) rheologies. As a consequence of the need to stay within the yield curve, the viscosity and/or elasticity needs to change. It has been found that models are more capable of reproducing features in the sea ice if the processes happening at a lower scale than the model spatial resolution are parametrized. This has resulted in the development of the the Elasto-Brittle (EB), the Maxwell-Elasto-Brittle (MEB) and the Brittle-Bingham-Maxwell (BBM) rheologies. The latter is the current state-of-art model rheology successful in reproducing the multifractal nature of sea ice deformation in both space and time, i.e. the characteristic heterogeneity and intermittency.

Keywords: sea ice dynamics, sea ice rheology, brittle mechanics, multifractality.

Sommario

Il crescente interesse per il clima in generale e, in particolare, per il ruolo svolto dai processi artici al suo interno, ha portato a una crescente richiesta di previsioni accurate per il moto del ghiaccio marino. Tuttavia, il problema di trovare equazioni adeguate per descrivere con precisione la deriva e la deformazione della coperta di ghiaccio marino ha messo alla prova la comunità scientifica per molti anni. Questa tesi presenta gli sviluppi nella ricerca sulla modellizzazione del ghiaccio marino, dalle sue origini allo stato attuale, concentrandosi su modelli basati su una schematizzazione del ghiaccio come un mezzo continuo. Per fare ciò, descriveremo innanzitutto i parametri caratterizzanti lo stato del ghiaccio marino: la velocità di deriva, lo spessore, la concentrazione, gli sforzi interni e le proprietà del ghiaccio marino come la coesione, così come le equazioni che ne descrivono l'evoluzione temporale. Particolare attenzione sarà dedicata alla formulazione dello sforzo interno come funzione della (variazione di) deformazione, ovvero la reologia. Storicamente, si è passati da un'assenza di tale relazione, poiché i primi modelli non includevano gli sforzi interni, attraverso una semplice relazione lineare, simile a quella di un fluido viscoso, a reologie in cui il ghiaccio può presentare diverse relazioni al di sotto e al di sopra di una soglia critica data da una curva di resa. Saranno discusse la curva di Mohr-Coulomb e le curve di resa ellittiche. Il comportamento subcritico del ghiaccio è elastico, viscoso o una combinazione dei due. Il ghiaccio supercritico si deforma plasticamente. Esempi di tali reologie discusse sono le reologie elastico-plastiche (EP) e viscoso-plastiche (VP). A causa della necessità di rimanere entro la curva di resa, la viscosità e/o l'elasticità devono cambiare. Si è scoperto che i modelli sono più capaci di riprodurre le caratteristiche del ghiaccio marino se i processi che avvengono su una scala inferiore rispetto alla risoluzione spaziale del modello sono parametrizzati. Ciò ha portato allo sviluppo delle reologie note con il nome di Elasto-Brittle (EB), Maxwell-Elasto-Brittle (MEB) e Brittle-Bingham-Maxwell (BBM). Quest'ultima è la reologia implementata dal modello attualmente più avanzato, che si è dimostrata capace di riprodurre la natura multifrattale della deformazione del ghiaccio sia nel dominio spaziale che in quello temporale, ovvero l'eterogeneità e l'intermittenza caratteristiche.

Parole chiave: dinamica del ghiaccio marino, reologia del ghiaccio marino, meccanica dei mezzi fragili, multifrattalità.

Alle mie care nonne,
Adele e Prima

Contents

Abstract	v
1 Introduction	1
2 Sea ice dynamics modeling	5
2.1 A continuum model of the sea ice cover	5
2.1.1 The continuum scale	5
2.1.2 A two-dimensional theory	6
2.2 Ice kinematics	7
2.2.1 Deformation of drift ice	7
2.2.2 Sea ice internal stress	9
2.3 The state of the ice cover	10
2.3.1 Ice thickness distribution	10
2.3.2 The ice state variables	11
2.4 Sea ice rheology	12
2.5 Governing equations	12
2.5.1 Evolution of the ice thickness and concentration	12
2.5.2 Evolution of the ice thickness distribution	14
2.5.3 The momentum equation	15
2.6 Atmospheric and oceanic coupling with ice	16
2.7 A full sea ice model	16
3 Toward rheology-based sea ice models	19
3.1 Early sea ice models	19
3.1.1 Equilibrium drift theories	20
3.2 Viscous and Plastic Rheologies	24
3.2.1 Viscous rheologies	24
3.2.2 Plastic rheologies	26
Elastic-plastic rheology (EP)	28
Viscous-plastic rheology (VP)	29
Mohr-Coulomb failure	31
3.3 A summary of rheology-based sea ice dynamics up to the current state . .	32
4 Sea ice brittle modeling	35
4.1 A new modeling paradigm	35
4.1.1 A quantitative approach to study scale-invariance	35
4.1.2 The multifractal scaling properties of sea ice deformation	36
4.1.3 A new validation metric for sea ice models	36
4.2 The Elasto-Brittle rheology (EB)	38
4.2.1 Toward an elasto-brittle approach for sea ice rheology	38
4.2.2 Constitutive law	39
4.2.3 Damage criterion	41
4.2.4 Progressive damaging and healing	42

4.2.5	Results and known limitations of the EB rheology	44
4.3	The Maxwell elasto-brittle rheology (MEB)	45
4.3.1	Motivation	45
4.3.2	Constitutive model	46
4.3.3	Damage criterion	47
4.3.4	Progressive damaging	47
4.3.5	Coupling of damage with mechanical parameters	48
4.3.6	Some results and known limitations of the MEB rheology	49
4.4	The brittle Bingham-Maxwell rheology (BBM)	49
4.4.1	Motivation	49
4.4.2	Constitutive model	50
4.4.3	Damage criterion	51
4.4.4	Damage propagation and coupling with mechanical parameters	51
4.4.5	Results	52
4.5	A timeline of sea ice brittle modeling	53
5	Summary and concluding remarks	57
A	Discontinuous Galerkin solver in sea ice modeling	59
A.1	Continuity equation	59
A.1.1	Finite dimensional approximation	60
A.1.2	Advection equation	61
A.1.3	Finite dimensional approximation	62
	Ringraziamenti	65
	Bibliography	67

Chapter 1

Introduction

The sea ice cover

Sea ice is what we call any form of frozen seawater floating on the ocean surface. The main components are brittle floes, irregularly shaped pieces of ice, with large horizontal dimensions, normally between 100 m and 5 km, several meters thick, which form a *continuous cover* by welding together during winter (see Figures 1.1 and 1.2). The presence of the atmosphere and the ocean bounding sea ice contribute to its deformation and motion: wind and water stress cause the cover to *fracture* and to *drift* over the ocean. As a result of the external forcing the cover fails to form a set of cracks. When these narrow features align together they form long regions of open water (or very thin ice) called *leads*. If sea ice is very compact and subject to a high stresses, it can pile up to form *pressure ridges* (Nansen, 1897). Remote sensing observations processed during the first RADARSAT program (1995-2013) using synthetic aperture radar imagery showed the existence of localized regions of shear in the sea ice cover, known as *Linear Kinematic Features* (LKFs; Kwok et al. 1998; Kwok 2001). Consisting of leads and ridges, these are basically regions of strong weakness of the cover and their properties give us critical information about the nature of the mechanical behavior of sea ice both at the smaller and at the larger scales.

Motivation for the study

Sea ice is a critical component of the Earth's cryosphere. It is profoundly important in regulating the planet's climate and in influencing various interconnected systems. The albedo effect, a key mechanism associated with sea ice, plays a pivotal role in climate regulation. With its high albedo, sea ice reflects back a substantial portion of incoming solar radiation. This reflective quality helps to maintain Earth's energy balance by preventing the excessive absorption of solar energy in the underlying ocean. As sea ice diminishes, the reduction of this reflective surface contributes to a positive feedback loop, amplifying warming trends.

Beyond its albedo effect, sea ice actively participates in driving global ocean circulation patterns. The formation of sea ice in polar regions contributes to the production of dense, cold water, fostering the global thermohaline circulation¹. Alterations in sea ice dynamics can influence these circulation patterns, thereby impacting climate systems on a global scale.

Changes in sea ice can also influence atmospheric circulation patterns, potentially altering weather systems globally. This includes shifts in storm tracks and precipitation patterns, which can have far-reaching consequences for regional climates.

¹Thermohaline circulation, also known as the "global conveyor belt", is a deep-ocean current system resulting from temperature and salinity-driven density variations. In polar regions, cold temperatures cause seawater to freeze into ice, leaving behind saltier water that sinks due to increased density. This sinking initiates a continuous cycle of deep-ocean currents, playing a vital role in redistributing heat and momentum worldwide.



FIGURE 1.1: The picture shows sea ice floes as present in the Nares Strait during the Enduring Ice Project (see <https://albedo.cool/>).
Credit: Cristopher Horvat.

Sea ice's dynamic nature affects various maritime activities, including shipping routes and resource extraction such as oil and gas. Diminishing sea ice opens up new possibilities for navigation in the Arctic. This presents both opportunities and challenges for human endeavors in polar regions.

Reports, such as those from the *US National Snow & Ice Data Center*, indicate an undoubted decline in the Arctic's sea ice cover extent. This decline, measured as the area of the ocean covered by sea ice for a fractional portion of at least 15%, has been observed since the systematic collection of data commenced in 1979.

Motivated by this an international effort to create an advanced continuum sea ice model for climate research has been initiated: the Scale-Aware Sea Ice Project - SASIP. SASIP aims at radical knowledge step in the understanding of the sea-ice processes and on our ability to model them. The project's scope is to accurately capture sea ice dynamics, i.e. the drift and deformation, and thermodynamics, i.e. the melting/growing by incorporating physical accuracy, data adaptability, high parallelization and computational efficiency. SASIP intends to leverage machine learning and data assimilation techniques, utilizing extensive datasets from simulations and remote sensing to enhance its capabilities.

A multiscale dynamics

Sea ice is a complex medium with a very heterogeneous (granular) nature at the smaller scales and a quasi-continuum nature at the larger scales. This is especially true during the colder seasons (see Figure 1.2). As will be discussed in this work, sea-ice deformation exhibits multifractal properties: it is characterized by many intense events isolated in time and the deformation is strongly localized in space around the LKFs. This renders it necessary to adopt a multiscale modeling approach.

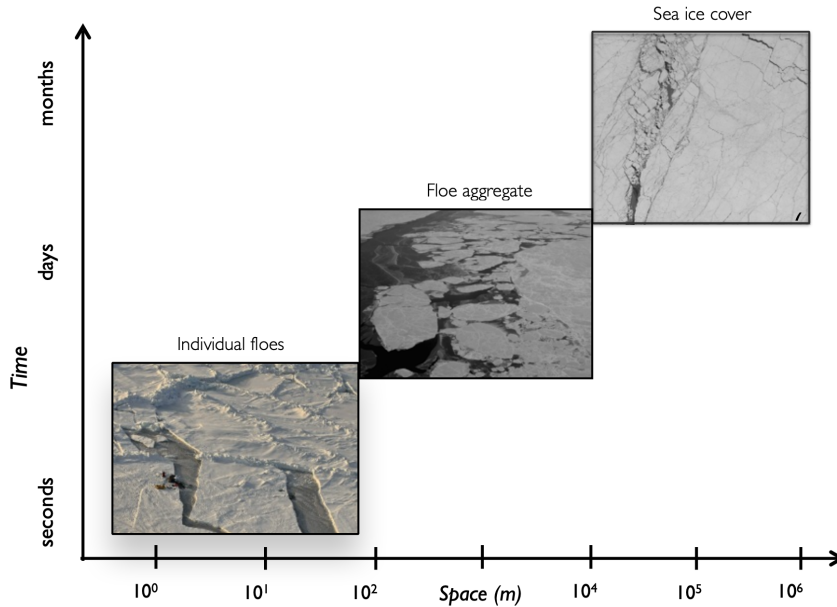


FIGURE 1.2: Aerial pictures of sea ice (from bottom to top) at the scale of 100 m, ~ 5 km and 60 km. At the smallest time and space scales, the discontinuous nature of the ice cover cannot be ignored when modeling its deformation and drift. At large scales (10^4 m), the ice cover is constituted by a large number of individual ice floes of different shapes and sizes and is described by mean quantities in continuum models.

From Dansereau (2016)

Aiming to build a model that is consistent with observations, makes the resolution at which observations are obtainable a critical factor. Current resolution for sea ice deformation measurements from the RADARSAT Geophysical Processor system (RGPS), that is the main source of observations for this kinematic quantity in the Arctic to date, is of the order of 10 km.

In this work we focus on the larger scales, which allows for the use and development of a continuum theory approaches. This approach is also the one that is currently taken by sea ice models effectively implemented into larger climate models (e.g. The CMIP6 Sea-Ice Model Intercomparison Project; Notz et al. 2016).

Coupling to thermodynamics

In this thesis the mechanical behavior of sea ice is analyzed ignoring the thermodynamics. Mechanical growth occurs at very short time scales compared to thermal production, therefore, in the long run, thermal production of ice volume usually exceeds mechanical production (Leppäranta, 2011). This strongly impacts the time horizon until when the model can provide a faithful description of reality. This is one of the main reasons why these mechanical models are used is a stand-alone (non-coupled) implementation. Large coupled climate models (ice-ocean-atmosphere-land) are usually run for longer timescales, thus in those cases it is unavoidable to include ice thermodynamics. Forcing provided by solar radiation and heat exchange with water and air lead to ice growth and melt both in the interior and at the boundaries. Freezing and melting are thus responsible for changing ice material properties. To account for this, the conservation laws for these properties should contain appropriate sink/source terms. However, models of thermodynamics are, to a good approximation, vertical (Maykut and Untersteiner, 1971). This partly supports

the commonly adopted perspective of treating sea ice as a flat, two-dimensional sheet whose motion is happening in the horizontal plane.

Structure of the thesis

This work is meant to provide the theoretical basis underlying continuum models of sea ice dynamics and review some of the main approaches employed in the modeling of its rheological behavior. The structure is the following:

- Chapter 2 explains why we treat ice as a two-dimensional continuous sheet. The relevant quantities entering the mechanical description of its drift and deformation are presented. The concept of sea ice rheology is introduced in a general manner. Following this, we then describe the governing equations. At the end of the chapter we provide a diagram illustrating the big picture on the physics of a sea ice model.
- In the first part of Chapter 3 the early (equilibrium-based) drift models of sea ice, lacking a rheological parametrization, are presented. In the second part, the main rheologies historically employed in sea ice mechanical behavior are outlined, ranging from the simplest viscous to the plastic ones.
- Eventually, Chapter 4 addresses the new solid-like brittle rheology approach that is the subject of recent research efforts. The description of the brittle-based rheologies follows an introduction of this new paradigm and an evaluation of the extent to which it is able to reproduce the observed multifractal properties of sea ice deformation.

Chapter 2

Sea ice dynamics modeling

This chapter wants to provide the physical framework to study continuum theories of sea ice dynamics. First, the working hypothesis and the physical quantities relevant to the study of the problem are specified. Then, the governing equations are presented. At the end of the chapter, a diagram providing an overview on the physical components of a full sea ice model is given.

2.1 A continuum model of the sea ice cover

In this work, we focus on the study of models capable of explaining sea ice deformation and motion, i.e. its dynamics.

Ever since the first sea ice-dynamics modeling attempts were made, in which the wind-driven drift of a single floe was considered (e.g. Gudkovich and Nikiforov, 1963), it was clear that the kinematics depended upon the floe size and shape (see Figure 2.1 for the sketch of a free floe). However, successive developments have taught that velocities alone are poor indicators of ice behavior (Rothrock, 1975b) and that it is necessary to account for interactions between the floes. These may be in direct contact, freezing together forming aggregates, or separated by open water or very thin ice, normally refrozen leads.

In the following, sea ice dynamics is analyzed, in particular in its continuum-scale approach, and the rationale behind the development of a two-dimensional theory for sea ice-dynamics is given.

2.1.1 The continuum scale

As outlined in chapter 1, the sea ice cover displays a great spatial and temporal variability ranging from the purely discontinuous character at the shorter scales to the approximately continuous one at the larger scales. In the latter case, the subject of study are drift ice particles, continuum elements containing several ice floes¹. In the sea ice community it is common to speak of *ice fields*: any area of floating ice consisting of any size of floes, which is greater than 10 km across (WMO, 2014).

If we let d denote the characteristic floe size, a material particle of size D will contain $n \approx (D/d)^2$ floes. For the continuum approximation to hold, we need n to be large enough, say $n > 100$, which means that the single continuum element's dimension should be at least an order of magnitude greater than the floe size. In addition to that, it is clear that any property of the ice field should have much larger spatial variability \tilde{D} than the previous length scales; formally, the scales should satisfy (Rothrock, 1975b):

$$d \ll D \ll \tilde{D}. \quad (2.1)$$

¹Until recently drift ice was indicated as pack ice, but now the latter term *pack ice* refers to very densely packed ice (WMO, 2014).

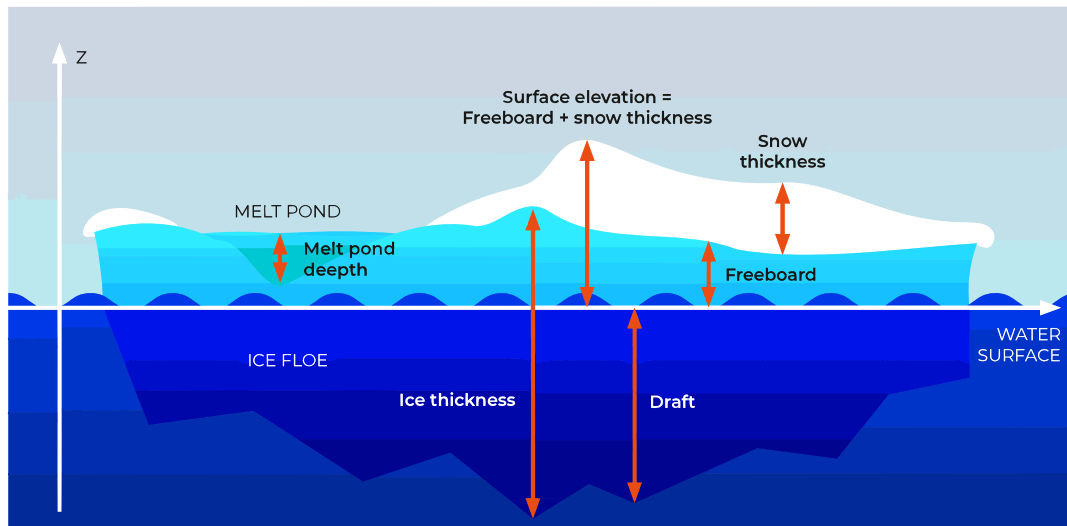


FIGURE 2.1: Schematic picture of a free ice floe. The freeboard and draft are, respectively, the portion of the ice floe outside of and submerged into the sea. In many cases the floe might be partially covered by snow. The melt pond consists of a pool of open water formed on the sea ice.

Taken from: A. Grobe and H. Grobe (2007).

In practice, most (numerical) sea ice models work with a mid-coarse spatial resolution (e.g 10 km in Rampal et al. 2016; 12 km in Boutin et al. 2023), i.e. the smallest resolved spatial scale, which guarantees each grid cell to contain enough floes while simultaneously keeping computation cost reasonable. As D approaches d (higher resolution), a system of a few floes is being resolved: field properties change abruptly at the floes' boundaries, thus requiring some sort of spatial smoothing.

Recently, efforts have been made to include evolving information about the distribution of floe sizes into the models (e.g. Horvat and Tziperman, 2015). At present time, however, all IPCC-class climate models employ a continuous description of the sea ice cover. I.e. in the following we will consider sea ice to be a continuous medium.

2.1.2 A two-dimensional theory

In the modeling approach described hereafter, the sea ice cover is considered as a thin plate, due to its large aspect ratio, with the horizontal length scales being many orders of magnitude larger than the vertical scales. As such, a two-dimensional dynamical theory is believed to be adequate. In particular, the kinematics and constitutive properties of the ice sheet will be described by a two-dimensional horizontal velocity field \mathbf{u} and the planar stress hypothesis will be taken (Timoshenko and Goodier, 1951; Zienkiewicz and Taylor, 2000).

In a key study, Nye (1973) provided evidence that such an approach is justified at the mesoscale and larger. A detailed derivation of the two-dimensional conservation laws and constitutive relations from the fundamental three-dimensional equations integrating through the ice layer depth can be found in Gray and Morland (1994) and Leppäranta (2011)².

The greatest bulk of research in sea ice dynamics has been concerned with the development of two-dimensional models.

²Gray and Morland (1994) made use of the theory of interacting continua, so their result is technically valid for a mixture of ice and water.

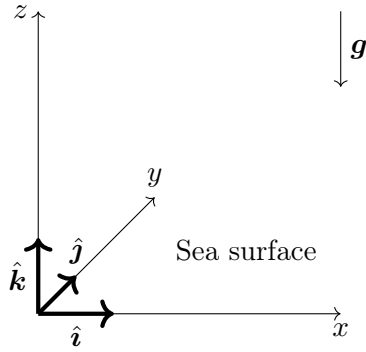


FIGURE 2.2: Cartesian coordinate system at the sea level used to formulate the theory.

It is customary to consider the vertically-integrated linear momentum balance equation as the governing equation of motion of the ice cover (see Section 2.5.3).

In the following we present the sea ice dynamics in a two-dimensional Cartesian frame defined by orthonormal vectors \hat{i} and \hat{j} (see Figure 2.2).

2.2 Ice kinematics

Let $\mathbf{u}(x, y; t)$ be the horizontal sea ice velocity. As our main concern will be the large scale modeling, where multiple floes are considered, we assume \mathbf{u} to be sufficiently smooth. More specifically, we assume it is to at least second order (Coon et al., 1974; Hunter, 1983).

For the reasons outlined in Section 2.1.2, a plane stress condition is assumed, which means only the horizontal components of internal stress and strain (deformation) tensors are considered.

2.2.1 Deformation of drift ice

The motion of a continuum element of the ice cover can be decomposed into a rigid translation, rigid rotation and strain. Clearly, in a two-dimensional continuum flow model of ice, translation can happen in the plane and an eventual rotation is just about the vertical axis. On the other hand, strain, the physical deformation of drift ice particles (continuum elements) may be of three different modes: tensile strain or extension, compressive strain or contraction and shear strain. The first two modes are normal to the surface and are responsible for changing lengths and therefore causing a relative volume variation. Shear strain, instead, is responsible for changing the shape of the continuum.

In the following treatment the reference frame is the sea surface Cartesian system shown in Figure 2.2. Let $\mathbf{x}(t)$ be the coordinate of an ice particle. The material deformation, without considering pure translation, is given by the two-dimensional displacement gradient $\nabla \mathbf{x} - \mathbf{I}$. The displacement gradient is made up of two parts: a symmetric one, the strain $\boldsymbol{\varepsilon}$, and an antisymmetric one, the rotation $\boldsymbol{\omega}$. It can be easily seen that the velocity gradient, $\frac{\partial u_{ij}}{\partial x_k}$, $i, j, k = 1, 2$, a second-order tensor with matrix representation

$$\nabla \mathbf{u} = \begin{bmatrix} \frac{\partial u_x}{\partial x} & \frac{\partial u_x}{\partial y} \\ \frac{\partial u_y}{\partial x} & \frac{\partial u_y}{\partial y} \end{bmatrix} \quad (2.2)$$

corresponds to the rate of displacement gradient, the latter being composed of two parts:

$$\nabla \mathbf{u} = \dot{\boldsymbol{\varepsilon}} + \dot{\boldsymbol{\omega}} \quad (2.3)$$

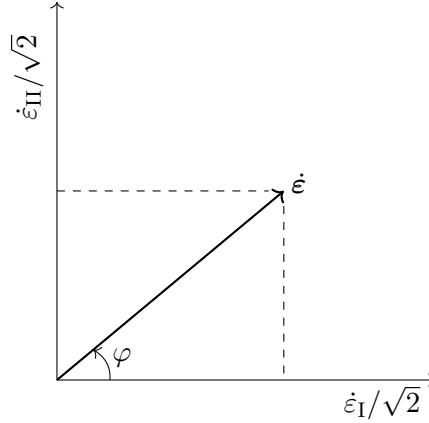


FIGURE 2.3: Strain-rate representation in the principal axes system. The modes of deformation are determined by the angle φ .

where we have introduced the *strain-rate*:

$$\dot{\epsilon} = \frac{1}{2} [\nabla \mathbf{u} + (\nabla \mathbf{u})^T] . \quad (2.4)$$

The strain-rate gives us the deformation rate of the sea ice cover and it can be decomposed into a isotropic (pure compression/dilatation) and deviatoric part (pure shear deformation): $\dot{\epsilon} = \dot{\epsilon}_s + \dot{\epsilon}' = (\frac{1}{2} \text{tr } \dot{\epsilon}) \mathbf{I} + \dot{\epsilon}' = (\frac{1}{2} \nabla \cdot \mathbf{u}) \dot{\epsilon} + \dot{\epsilon}'$. As second-order tensors, the strain and the strain rate have a 2×2 matrix representation in the Cartesian orthogonal system considered:

$$\epsilon = \begin{bmatrix} \epsilon_{11} & \epsilon_{12} \\ \epsilon_{21} & \epsilon_{22} \end{bmatrix} \quad \dot{\epsilon} = \begin{bmatrix} \dot{\epsilon}_{11} & \dot{\epsilon}_{12} \\ \dot{\epsilon}_{21} & \dot{\epsilon}_{22} \end{bmatrix} . \quad (2.5)$$

The magnitude of the strain-rate is given by the Frobenius norm of the strain-rate tensor:

$$\|\dot{\epsilon}\| = \sqrt{\dot{\epsilon}_{11}^2 + \dot{\epsilon}_{12}^2 + \dot{\epsilon}_{21}^2 + \dot{\epsilon}_{22}^2} . \quad (2.6)$$

Since the dimension is 1/time, this value defines the timescales of strain and rotation. In the principal axes coordinate system the normal strain-rates are given by the principal values (eigenvalues):

$$\dot{\epsilon}_{1,2} = \frac{1}{2} \text{tr } \dot{\epsilon} \pm \frac{1}{2} \sqrt{(\text{tr } \dot{\epsilon})^2 - 4 \det \dot{\epsilon}} \quad (2.7)$$

with $\dot{\epsilon}_1 \geq \dot{\epsilon}_2$. One way to visualize the strain-rate is through the invariants:

$$\dot{\epsilon}_I \equiv \dot{\epsilon}_1 + \dot{\epsilon}_2 = \text{tr } \dot{\epsilon} \quad (2.8a)$$

$$\dot{\epsilon}_{II} \equiv \dot{\epsilon}_1 - \dot{\epsilon}_2 = \sqrt{(\text{tr } \dot{\epsilon})^2 - 4 \det \dot{\epsilon}} \quad (2.8b)$$

which are themselves functions of the invariants of 2×2 matrices: $\text{tr } \dot{\epsilon}$ and $\det \dot{\epsilon}$. The first invariant equals the divergence of the velocity while the second one equals twice the maximum shear rate. In terms of these two invariants, the magnitude of the strain-rate tensor (Equation 2.6) reads:

$$\|\dot{\epsilon}\| = \sqrt{\frac{\dot{\epsilon}_I^2 + \dot{\epsilon}_{II}^2}{2}} . \quad (2.9)$$

We have a simple but handy visualization of the mode of deformation, that is, as a vector in the $(\dot{\epsilon}_I, \dot{\epsilon}_{II}) \sqrt{2}$ upper-half plane (see Figure 2.3):

$$\begin{cases} \dot{\epsilon}_I = \sqrt{2} \|\dot{\epsilon}\| \cos \varphi \\ \dot{\epsilon}_{II} = \sqrt{2} \|\dot{\epsilon}\| \sin \varphi \end{cases} \quad \varphi = 2 \arctan \left(\frac{\dot{\epsilon}_{II}}{\dot{\epsilon}_I + \sqrt{2} \|\dot{\epsilon}\|} \right), \quad 0 \leq \varphi \leq \pi \quad (2.10)$$

where the vector's direction φ represents the ratio of rates of shearing and divergence and the vector's length the magnitude of the deformation-rate. The main deformations mode are the following: pure divergence ($\varphi = 0$), uniaxial tension ($\varphi = \pi/4$), pure shear ($\varphi = \pi/2$), uniaxial contraction ($3\pi/4$) and pure convergence (π).

2.2.2 Sea ice internal stress

In keeping with the preceding sections, sea ice motion is considered to take place in the horizontal plane. In this work, as in the models of Ólason et al. (2022), Bouillon and Rampal (2015b), Sulsky et al. (2007), the two-dimensional *horizontal internal stress* is indicated with $\boldsymbol{\sigma}$ and it is given by:

$$\boldsymbol{\sigma} = \boldsymbol{\sigma}^{\text{tot}} - p\mathbf{I} \quad (2.11)$$

where $\boldsymbol{\sigma}^{\text{tot}}$ is the (horizontal) Cauchy stress tensor (e.g. Hunter, 1983) while $-p\mathbf{I}$ represents an isotropic averaged stress due to gravity working on the ice.

Since the equation of motion is obtained through vertical integration of the three-dimensional momentum equation (see Section 2.5.3) it is customary in the sea ice modeling community to refer to the *sea ice internal stress*, $\boldsymbol{\sigma}_{\text{ice}}$, as the tensor whose components are the depth-integrated horizontal components of the three-dimensional internal stress³ (e.g. Gray and Morland, 1994; Sulsky et al., 2007). However, in practice, the homogeneity of the stress in the ice volume is often assumed (e.g. Ólason et al., 2022; Rampal et al., 2016), the sea ice internal stress simply being given by $\boldsymbol{\sigma}_{\text{ice}} = \boldsymbol{\sigma} \hat{h}$, where $\boldsymbol{\sigma}$ is given by Equation 2.11 and \hat{h} is the mean ice thickness (see Section 2.3.1).

Similarly to the strain and strain rate, the ice internal stress has a 2×2 matrix representation with respect to the usual orthogonal reference frame,

$$\boldsymbol{\sigma} = \begin{bmatrix} \sigma_{11} & \sigma_{12} \\ \sigma_{21} & \sigma_{22} \end{bmatrix}, \quad (2.12)$$

where the symmetry (e.g. Hunter, 1983) ensures the independence of σ_{11}, σ_{22} , related to the normal stress, and σ_{12} , related to shear stress. The of normal stress, σ_N , and shear stress τ , respectively given by:

$$\sigma_N = \frac{\sigma_{11} + \sigma_{22}}{2} \quad (2.13)$$

$$\tau = \sqrt{\left(\frac{\sigma_{11} + \sigma_{22}}{2}\right)^2 + \sigma_{12}^2} \quad (2.14)$$

are two invariants of $\boldsymbol{\sigma}$.

The horizontal stress is usually characterized by the two invariants, σ_I, σ_{II} , given by:

$$\sigma_I \equiv \sigma_1 + \sigma_2 = \text{tr } \boldsymbol{\sigma} \quad (2.15a)$$

$$\sigma_{II} \equiv \sigma_1 - \sigma_2 = \sqrt{(\text{tr } \boldsymbol{\sigma})^2 - 4 \det \boldsymbol{\sigma}} \quad (2.15b)$$

where the principal stresses $\sigma_{1,2}$, i.e. the eigenvalues of the internal stress tensor, are obtained by replacing $\dot{\epsilon}$ with $\boldsymbol{\sigma}$ in Equation 2.7. Ice is said to possess a *stress-state* given by a point in the $\{\sigma_I, \sigma_{II}\}$ plane.

Section 2.5.3 explains how the internal stress of the ice enters the equation of motion.

³We point out to the reader that $\boldsymbol{\sigma}$ has units of N m^{-2} (Pa) while $\boldsymbol{\sigma}_{\text{ice}}$ of N m^{-1} .

2.3 The state of the ice cover

Due to its complex and diverse physics, it is not easy to identify a reasonable set of material properties to parametrize the state of the ice cover. Sea ice thickness, i.e. ice volume per unit area, has proved an important indicator of the state of the cover: many of the quantities linked to ice mechanical behavior, e.g. the internal resistance to the motion, are very sensible to its change. Another important property is given by sea ice concentration, i.e. the fractional area of ocean covered by ice, which, combined with ice thickness, provides an estimate of ice volume. Here we will discuss how these concepts enter the description of sea ice as a continuous medium.

2.3.1 Ice thickness distribution

Local measurements tell us that the ice cover is a horizontally nonuniform mixture of ice of different thicknesses, each of which may respond differently to similar thermal and mechanical forcing (Maykut, 1982). Due to ridges and leads, sea ice thickness will vary on scales even smaller than the sizes of the sea ice floes. In order to incorporate the sea ice thickness into a continuous theory for sea ice dynamics, these subscale variations of sea ice thickness are customarily represented as a thickness distribution⁴. I.e. the sea ice thickness per unit of area in a continuous sea ice model at point \mathbf{x} can be given as (Thorndike et al., 1975; Rothrock, 1986):

$$\hat{h}(\mathbf{x}, t) = \int_0^{\infty} hg(h; \mathbf{x}, t) dh \quad (2.16)$$

with $g(h; \mathbf{x}, t)dh$ the probability to find a sea ice thickness between h and $h + dh$ at location \mathbf{x} .

No simple general form exists for g , so often histogram approximations are employed. In one extreme, but frequently applied, approach one makes a binary division between ice and no-ice. I.e. a function “ice”, I , is defined as follows (Leppäranta, 2011):

$$I(h, h_0) = \begin{cases} 0 & \text{if } h \leq h_0 \\ 1 & \text{if } h > h_0 \end{cases} \quad (2.17)$$

where h_0 is the so-called *demarcation thickness*. In terms of Heaviside step-function H , $I = H(h - h_0)$. This way, what is considered by the theory as mechanically active ice has been separated from very thin ice, just considered as a region of weakness in the ice cover. The choice made by some modelers to exclude very thin ice from the mean ice thickness is also motivated by a certain difficulty of detection by the means of remote sensing techniques. Combining the definition in Equation 2.17 with the sea ice thickness distribution allows to introduce a variable *sea ice concentration* or *compactness* as:

$$A(\mathbf{x}, t) = \int_0^{\infty} I(h, h_0)g(h; \mathbf{x}, t) dh. \quad (2.18)$$

The constraint $0 \leq A \leq 1$ is straightforward from the definition. Basically $A(\mathbf{x})$ gives $P(I = 1; \mathbf{x})$, the probability to encounter sea ice when randomly sampling at location \mathbf{x} . Consequently, the probability to encounter open water or negligible thin ice, i.e. the no-ice condition, is given by $1 - A$. The practice of expressing compactness in multiples

⁴While this seems a reasonable mathematical assumption which grants us a possibility to estimate the statistics of the ice thickness, in physical terms there is no intrinsic randomness associated with h . As a matter of fact, the dynamical change of volume of the ice cover can be explained in terms of Newtonian mechanics, a deterministic theory.

of 0.1 is typically applied to observed or measured sea ice concentration (WMO, 2014). This method is used to provide a more detailed and standardized way of reporting sea ice coverage, especially in the context of remote sensing and satellite observations; it allows for a finer resolution in reporting variations in sea ice extent.

Using Bayes' theorem, the average thickness of the sea ice floats, also known as the *ice slab thickness* (e.g. in Ólason et al., 2022), at location \mathbf{x} in this binary division is given as

$$\begin{aligned}\hat{h}_{\text{thick}}(\mathbf{x}, t) &= \int_0^\infty hg(h|I = 1; \mathbf{x}, t) dh \\ &= \frac{1}{P(I = 1; \mathbf{x}, t)} \int_0^\infty hg(I = 1|h; \mathbf{x}, t)g(h; \mathbf{x}, t) dh \\ &= \frac{1}{A(\mathbf{x}, t)} \int_{h_0}^\infty hg(h; \mathbf{x}) dh \\ &\approx \frac{1}{A(\mathbf{x}, t)} \hat{h}(\mathbf{x})\end{aligned}\tag{2.19}$$

neglecting any mass in ice below the demarcation thickness in line with the histogram approximation. The evolution equations for sea ice thickness and compactness will be presented in Section 2.5.

2.3.2 The ice state variables

In this work we indicate with \mathcal{J} the set of ice state variables chosen by a model. There are two main approaches to choose how to model the material properties of sea ice.

The first approach is based on defining ice categories, each of which must obey the conservation laws in Section 2.5. In this case $\mathcal{J} = \{A, h_1, \dots\}$, where A is the sea ice concentration, defined by Equation 2.18, and h_1, \dots are the thicknesses of the various ice categories. Ice concentration or ice thickness have been proved to be poor indicators of the actual state of the ice cover by themselves and proper characterization of ice properties requires combination of concentration with at least 1 sea ice category (Nikiforov, 1957; Doronin, 1970). Examples of using a single sea ice thickness category in combination with sea ice concentration are Nikiforov (1957), Doronin (1970), and Bouillon and Rampal (2015b). Another example is given by neXtSIM model equipped with thermodynamics (Rampal et al., 2016) which contains variables for the thickness of regular sea ice and snow (see Figure 2.1) as well as sea ice concentration. In general, the number of sea ice categories in the model depend upon their dynamical significance and observability (Haapala, 2000).

The second approach is to take the thickness distribution as state variable and to determine the optimal degree of resolution of the distribution. In other words, how many different discrete thicknesses classes should be used in the model to maintain the desired accuracy while keeping (computational) complexity as low as possible? This approach makes sense whenever more than a few thickness classes are considered, otherwise the information about the actual thickness class can easily be lost. An example of a model implementing this second approach is the AIDJEX sea ice model introduced by Coon et al. (1974).

In the context of brittle-based models, a typical variable encompassed by \mathcal{J} is the material's cohesion, i.e. its inherent shear strength (see e.g. Equation 4.11), which can be used as a means of characterizing the material's natural heterogeneities.

2.4 Sea ice rheology

Rheology is branch of physics concerned with studying the deformation and flow of materials, both solids and liquids. The aim of rheological studies is mainly to provide an extension of continuum mechanics to characterize the flow of materials exhibiting both solid-like (elastic, plastic, brittle) and fluid-like (viscous, non-Newtonian) behavior (Barnes et al., 1989).

In the case of sea ice, observational evidence shows that drift ice deforms and fractures under the action of external forcing, presenting itself as a large field broken into floes (Feltham, 2008). In this context, *sea ice rheology* is what we call the relationship between the sea ice internal stress to the large-scale deformation of the ice cover and the state of the ice cover.

If we exactly knew the form of the constitutive equation for sea ice, we would not need to pay attention to the mechanisms of floe interaction (Rothrock, 1975b). However, performing a field experiment capable of furnishing enough information to conclusively establish the constitutive law for sea ice has not been possible. The determination of suitable constitutive relations to describe sea ice rheology has guided sea ice-dynamics research since it began. To this day it remains an outstanding problem that limits the success of sea ice models (Feltham, 2008).

The main stress-generating mechanisms affecting sea ice are the following:

- Ice *ridging* processes due to convergence of very compact ice;
- Ice *opening*, causing the creation of leads;
- Edge shear tractions between floes;
- Thin pieces of ice sliding over each other as a consequence of currents or winds' push, known as *rafting*;
- Interaction between floes and leads.

The knowledge of these mechanisms along with some observational insights about the ice cover guide the development of a constitutive law for sea ice. The constitutive equation relating stress and deformation for drift ice has the generic form:

$$\boldsymbol{\sigma} = \boldsymbol{\sigma}(\mathcal{J}, \boldsymbol{\varepsilon}, \dot{\boldsymbol{\varepsilon}}) \quad (2.20)$$

where the ice state \mathcal{J} is determined by the material properties (sea ice concentration, sea ice thickness, cohesion, etc.) as well as model dependent parameters, while the strain $\boldsymbol{\varepsilon}$ and strain rate $\dot{\boldsymbol{\varepsilon}}$ are determined by the (large-scale) deformation of the sea ice. Determining the appropriate constitutive relation for sea ice has proven to be very difficult both because of its highly non-linear character (see Figure 2.4 for a one-dimensional illustration) and for the initial lack of useful data.

In chapter 3 and 4 the different rheological models for $\boldsymbol{\sigma}(\mathcal{J}, \boldsymbol{\varepsilon}, \dot{\boldsymbol{\varepsilon}})$ are presented.

2.5 Governing equations

In this section the general equations for the evolution of the model variables are presented.

2.5.1 Evolution of the ice thickness and concentration

As mentioned in Section 2.3.2, \mathcal{J} contains the sea ice state variables that are advected by the flow. The actual variables J contained in \mathcal{J} are model dependent, but they should

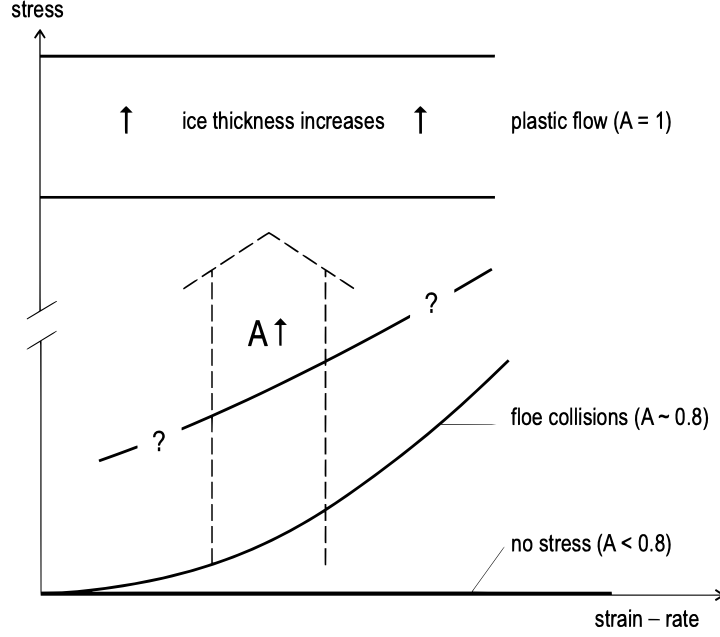


FIGURE 2.4: Schematic representation of the change in quality of sea ice rheology as a function of ice compactness A and thickness h . When the plastic regime is reached the stress becomes independent of the strain-rate. Taken from: Leppäranta (2011).

follow the advection equation (see Appendix A for an example of how such an equation would be implemented in a sea ice model like neXtSIM_{DG}; Richter et al. 2023):

$$\frac{\partial J}{\partial t} + (\mathbf{u} \cdot \nabla)J = S_J \quad (2.21)$$

where \mathbf{u} is the two-dimensional velocity of the ice sheet, S_J represents changes in sea ice state variables due to mechanical and thermodynamic processes (Dansereau, 2016), the latter being outside the scope of this work. The left-hand side of Equation 2.21 can be rewritten using the Lagrangian (material) derivative $D/Dt = \partial/\partial t + (\mathbf{u} \cdot \nabla)$ as $\frac{DJ}{Dt}$.

The mass conservation of ice is a necessary condition for any ice state. When ice density, ρ , is assumed to be constant (neglecting compressibility), the conservation of mean sea ice thickness is equivalent to the conservation of mass. In this incompressible case, the mean ice thickness can change due to the divergence of ice motion or by thermal growth/melt, so the conservation equation reads (see Appendix A for an example of how such an equation would be implemented in a sea ice model like neXtSIM_{DG}; Richter et al. 2023):

$$\frac{D\hat{h}}{Dt} = -\hat{h}\nabla \cdot \mathbf{u} + S_h, \quad \hat{h} \geq 0 \quad (2.22)$$

where \hat{h} is given by Equation 2.16 and S_h is a potential thermodynamic source/sink term.

The equation obeyed by compactness A is somewhat more complex to determine and depends on the chosen level of mechanical deformation complexity. In simpler two-level models in which a selected surface of the ocean S is assumed to be partially covered by ice, S_{ice} , and by open water, $S - S_{ice}$, the change in compactness is given by (Rothrock, 1975b):

$$\frac{DA}{Dt} = \frac{D}{Dt} \frac{S_{ice}}{S} = \frac{1}{S} \frac{DS_{ice}}{Dt} - \frac{S_{ice}}{S^2} \frac{DS}{Dt} = -A\nabla \cdot \mathbf{u} \quad (2.23)$$

where $(1/S)(DS/Dt) = \nabla \cdot \mathbf{u}$ by definition and the ice-covered area is assumed to be

conserved (Nikiforov, 1957). Including a thermodynamic term, the complete conservation law for concentration assumes the form

$$\frac{DA}{Dt} = -A\nabla \cdot \mathbf{u} + S_A, \quad 0 \leq A \leq 1. \quad (2.24)$$

The constraint $A \leq 1$ is enforced by specifying a mechanical redistribution mechanism. Simplified versions of mechanical redistribution in which A is clipped at 1 are popular (Hibler, 1979; Dansereau, 2016). Despite their simplicity, several sea ice models employ Equations 2.22 and 2.24; for instance Hibler (1979) and Bouillon and Rampal (2015b).

Additional complexity can be considered if the changes due to mechanical deformation are let depend on the deformation mode φ (see Equation 2.10), and from the magnitude of the strain rate $\|\dot{\boldsymbol{\epsilon}}\|$ (e.g. Thorndike et al., 1975), rather than simply the divergence of the flow.

2.5.2 Evolution of the ice thickness distribution

In those more sophisticated models implementing thickness distribution as the ice state its evolution equation must be evaluated. Mechanics and thermodynamics have different roles in this context. Freezing and melting are source/sink terms in the thickness distribution in the thickness space, i.e. for rearranging relative amounts of ice in different categories (Hibler, 1980). On the other hand, how dynamics affects the form of the distribution is a model prescription. Generally, thinner ice is produced as a result of a diverging motion, while thicker ice is produced through convergence of thinner ice, i.e. through ridging.

In Lagrangian form, the equation for the evolution of the thickness distribution $g(h; \mathbf{x}, t)$ reads (Thorndike et al., 1975; Rothrock, 1986):

$$\frac{Dg}{Dt} = \Psi - g\nabla \cdot \mathbf{u} - g\frac{\partial\Phi}{\partial h} \quad (2.25)$$

where the first term on the right-hand side represents the mechanical redistribution due to opening and ridging, the second term is the flux divergence, the third term is the ablation and accretion with Φ the accretion rate. Equation 2.25 is non-linear since each function may depend on g itself. The mechanical complexity of the model is enclosed in the redistribution function Ψ . This function may depend on the thickness h , on the strain rate $\dot{\boldsymbol{\epsilon}}$ and may have a functional dependence on the thickness distribution g . Any redistribution function must satisfy these two strong constraints (Thorndike et al., 1975):

$$\int_0^\infty h\Psi dh = 0 \quad (2.26)$$

$$\int_0^\infty \Psi dh = \nabla \cdot \mathbf{u}. \quad (2.27)$$

Equation 2.26 ensures that the mean ice thickness will not change due to redistribution, while Equation 2.27 imposes that the area of ice imported by convergence must exactly accommodate the new open water area on top of the area lost by ridging. It is obtained by integration of Equation 2.25.

In his work Thorndike et al. (1975) concluded that, when shearing occurs along a crack, the components of the displacement vector normal to the crack will locally cause a redistribution very similar to the ridging/opening events observed in pure convergence/divergence configurations⁵. On the other hand, g is not changed by displacements along the crack.

⁵See Fig. 10 of Thorndike et al. (1975) or Fig. 2.9 of Coon et al. (1974) for a schematic diagram of the formation of leads and pressure ridges during pure shearing deformation.

On these bases, a general redistribution function should be the combination of the two following modes (e.g. Feltham, 2008; Thorndike et al., 1975):

$$\Psi = \sqrt{2} \|\dot{\boldsymbol{\epsilon}}\| [\alpha_r(\varphi)w_r(h) + \alpha_o(\varphi)w_o] \quad (2.28)$$

where φ gives the deformation mode (see Equation 2.10), α_r and α_o are the ridging and opening coefficients describing the relative amount of deformation realized through pure convergence-type ridging and through pure divergence-type opening such that $\alpha_o(0) = 1$, $\alpha_r(\pi) = -1$ and $\alpha_o = \alpha_r + \cos \varphi$ (Feltham, 2008). The opening mode w_o provides a source of open water and it is defined as twice the Dirac-delta: $\int_0^{+\infty} w_o(h) dh = 1$, $w_o(h) = 0, \forall h > 0$. Finally, the ridging mode w_r specifies how ice is moved between the thickness categories, i.e. the loss and gain of different thicknesses in ridging. Several ridging models have been developed, prescribing an expression for w_r (e.g. Parmerter and Coon, 1973; Coon et al., 1974).

2.5.3 The momentum equation

The two-dimensional momentum equation is of the general form

$$\rho \hat{h} \left[\frac{\partial \mathbf{u}}{\partial t} + (\mathbf{u} \cdot \nabla) \mathbf{u} \right] = \mathbf{F}_{\text{int}} + \mathbf{F}_{\text{ext}} \quad (2.29)$$

where ρ is the sea ice density, \mathbf{u} the (horizontal) velocity of the ice sheet and the two terms on the right-hand side represent, respectively, the vertically-integrated internal force and the total external forcing acting on the ice cover. The external forcing typically comes from the air and ocean drags, the Coriolis force and the sea surface tilt. On the other hand, the internal force arises from the sum of all mechanical interactions between ice floes. The vertically-integrated internal force is given by (Gray and Morland, 1994; Hunter, 1983):

$$\mathbf{F}_{\text{int}} = \nabla \cdot (\hat{h} \boldsymbol{\sigma}) \quad (2.30)$$

where the (vertically integrated) ice stress $\boldsymbol{\sigma}_{\text{ice}}$ has been written explicitly in terms of the two-dimensional horizontal stress given by Equation 2.11 (Bouillon and Rampal, 2015b; Ólason et al., 2022).

Inserting expressions for these forces into (Equation 2.29) gives us the following momentum equation (Ólason et al. (2022), Bouillon and Rampal (2015b), Dansereau (2016)):

$$\rho \hat{h} \frac{D\mathbf{u}}{Dt} = \nabla \cdot (\boldsymbol{\sigma} \hat{h}) + A(\boldsymbol{\tau}_a + \boldsymbol{\tau}_w) - \rho \hat{h} f_c \hat{\mathbf{k}} \times \mathbf{u} - \rho h g \nabla H \quad (2.31)$$

with

- $\boldsymbol{\tau}_a$ and $\boldsymbol{\tau}_w$ the surface wind (air) and ocean (water) stresses, respectively;
- $-\rho \hat{h} f_c \hat{\mathbf{k}} \times \mathbf{u}$ the horizontal component of Coriolis pseudo-force, with $f_c = 2\omega \sin \phi$, ω being Earth's angular speed and ϕ the latitude and
- $-\rho h g \nabla H$ the force due to gradients in the sea surface dynamic height, H .

Commonly employed parametrizations of $\boldsymbol{\tau}_a$ and $\boldsymbol{\tau}_w$ are presented in Section 2.6. Furthermore, as is customary in ocean dynamics, the part of the Coriolis force arising from vertical motion is very small compared to the horizontal one and has therefore been neglected. The horizontal gradient of the sea surface atmospheric pressure should be taken into account with a $-\hat{h} \nabla p_a$ term on the right-hand side of Equation 2.31 but it is small compared to the others (Rothrock, 1975b) and thus usually neglected.

Some models (e.g. Rampal et al., 2016) implement an additional (vertically integrated) pressure gradient term, $-\nabla P$, on the right-hand side of Equation 2.31 which is meant to avoid excessive convergence for very densely-packed and highly damaged ice. Other models (e.g. Lemieux et al., 2015), include an extra basal term $\boldsymbol{\tau}_b$ on the right hand side of the momentum equation 2.31 (e.g. Rampal et al., 2016; Ólason et al., 2022) to account for land fast ice. This is however outside the scope of this work.

2.6 Atmospheric and oceanic coupling with ice

Sea ice provides an interface between the atmosphere and the underlying ocean and it exchanges momentum with both. This momentum transfer between the mean flow in the atmosphere and the ocean is intermediated by the atmospheric boundary layer (ABL) and oceanic boundary layer (OBL). The ABL over sea ice has been thoroughly examined (e.g. Rossby and Montgomery, 1935; Brown, 1980). The OBL beneath sea ice, on the other hand, still contains unknown details (Leppäranta, 2011; McPhee, 2017). These boundary layers are made up of two parts: a turbulent surface layer next to ice, in which the stress is approximately constant and an Ekman layer (e.g. Cushman-Roisin, 1994; Ekman, 1905) in which the velocity “rotates” as a result of the Coriolis effect, with stress gradually decreasing moving farther away from the ice boundary. The height of such layers varies based on different conditions, but it is of the order of the km for the ABL and ~ 50 m for the OBL (Leppäranta, 2011). The dominant balance in the momentum equations in the first layer is between pressure gradient and turbulent dissipation terms, while in the second layer it is between pressure gradient, turbulent dissipation and Coriolis terms. The latter cause the horizontal velocity within the Ekman layer to turn in the vertical. Consequently, the direction of the stress exerted by the atmosphere (ocean) on the the sea ice differs from the direction of the main flow in the lower atmosphere (upper ocean). Formally, the atmospheric (oceanic) stress on the sea ice is given by (e.g. Brown, 1980)

$$\boldsymbol{\tau}_a = \rho_a C_a \|\mathbf{u}_a\| [\mathbf{u}_a \cos \theta_a + \hat{\mathbf{k}} \times \mathbf{u}_a \sin \theta_a] \quad (2.32a)$$

$$\boldsymbol{\tau}_w = \rho_w C_w \|\mathbf{u}_w - \mathbf{u}\| [(\mathbf{u}_w - \mathbf{u}) \cos \theta_w + \hat{\mathbf{k}} \times (\mathbf{u}_w - \mathbf{u}) \sin \theta_w] \quad (2.32b)$$

where C_a, C_w are the air drag and water drag, ρ_a, ρ_w the air and water density, \mathbf{u}_a (\mathbf{u}_w) is the main flow (large-scale) velocity at the bottom of the atmosphere (top of the ocean)⁶ and θ_a (θ_w) the angle between the stress $\boldsymbol{\tau}_a$ ($\boldsymbol{\tau}_w$) and the main flow at the bottom of the atmosphere (top of the ocean). Different boundary layer theories exist giving rise to different values for $C_a, C_w, \theta_a, \theta_w$. The treatment of these theories is beyond the scope of this work.

2.7 A full sea ice model

The goal of the diagram in Figure 2.5 is to provide an overview on the various physical components that have to be integrated into a sea ice model. In the case of a stand-alone model, the contribution of the atmosphere and the ocean to the dynamics is given by external forcing, prescribed through the air/ocean drags. In coupled models, the feedback from the ice is connected to the air/ocean variables through a coupler.

⁶This is the velocity immediately outside of the boundary layer, free from the frictional influence of the surface, and it is usually close to the geostrophic (free-stream) velocity. In coupled models, this is determined by the atmospheric/oceanic model employed.

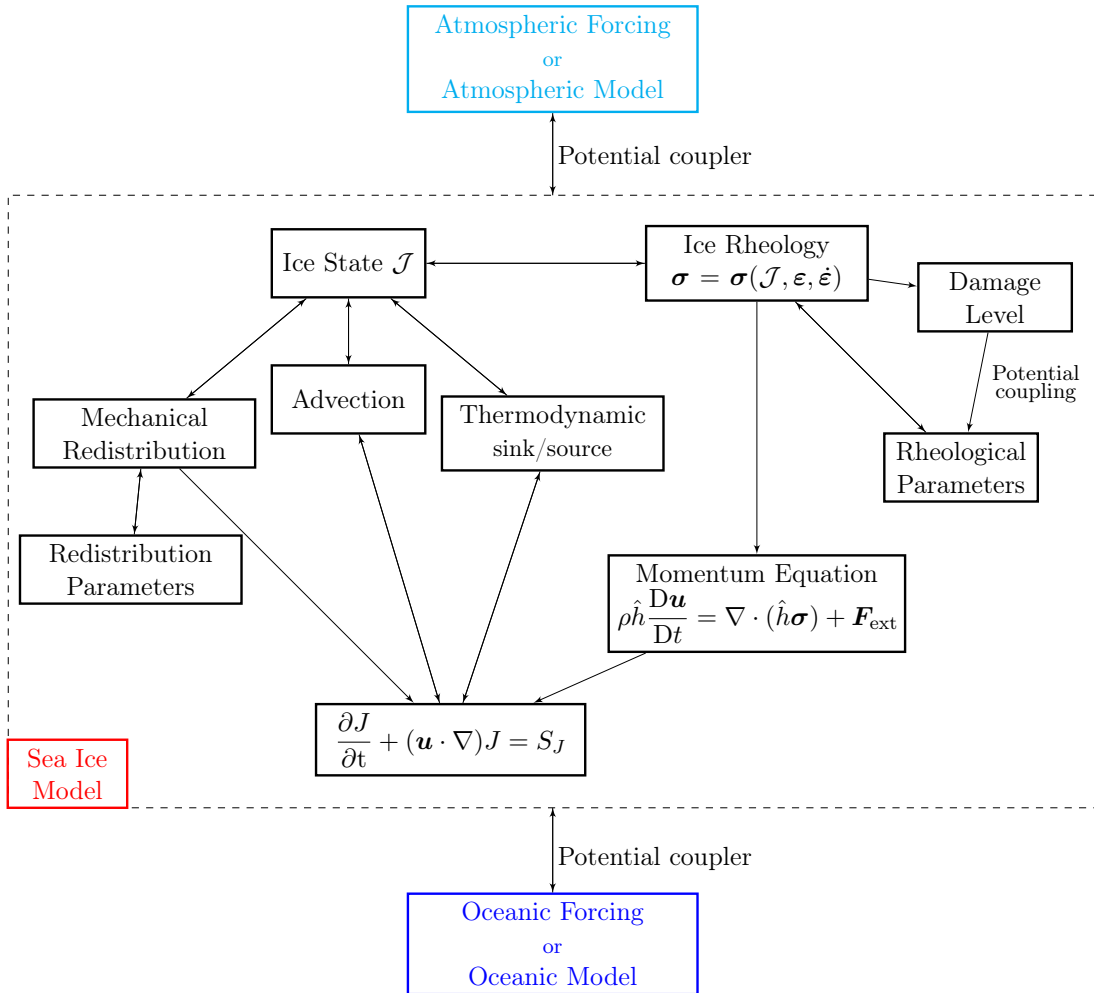


FIGURE 2.5: Diagram showing the physical components of a full sea ice model. Each scalar variable J encompassed by the ice state (set of material properties), \mathcal{J} , is advected and is subject to mechanical and thermodynamic changes (not considered in the present work). The internal stress of ice, σ , is related to deformation and the ice state through the rheology (see chapters 3 and 4). The fundamental dynamical equation, given the evolution of the drift velocity \mathbf{u} is given by the linear momentum balance, in which external forcing from the air/ocean and from the Coriolis effect is applied. If an oceanic/atmospheric model is considered, a coupler is responsible for updating the external air/ocean variables (as a result of feedback from the ice) and for providing the forcings to the ice.

Chapter 3

Toward rheology-based sea ice models

This chapter is meant to be a review of the sea ice dynamics modeling, concentrating on the development of rheological models. Section 3.1 consists of a brief history of the early modeling approaches of sea ice. Section 3.2 then proceeds to introduce rheological models which have been used to model sea ice leaving the latest developments based on brittle mechanics concepts for a separate discussion in Chapter 4. Eventually, Section 3.3 reviews the developments in rheology-based dynamics up to the current state.

3.1 Early sea ice models

Early investigations into sea ice dynamics began in the late 1800s when the first expeditions to the northern polar region took place. The relevance of the sea ice drift problem was first highlighted by Fridtjof Nansen’s observation of the wind-driven drift of ice subsequent to his 1893–1896 *Fram* expedition across the Eurasian Arctic Ocean (Nansen, 1902). Based on his observations, he concluded that ice does not exactly drifts in the same direction as the wind blows as was commonly believed at the time. Instead he found that it was deviating about $20^\circ - 40^\circ$ to the right of it. His suggestion, later confirmed by Ekman’s mathematical work (Ekman, 1902), was that this deviation is due to the Coriolis force turning the flow in clockwise direction (in the Northern hemisphere). Building on these observations, Ekman formulated his theory of oceanic drift currents (Ekman, 1905).

Wind-driven ice drift was further examined in the case of the oceanic and atmospheric drag forces by Sverdrup (1928), Rossby and Montgomery (1935) and Shuleikin (1938).

In particular, Rossby and Montgomery (1935) were the first to implement a Prandtl-type boundary layer in the study of steady ice drift. Their aim was to develop a quantitative theory relating the eddy-viscosity coefficient¹ to the physical parameters of the layer. Then, Shuleikin (1938) was able to complete a model of ice in the *free drift* regime, i.e. a regime in which internal stresses are neglected.

Subsequent empirical studies performed by Soviet scientists, notably Zubov, Somov and Gordienko, were key to more accurately clarify the relation between wind and drift. For instance, Zubov (1945) contributed with the development of some semi-empirical modifications of Nansen-Ekman drift law previously derived, and of the isobaric drift law among other things. With the introduction of the ice conservation law (Nikiforov, 1957) and with the first attempts to gain a more quantitative knowledge of ice internal resistance through a rheological equation (Laikhtman, 1958; Ruzin, 1959; Reed and Campbell, 1960) the ice dynamics problem reached a critical turning point.

¹In ocean dynamics, large-scale turbulent stresses have a first-order approximation as linear viscous stresses (see Equation 3.10), with the “viscosity” then called eddy viscosity (e.g. Gill, 1982).

3.1.1 Equilibrium drift theories

As in most situations ice accelerations are negligible, the great bulk of early research on sea ice dynamics has been concerned with equilibrium, or steady-state, drift theories. Analytical solutions to the steady-state motion of ice may be derived in many cases by algebraic means, while the general accelerated problem requires numerical integration of systems of non-linear differential equations (Reed and Campbell, 1960).

For the matter of this section, the most general steady-state momentum equation considered reads (Campbell, 1965):

$$\boldsymbol{\tau}_a + \boldsymbol{\tau}_w - \rho h f_c \hat{\mathbf{k}} \times \mathbf{u} - \rho h g \nabla H + \mathbf{F}_{\text{int}} = \mathbf{0} \quad (3.1)$$

where all the physical quantities had been defined when discussing the momentum equation (Equation 2.31) in Section 2.5. In Equation 3.1 we see that the internal force has not been explicitly written in terms of internal stress divergence (see Equation 2.30). At this early research stage, indeed, the lack of information about how internal stress was transmitted through drift ice forced sea ice scientists to enclose all the information about the internal resistance of ice into a term, \mathbf{F}_{int} , whose form was then prescribed. The first attempts, relating ice internal force to its drift velocity (e.g. Sverdrup, 1928), were source of misunderstanding since ice stress is actually linked to relative movement of the material, i.e. strain or strain-rate (Rothrock, 1975b).

Because of the lack of computational power at the time, it was almost impossible to numerically solve sea ice models. Various authors addressed the problem and developed equilibrium theories making different assumptions on which terms to retain from Equation 3.1.

What follows is a presentation of the main developments in sea ice steady-state modelling up to the 1960s (Campbell, 1965). All the force-balance diagrams are assumed to be located in the Northern Hemisphere, where $f_c > 0$.

Nansen (1902) neglected ice stress and the pressure gradient force due to the sea surface tilt reducing Equation 3.1 to:

$$\boldsymbol{\tau}_a + \boldsymbol{\tau}_w - \rho h f_c \mathbf{k} \times \mathbf{u} = \mathbf{0} \quad (3.2)$$

where the wind and ocean stress were parametrized as follows:

$$\boldsymbol{\tau}_{a,w} = \frac{\|\boldsymbol{\tau}_{a,w}\|}{\|\mathbf{u}_{a,w} - \mathbf{u}\|} \begin{bmatrix} \cos \theta_{a,w} & \sin \theta_{a,w} \\ -\sin \theta_{a,w} & \cos \theta_{a,w} \end{bmatrix} (\mathbf{u}_{a,w} - \mathbf{u}) \quad (3.3)$$

with $\mathbf{u}_{a,w}$ the main flow velocity and $\theta_{a,w}$ the air/water turning angle between the main flow and the surface stress (see Section 2.6). In his model the Ekman spiral² starts directly below the ice-water interface. I.e. the Ekman spiral in the ocean is assumed to be similar to the case in which no sea ice is present. Figure 3.1 shows the balance of force in Nansen (1902). This approach turned out to overestimate the angle between the wind stress $\boldsymbol{\tau}_a$ and the ice velocity \mathbf{u} . To fit the observations Nansen (1902) tried to add a wind-independent gradient current, similar to the term $-\rho h g \nabla H$ in Equation 3.1, to the description. However, this addition did not successfully describe correctly newly-available drift data.

²In the context of the Ekman transport, this phenomenon occurs as a consequence of the Coriolis effect. As the wind applies a shear stress on the Ocean's water, the latter's surface starts moving but the Coriolis forces a deflection to the right in the Northern Hemisphere and on the left in the Southern Hemisphere. This deflection is then transmitted from the surface to deeper layers of the ocean. As a result, the velocity-depth profile assumes a spiraling pattern.

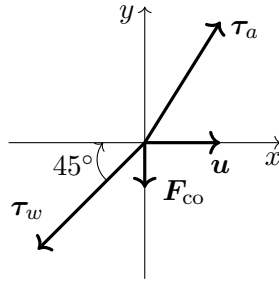


FIGURE 3.1: Balance of forces in Nansen (1902) according to Equation 3.2. Because of the Ekman layer starting at the sea surface, τ_w forms a 45° angle with the surface velocity \mathbf{u}_0 , which is in the same direction as the ice velocity \mathbf{u} . \mathbf{F}_{co} represents the Coriolis force.

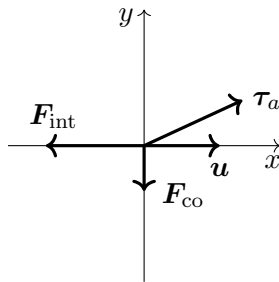


FIGURE 3.2: Force diagram in Sverdrup (1928) model.

Sverdrup (1928) proposed an equilibrium drift theory that neglected the pressure gradient force and the water stress:

$$\tau_a - \rho h f_c \hat{\mathbf{k}} \times \mathbf{u} + \mathbf{F}_{\text{int}} = \mathbf{0} \quad (3.4)$$

where he considered the internal force to be linearly related to the drift velocity through $\mathbf{F}_{\text{int}} = -k\rho\mathbf{u}$, where k is a friction coefficient. As outlined earlier such an approach has no real physical basis and it is appropriate for the expression of the friction between a moving object and a stationary object (Rothrock, 1975b). The balance of forces is shown in Figure 3.2. Sverdrup's theory was successful with data from the North-Siberian shelf but failed within other regions (Campbell, 1965).

Rosby and Montgomery (1935) developed three different theories to study sea ice. In the first theory, ice was assumed to be a two-dimensional internal stress-free plate with negligible thickness, hence with a negligible Coriolis contribution to the motion. Consequently, Equation 3.1 reads:

$$\tau_a + \tau_w = \mathbf{0}. \quad (3.5)$$

This theory was the first to include a Prandtl boundary layer (Prandtl, 1905) beneath the ice. Albeit furnishing results well in agreement with air stress and ice velocity values in the study region of the Weddell Sea, their solution underestimated the angle between ice drift and wind velocity (see Figure 3.3a). This first attempt was followed by an extension of the previous theory to include Coriolis force and a Sverdrup type of internal force with a general equilibrium equation of the form:

$$\tau_a + \tau_w - \rho h f_c \mathbf{k} \times \mathbf{u} - k\rho\mathbf{u} = \mathbf{0} \quad (3.6)$$

Although in good agreement with observations from the Weddell Sea, predictions from

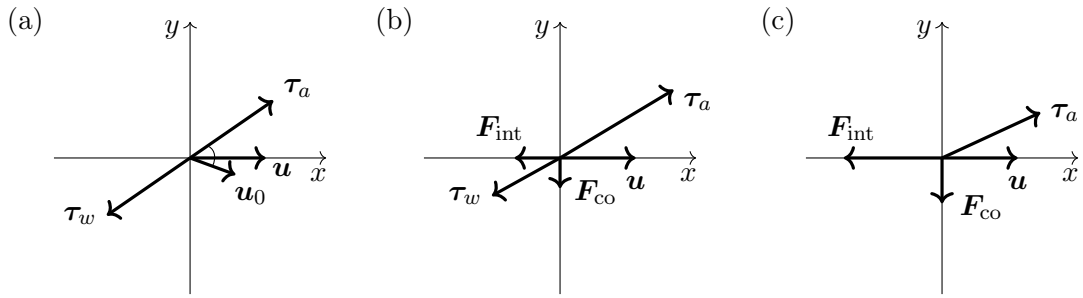


FIGURE 3.3: Balance of forces in the three equilibrium-drift theories developed in Rossby and Montgomery (1935). Figure (a) shows the stress and Coriolis-free case (Equation 3.5). \mathbf{u}_0 indicates the ocean's surface velocity. The highlighted angle was calculated to be around 54° . Fig. (b) shows the extended model where Coriolis force was included (Equation 3.6). Eventually, when water drag is neglected the balance diagram is like the one in Fig. (c).

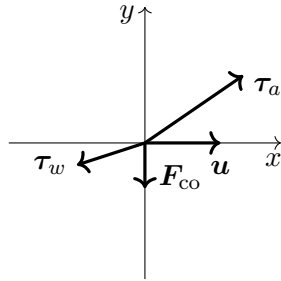


FIGURE 3.4: The figure shows the force balance in Shuleikin (1938) theory. The water stress form an angle of 18° with the drift direction.

Equation 3.6 were found to deviate from observations collected from the North-Siberian shelf (Campbell, 1965). Consequently, Rossby and Montgomery (1935) water stress was put aside and an equation like 3.4 was employed. The force balance diagram for these two latter two theories is shown in Figure 3.3b and Figure 3.3c, respectively. This theory successfully fitted summer data characterized by a strong stability of the surface waters, but failed with winter data when neutral stability conditions were approached (Campbell, 1965).

Shuleikin (1938) proposed a solution of Equation 3.2 with a constant angle between the water drag and the surface drift velocity. In order to close the solution to the problem, a relationship between the ocean surface velocity \mathbf{u}_0 and the wind flow velocity \mathbf{u}_a was needed. Shuleikin (1938) made use of the following empirical expression derived by Ekman on the basis of Mohn and Nansen³:

$$\frac{\|\mathbf{u}_0\|}{\|\mathbf{u}_a\|} = \frac{0.0127}{\sqrt{\sin \phi}}. \quad (3.7)$$

It can be shown that this formulation yields a turning angle $\theta = 18^\circ$ in Equation 3.3 (see Figure 3.4). This is contrast to $\theta = 45^\circ$ expected from Ekman's theory (Ekman, 1902). Results were in agreement with selected drift segments data coming from the first Arctic Ocean drift station, North Pole 1, landed by the Soviet Union in 1937. Shuleikin work was critical to show the importance of the boundary layer.

³Eq. 3.7 was derived in open water conditions with a different turbulent regime than under the ice sheet.

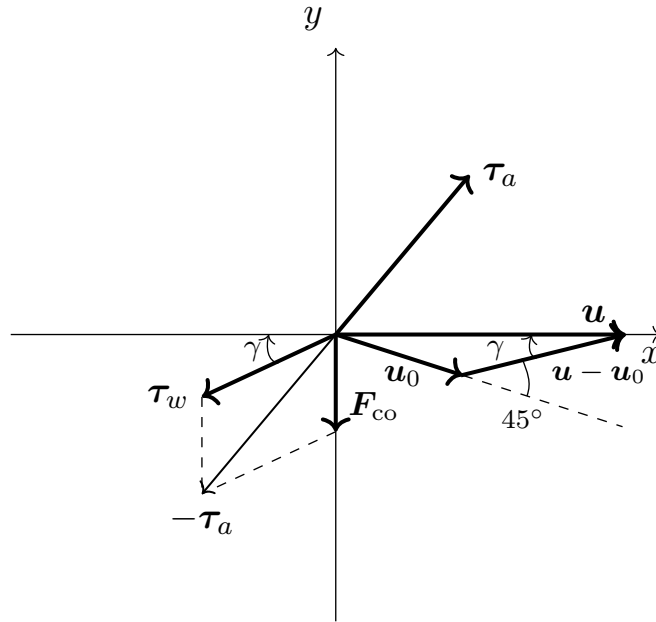


FIGURE 3.5: Force diagram in Reed and Campbell (1960) equilibrium theory. The velocity \mathbf{u}_0 is the current velocity at the interface between the boundary layer and the deeper layer in which the Ekman spiral is assumed to prevail.

Felzenbaum (1958) proposed yet another steady-state model where the pressure gradient force, derived from a simple ocean model in which density and eddy viscosity are uniform. He considered wind and water stress forces on the ice, along with Coriolis force, though in a form independent of latitude, while neglecting any large scale resistance to strain within the ice cover. His study was also important because he stressed on the fact that ice flow needs to be studied in relation to the whole ice cover and on the importance of considering sea as a dynamic unit (Campbell, 1965).

Reed and Campbell (1960) studied the equilibrium drift of an isolated floe of ice following the path traced by Shuleikin (1938). In their work, they first replaced the contribution of internal ice force \mathbf{F}_{int} with wind and water pressure acting on the exposed vertical edges of the floe. They reasoned that, since the integrated stress over the horizontal faces of the floe increases with the square of the radius while the side pressure increase only with the radius itself, the latter could be neglected by taking a sufficiently large floe. Therefore they ended up analytically solving Equation 3.2. They did this purely on theoretical grounds without resorting to the empirical expression of Equation 3.7. In particular, to close the system of equations they derived a theoretical relationship:

$$\|\mathbf{u}_0\| = B(\|\mathbf{u}\| - \|\mathbf{u}_0\|)^{3/2} \quad (3.8)$$

where B depends on the physical quantities of the boundary layer. The balance of forces is shown in Figure 3.5. In Reed and Campbell (1960) the authors collected data from the drift ice station Alpha, historically the first non-Soviet floe-station established and maintained by a Western country (Cabaniss et al., 1965). Their main conclusion was that the pressure gradient force due to a dynamic change in the sea elevation and the internal ice stress play a key role in the dynamics of the ice cover and cannot be neglected.

This conclusion served as the main impetus for the development of the first rheology-based models which were just getting underway at that time.

3.2 Viscous and Plastic Rheologies

In this section we will take a first look into rheologies employed in continuum sea ice models. We can take as an axiom that any real material, sea ice included, possesses all the rheological properties (Mellor, 1986). However, developing a model taking into considerations all of them is not, in practice, feasible. As a result, the modeler has to evaluate the significance of each rheological property by studying the material response over a wide range of temporal/spatial scales and in multiple stress-strain configurations. Historically, a hierarchy of models ranging from simple to complex can be discerned. Here the complexity of a model is determined by the number of aforementioned processes included and the degree of nonlinearity of the stress-strain rate relationship (Mellor, 1986).

An apt sea ice rheology is one that is able to display the main physical features of sea ice: weakness in tension, mild strength in shear and largest strength in compression. In particular, strain hardening is observed in compression and softening or instability in pure shear. Furthermore, it should reflect the observations that stresses are constrained to specific range (Rothrock, 1975b).

Note on the chosen convention in the formulation of a rheology

In this work, unlike in most of the sea ice dynamics literature, we formulate the rheologies in terms of the horizontal two-dimensional stress, $\boldsymbol{\sigma}$, given by Equation 2.11 rather than in terms of the vertically integrated stress, $\boldsymbol{\sigma}_{\text{ice}}$. The motivation for stating the laws in terms of $\boldsymbol{\sigma}$ lies in the more apparent physical meaning of the two-dimensional stress tensor, possessing the unit of a pressure. In addition to that, in brittle-based rheologies, presented in Chapter 4, this allows a direct comparison between the local state of stress and the critical stresses ($\sigma_{N,\text{max}}, \sigma_{T,\text{max}}$; see Section 4.2.3) when estimating how far the stress state is from the failure envelope.

The relationship between rheological parameters appearing in the constitutive equations hereafter and the ones in the $\boldsymbol{\sigma}_{\text{ice}}$ -formulated version are consistent with $\boldsymbol{\sigma}_{\text{ice}} = \boldsymbol{\sigma} \hat{h}$, where \hat{h} is the mean sea ice thickness (see Equation 2.16).

3.2.1 Viscous rheologies

When ice is assumed to act as a fluid in response to stress, a fluid-like constitutive law of the form $\boldsymbol{\sigma} = \boldsymbol{\sigma}(\mathcal{J}, \dot{\boldsymbol{\epsilon}})$ is employed. The Reiner-Rivlin fluid model provides a general viscous model applicable to sea ice (e.g. Hunter, 1983):

$$\boldsymbol{\sigma} = \alpha \mathbf{I} + \beta \dot{\boldsymbol{\epsilon}} + \gamma \dot{\boldsymbol{\epsilon}}^2 \quad (3.9)$$

where the last quadratic term (matrix multiplication is implied) is generally neglected in sea ice modeling. The coefficients α , β , γ may depend on the material properties, \mathcal{J} and on the strain-rate invariants, $\dot{\epsilon}_{\text{I}}, \dot{\epsilon}_{\text{II}}$.

Linear viscous model

Although too crude for a realistic representation of sea ice mechanical behavior by themselves, viscous laws were the first class of applied sea ice rheologies. The first and simplest approach was to consider ice as a highly viscous Newtonian fluid. I.e. it was assumed to possess a constitutive equation of the form (Laikhtman, 1958; Ruzin, 1959; Campbell, 1965):

$$\boldsymbol{\sigma} = 2\eta \dot{\boldsymbol{\epsilon}}' \quad (3.10)$$

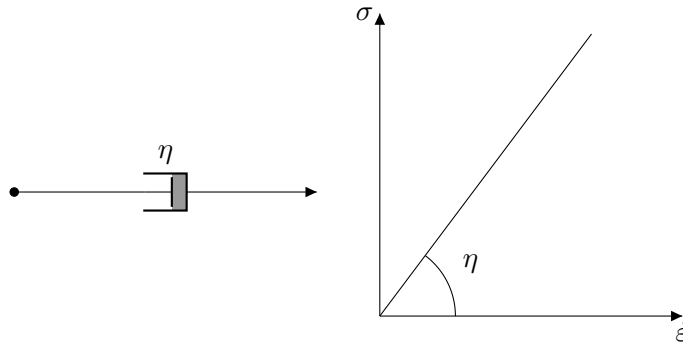


FIGURE 3.6: One-dimensional illustration of the linear-viscous response. The mechanical analog is the dashpot model. The stress is directly proportional to the strain-rate.

where η is the shear (linear) viscosity and $\dot{\boldsymbol{\epsilon}}'$ is the deviatoric part of the strain rate (see Section 2.2.1). In this simple model, the stresses are along on the σ_{II} -axis and consequently convergence is unopposed. Typical values of viscosity are in the range $10^8 - 10^{12} \text{ kg } \hat{h}^{-1} \text{ s}^{-1}$ (e.g. Campbell, 1965), where \hat{h} is the mean ice thickness (Equation 2.16). The 1D mechanical analogue of linear viscosity is given by a dashpot (see Figure 3.6). When ice is modeled as an incompressible Newtonian fluid governed by Equation 3.10 then the internal force, \mathbf{F}_{int} , in the momentum equation 2.31 is simply given by $\hat{h}\eta\nabla^2\mathbf{u}$.

A more general, yet still linear, model is given by (Hibler, 1974; Campbell and Rasmussen, 1972):

$$\boldsymbol{\sigma} = \zeta \text{tr } \dot{\boldsymbol{\epsilon}} \mathbf{I} + 2\eta \dot{\boldsymbol{\epsilon}}' \quad (3.11)$$

where the bulk viscosity ζ has been introduced. In order to better fit data, Campbell and Rasmussen (1972) and Rothrock (1975b) proposed a version of Equations 3.11, 3.10 with stepwise viscosities, smaller in diverging flows and larger in converging ones. This supports the observed resistance of ice against convergence and absence of it against tension. In the case of constant viscosities, $\mathbf{F}_{\text{int}} = \hat{h}\zeta\nabla(\nabla \cdot \mathbf{u}) + \hat{h}\eta\nabla^2\mathbf{u}$.

Another linear modeling approach consisted in considering a pressure term in the rheology active only during convergence. For instance, Kheisin and Ivchenko (1973) added such a term, $-p_s\mathbf{I}$, to Equation 3.10 where $p_s = k\delta A$ for $\delta A > 0$ and null otherwise, with δA small compactness variations and k the elastic bulk modulus, effectively developing a linear viscoelastic model, e.g. the linear Maxwell model in Section 4.3.2.

Linear viscous models can satisfy realistic boundary conditions and provide first-order approximation for basin-wide ice circulation (Leppäranta, 2011).

Nonlinear viscous model

The general form of a isotropic, homogeneous nonlinear viscous law reads (Glen, 1970)

$$\boldsymbol{\sigma} = (-p + \zeta \text{tr } \dot{\boldsymbol{\epsilon}}) \mathbf{I} + 2\eta \dot{\boldsymbol{\epsilon}}' \quad (3.12)$$

with $\zeta = \zeta(\mathcal{J}, \dot{\boldsymbol{\epsilon}}_{\text{I}}, \dot{\boldsymbol{\epsilon}}_{\text{II}})$, $\eta = \eta(\mathcal{J}, \dot{\boldsymbol{\epsilon}}_{\text{I}}, \dot{\boldsymbol{\epsilon}}_{\text{II}})$ and $p = p(\mathcal{J})$ to account for (vertically-averaged) hydrostatic pressure (Leppäranta, 2011).

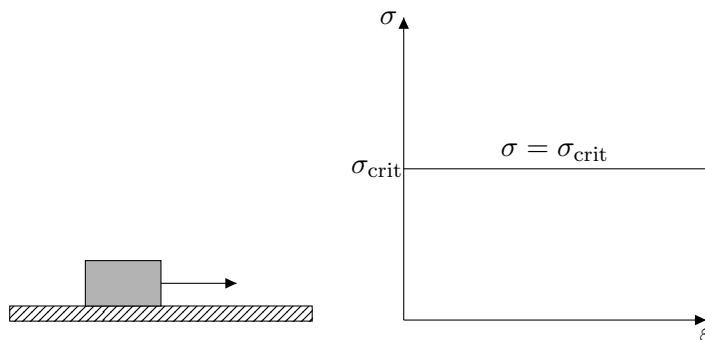


FIGURE 3.7: One-dimensional illustration of the rigid-plastic response. The mechanical analog is the dry friction of a block. From this simple model it is not possible to determine any functional relation between σ and ε for $\sigma < \sigma_{\text{crit}}$.

3.2.2 Plastic rheologies

Rationale behind a plastic model of sea ice

The adoption of a plastic rheology finds its strongest argument in the mechanical behavior of compact ice. In fact, despite relatively smooth variations in atmospheric and oceanic forcing fields, local events such as ridging and formation of leads occur sporadically and irreversibly, as though a critical stress state in the ice had been reached (Feltham, 2008).

Another argument in favor from rate-independent plastic theory was presented by Parmeter and Coon (1973) and Rothrock (1975a). They developed a kinematic model of ridging and showed that the shape of a pressure ridge and the loss of kinetic energy in the process are independent of the rate of formation. The rate independence of deformation is an important feature of ideal plastic behavior.

Lastly, observations of sea ice appearance and deformation suggest the analogy with granular mediums, e.g. soils. For these media, the plastic modeling approach has been shown to be successful (Schofield and Wroth, 1968).

A rigid-plastic model is unsatisfactory in that it does not allow for subcritical stresses to be calculated and thus leaves the subcritical rheological response undetermined. Therefore, in sea ice modeling, approximations of ideal plastic laws are used, prescribing simple subyield models. In the following, two plastic rheologies with different subyield behaviors, linear elastic (see Figure 3.8) and linear viscous (see Figure 3.6), respectively, are presented.

The yield curve and plastic flow

A material is said to possess a plastic behavior if it has the property of retaining a new shape even upon removal of forces of appropriate magnitude and direction (Lubliner, 2008). Ideal plasticity or rigid-plastic behavior is a simple rheological model in which there is no strain until a critical yield stress is reached. In 1D this is modeled by a block experiencing dry friction, i.e. which begins to move only when a strong enough forcing is applied (see Figure 3.7). The strong limitation of a rigid-plastic model is that it does not allow subcritical stresses to be calculated.

The general approach to model the plastic response of an ideal (i.e. rate-independent) plasticity theory is to postulate the existence of a yield criterion defining whether a stress state is critical, causing plastic deformation, subcritical, causing small deformation, or supercritical, causing the material's rupture. The yield criterion defines a region in the space spanned by the stresses that is bounded by a convex surface. This surface is referred

to as the *yield surface* (Phillips and Sierakowski, 1965) and can depend on the scalar parameters contained in the ice state \mathcal{J} . The allowed material's states are the ones lying on or inside the yield surface with the ones outside are unphysical.

A general, implicit, formulation of the yield criterion in a two-dimensional isotropic model is given by (Feltham, 2008)⁴

$$F(\sigma_I, \sigma_{II}; \mathcal{J}) = 0 \quad (3.13)$$

where F is the yield function, symmetric about the σ_I axis (Truesdell and Noll, 2004). Equation 3.13 defines a family of yield curves, parametrized by variations of the scalar properties of the ice. In plastic models of sea ice the approximation of a null tensile strength is normally employed. I.e. for all points on the yield curve $\sigma_{II} \leq 0$. In addition to that, to display a stronger resistance to compression rather than to shear, the yield curve must have a shape elongate in the σ_I axis.

Once the stress is on the yield curve, however, how the material deforms (plastically) remains to be specified. The flow must be such that the stress state keeps lying on the yield curve. The missing piece of information is given by the so-called *flow-rule* which allows strains to be calculated. Many theories employ Drucker's postulate: plastic flow is given by the solution that maximizes the rate at which plastic work is dissipated (Drucker, 1950). Its widespread use in sea ice plastic models is perhaps linked to its successful application to granular mechanics (Feltham, 2008).

The determination of the plastic yield curve has generally followed two main approaches (Feltham, 2008):

- a) By evaluation of the energetic budget of the subcontinuum-scale deformation (e.g. Rothrock, 1975a; Ukita and Moritz, 1995);
- b) By imposition of a scale-invariant Mohr-Coulomb rheology (e.g. Coon, 1974; Hibler and Schulson, 2000).

The methodology in a) is taken by mean-field or scale-dependent rheologies⁵ while b) by scale-invariant rheologies. In the context of approach a) and building on the developments in ridging modeling by Parmeter and Coon (1973), Rothrock (1975a) considered pressure ridges as the main sink of energy in the ice cover. By equating the plastic work of deformation to the gravitational potential energy due to the ridge creation plus the associated frictional loss in the formation he suggested two possible yield curve for the elastic-plastic model shapes: a teardrop shape and a lens shape. Ukita and Moritz (1995) also found the teardrop shape to be appropriate by extending Rothrock (1975a) reasoning with an energy sink due to the sliding motion of floes parallel to cracks. The teardrop and lens-shaped curves have been implemented by Zhang and Rothrock (2005) and have recently been suggested as a valid alternative to the standard elliptical curve for a high-resolution viscous-plastic rheological framework (Ringey et al., 2023). As for approach b), Pritchard (1977) found a wedge-shaped yield curve to be more appropriate for an elastic-plastic model. A Mohr-Coulomb (triangular) yield curve, usually applied in granular media mechanics (e.g. Tremblay and Mysak, 1997), was implemented by Coon (1974) in a ideal plastic model and by Hibler and Schulson (2000) in an anisotropic viscous-plastic model.

⁴The yield criterion can be equally written in terms of the invariants σ_1, σ_2 .

⁵The elastic-plastic rheology Coon et al. (1974) and the viscous-plastic rheology of Hibler (1979) both rely on this assumption.

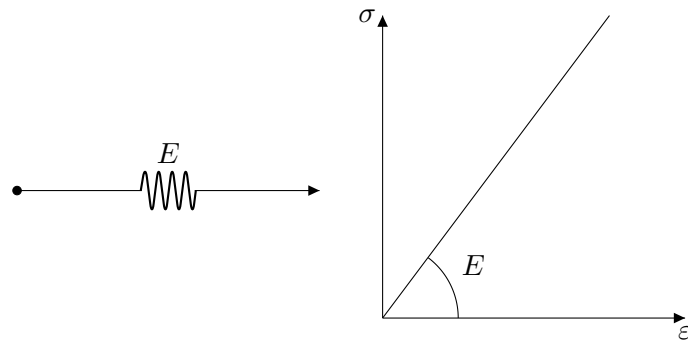


FIGURE 3.8: One-dimensional illustration of the linear elastic response. The mechanical analog is a dashpot. The stress is directly proportional to the strain through the elastic modulus E .

Elastic-plastic rheology (EP)

The elastic-plastic rheology (EP) arises when elastic subcritical behavior is coupled to a plastic law. The stress-strain relationship for such a model is shown in Figure 3.9. This approach was first taken by Coon et al. (1974) in the so-called AIDJEX model (see Section 3.3). They reasoned that for small deformations the stress-strain relationship is dominated by the elastic deformation of the thicker ice floats, while larger deformations also permanently rearrange thinner ice between them.

In postulating a material response, it is important to choose properly the reference configuration from which strain will be measured. In other words, a coordinate frame needs to be defined in which the strain is zero and with respect to which strain is measured. The choice of reference configuration is a constitutive assumption (Pritchard, 1974). However, in a fluid-like approach, ice is considered as material that has no permanent memory for any particular state (Truesdell and Noll, 2004) therefore no preferred configuration exists. In the AIDJEX model, elastic strains are evaluated with respect to a reference configuration evolving according to the plastic flow (Pritchard, 1975). It is commonly posed in plasticity theory that the strain rate, $\dot{\epsilon}$, is the sum of an elastic part, $\dot{\epsilon}_E$, and a plastic part, $\dot{\epsilon}_p$.

The EP constitutive model is given by the law of linear elasticity for an isotropic continuum, i.e. Hooke's law. In tensor form this reads

$$\boldsymbol{\sigma} = E\mathbf{K} : \boldsymbol{\epsilon} \quad (3.14)$$

where E is the elastic (Young) modulus and \mathbf{K} is the adimensional elastic stiffness tensor whose action on a generic symmetric tensor $\boldsymbol{\epsilon}$ is defined by

$$\mathbf{K} : \boldsymbol{\epsilon} = \frac{\nu}{(1+\nu)(1-2\nu)} \text{tr} \boldsymbol{\epsilon} \mathbf{I} + 2\frac{1}{2(1+\nu)} \boldsymbol{\epsilon} \quad (3.15)$$

ν being Poisson's ratio. An isotropic linear elastic material is always characterized by two independent elastic constants (Timoshenko and Goodier, 1951). Usually employed elastic constants are the adimensional (i.e. normalized by E) Lamé parameters

$$\Lambda = \frac{\nu}{(1+\nu)(1-2\nu)}, \quad G = \frac{1}{2(1+\nu)} \quad (3.16)$$

and the (adimensional) bulk modulus K and shear modulus G (corresponding to the second Lamé parameter), with $K = \Lambda + \frac{2}{3}G$.

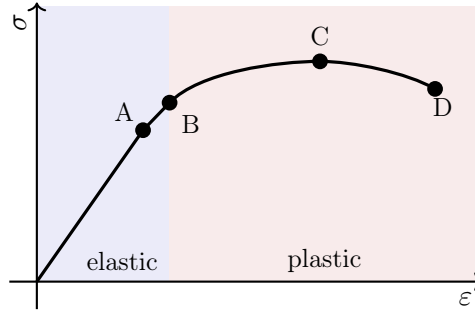


FIGURE 3.9: Typical 1D stress-strain diagram in tension for an elastic-plastic sea ice. The points in the figure have the following meaning: (A) is the elastic limit point, i.e. when the relation between σ and ε ceases to be linear, (B) is the yield strength, (C) the ultimate tensile strength and (D) the rupture point.

Usually, the time derivative of both sides of Equation 3.14 is taken in order to have a formulation in terms that can be evaluated directly from the velocity gradient (Pritchard, 1975). So, in terms of the rate-of-deformation tensor Equation 3.14 reads

$$\frac{D\boldsymbol{\sigma}}{Dt} = E[\text{Atr } \dot{\boldsymbol{\varepsilon}}(\mathbf{u}) \mathbf{I} + 2G\dot{\boldsymbol{\varepsilon}}(\mathbf{u})]. \quad (3.17)$$

Originally, Coon et al. (1974) stated the AIDJEX constitutive model in terms of the bulk and shear moduli and considered only compressive stresses to be allowed in the linear subcritical regime ($\boldsymbol{\sigma} = \mathbf{0}, \varepsilon_{E,I} \geq 0$). For ice with an average thickness $\hat{h} \approx 1$ m typical values of the dimensional (i.e. multiplied by E) bulk and shear moduli are $K = 10^7$ Pa, $G \approx \frac{1}{2}K$ (Leppäranta 2011; Coon and Pritchard 1974). The yield compressive strength P^* is around 10^5 Pa (Pritchard, 1980). These constants are one to two orders of magnitude larger at the smaller scales (Mellor, 1986). The yield curve is parametrized by the compressive strength P^* , which depends on the thickness distribution g (see Section 2.3.1) and on ice concentration A . The AIDJEX model employed a teardrop-shaped yield curve. Coon et al. (1974) chose the plastic flow to follow the associated or normal flow rule (Drucker, 1950):

$$\dot{\varepsilon}_I^p = \kappa \frac{\partial F}{\partial \sigma_I} \quad \dot{\varepsilon}_{II}^p = \kappa \frac{\partial F}{\partial \sigma_{II}} \quad (3.18)$$

where κ is a positive scalar determined as part of the solution to the dynamical equations and $\dot{\boldsymbol{\varepsilon}}^p$ is the plastic part of the strain rate, perpendicular to the yield curve.

Viscous-plastic rheology (VP)

A viscous-plastic (VP) sea ice rheological model was proposed by Hibler (1979). The physics remains essentially the same of the AIDJEX EP model by Coon et al. (1974), but a linear viscous response substitutes the linear elastic one. Nevertheless, there is a difference in how the EP and the VP rheology models compact ice subject to a high level of stress persisting over an extended period of time. The EP rheology allows stationary states with (almost) no relative motion to exist while the VP approximates these states as subject to a very slow, but nonzero, deformation, a phenomenon known as viscoplastic creep (Duval et al., 1983). Another benefit from using a viscous law over an elastic one is the fact that it is not necessary to keep track of an evolving stress-free configuration, unlike in the EP (Pritchard, 1975). I.e. in the EP model stress is a prognostic variable

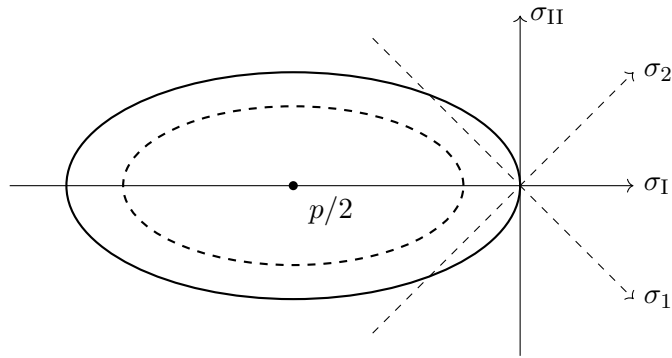


FIGURE 3.10: Elliptical yield curve used in the VP model. The concentric ellipse (dashed-lined) inside the yield curve represents the limiting curve in correspondence of upper bounds values for ζ and η (Hibler, 1977).

that has to be saved into memory, while in the VP model it is a diagnostic variable that can be calculated directly from the strain-rate field.

VP rheology follows from the assumption that the sea ice can be represented as the motion of floes randomly experiencing perfectly plastic interactions with each other averaged over sufficiently long time scales ($\gtrsim 1$ day). More specifically, Hibler (1977) demonstrated that if the floe interaction follow a rigid-plastic model with an elliptical yield curve, the resulting stress averaged over all interactions is the combination of a viscous term and an additional pressure term

$$\boldsymbol{\sigma} = 2\eta\dot{\boldsymbol{\epsilon}} + [\zeta - \eta]\text{tr}\dot{\boldsymbol{\epsilon}}\mathbf{I} - \frac{P}{2}\mathbf{I}. \quad (3.19)$$

Here $P/2$ is a pressure term, with P the ice strength and ζ, η are the bulk and shear viscosity, respectively, defined in Section 3.2.1.

If an elliptic yield curve

$$F(\sigma_I, \sigma_{II}, P) = \left(\frac{\sigma_I + P}{P}\right)^2 + \left(\frac{\sigma_{II}}{P}e\right)^2 - 1 = 0 \quad (3.20)$$

and a normal flow rule is assumed (see also figure 3.10) it is possible to obtain explicit expressions for ζ and η can be obtained (Hibler, 1977):

$$\zeta = \frac{P}{2\Delta}, \quad \eta = \frac{P}{4\Delta e^2} \quad (3.21)$$

such that the stress stays on the yield curve. Here

$$\Delta = \sqrt{(\dot{\epsilon}_{11}^2 + \dot{\epsilon}_{22}^2)(1 + e^{-2}) + 4e^{-2}\dot{\epsilon}_{12}^2 + 2\dot{\epsilon}_{11}\dot{\epsilon}_{22}(1 - e^{-2})}. \quad (3.22)$$

and e is the eccentricity of the ellipse, constituting a parameter of the rheology.

The VP rheology is closed by specifying an equation of state for the ice strength. Hibler (1979) used:

$$P = P^*\hat{h} \exp[-c^*(1 - A)] \quad (3.23)$$

where \hat{h} is the mean ice thickness⁶, and c^* is a (positive) compaction parameter, characterizing the strength reduction for lead opening.

⁶Hibler used a simple ice-open water model, so the mean ice thickness is exactly equal to $\hat{h}_{\text{thick}}A$.

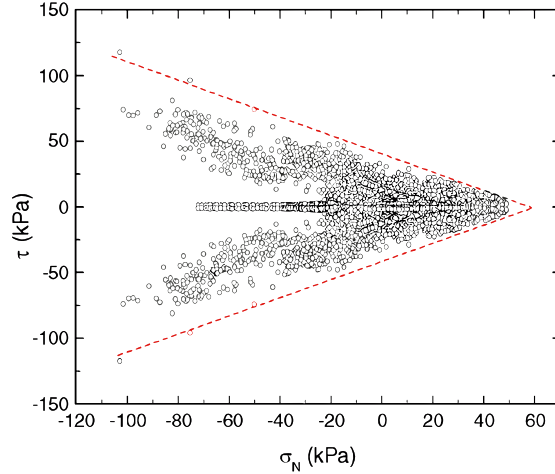


FIGURE 3.11: Stress states recorded during the SHEBA experiment in the Beaufort sea at one sensor, from mid-October, 1997, to end of June, 1998 (1 measure per hour). The figure is a plot in the shear versus normal stress space of $|\tau| = -\mu\sigma_N + C$ with $C = 40$ kPa and $\mu = 0.7$. Taken from Weiss et al. (2007).

Mohr-Coulomb failure

Another approach in the plastic modeling of sea ice has been to use Mohr-Coulomb fracture theory (Coulomb, 1776) to determine the point ice fails plastically. The idea is to assert a scale-invariant yield curve based on the idea of shear fracture or frictional sliding along flaws (Feltham, 2008). This is supported by the evident self-similarity (see Section 4.1.2) of fragmented and deformed sea ice on a wide range of scales (e.g. Rothrock and Thorndike, 1984; Weiss and Marsan, 2004; Matsushita, 1985) and by its granular deformation behavior. Erlingsson (1988) and Weiss and Schulson (2009) are example of studies where Coulombic faulting was observed to happen at both the micro (grain)-scale and the geophysical scale, with a scale-invariant (to a good approximation) angle of internal friction between the floes. Studies have shown that ice stress remains in an envelope resembling the Mohr-Coulomb form (see Figure 3.11; Weiss et al. 2007; Richter-Menge et al. 2002). If we consider a surface with unit normal \mathbf{n} in the sea ice horizontal plane, the traction exerted on a line with tangent unit vector \mathbf{t} is, by definition,

$$\boldsymbol{\sigma} \cdot \mathbf{n} = \sigma_N \mathbf{n} + \tau \mathbf{t} \quad (3.24)$$

where σ_N (Equation 2.13) and τ (Equation 2.14) are two invariants of $\boldsymbol{\sigma}$ respectively representing the normal stress across the line and the shear stress along it. The relationship between the normal and shear stresses and the other invariants σ_I, σ_{II} implicitly defines the Mohr circle in the $\{\sigma_N, \tau\}$ plane:

$$\tau^2 + (\sigma_N + \sigma_I)^2 = \sigma_{II}^2. \quad (3.25)$$

In a Mohr-Coulomb fracture theory, the failure criterion has a general form given by Mohr's law (e.g. Feltham, 2008):

$$|\tau| = \Omega(\sigma_N; \mathcal{J}). \quad (3.26)$$

Equation 3.26 states that the material fails when a certain shear stress-normal stress is reached. In practice, however, a simple form for Ω is chosen, giving rise to the Mohr-Coulomb shear stress criterion⁷ (Coulomb, 1776):

$$|\tau| = -\mu\sigma_N + C \quad (3.27)$$

where $\mu > 0$ is an internal friction coefficient (related to the angle of internal friction between the floes Θ through $\mu = \tan \Theta$ (constant) and C is the cohesion, i.e. inherent shear strength. Equation 3.27 defines a wedged-shaped yield curve, commonly referred to as Mohr-Coulomb envelope.

Coon (1974) proposed the first plastic sea ice rheological model assuming a Mohr-Coulomb criterion, namely of the form of Equation 3.27 with $\Theta = 35^\circ$ and $C = 0$.

The criteria described in this section will be widely employed in Chapter 4, when discussing the brittle-based rheological frameworks.

3.3 A summary of rheology-based sea ice dynamics up to the current state

The concept of a large-scale ice rheology to describe floe interaction mechanisms was first introduced in the works by Laikhtman (1958), Ruzin (1959) and Reed and Campbell (1960). There, the ice cover was treated like a thin film of Newtonian viscous fluid characterized by a uniform eddy viscosity. Viscous rheologies were employed through the 1960s to model the mechanical behavior of sea ice (e.g. Campbell, 1965; Doronin, 1970; Rothrock, 1970; Solomon, 1970; Glen, 1970).

A great advancement in sea ice dynamics understanding was made thanks to the Arctic Ice Dynamics Joint Experiment (AIDJEX) which took place between 1970 and 1978 (Untersteiner et al., 2007). The aim of the experiment was to gather a substantial amount of observations relating ice deformation to the external stress fields. Among the main achievements of the AIDJEX program, we find the introduction of elastic-plastic rheology (EP; Coon et al. 1974), in which a plastic failure law to model compact ice behavior was used, and the concept of ice thickness distribution (Thorndike et al., 1975). However, some of the underlying assumptions concerning ice mechanical behavior were later revised and found inadequate (Coon et al., 2007).

A step forward in sea ice dynamics research was moved with the viscous-plastic model (VP) by Hibler (1979). This is a two-categories model where ice is assumed to deform in a viscous manner with a high viscosity up to a plastic threshold. The yield curve in the stress plane was chosen to have elliptic shape.

Various improvements have been made to the original VP rheology, but the physical principles remain the same (Ólason et al. 2022; e.g. VP with JNKF in Lemieux et al. 2010). The elastic-viscous-plastic rheology (EVP; Hunke and Dukowicz 1997) was developed to address numerical issues related to the VP. Even in this case, several works continue to be aimed at improving the numerical efficiency of the EVP (e.g. Kimmritz et al. 2016, mEVP in Bouillon et al. 2013).

Virtually all current operational modeling platforms, whether assimilating data or not, and IPCC global coupled climate models including sea ice dynamics (e.g. the Coupled Model Intercomparison Project Phase 6, Notz and Community, 2020) use the VP or EVP rheological frameworks. For instance, the Los Alamos sea ice model (CICE) employs a revised version of the EVP rheology (Hunke et al., 2017). Despite its widespread use, the VP rheology has certain deficiencies both in the underlying assumptions (e.g. Coon et al.,

⁷Equation 3.27 is also referred to as Coulomb's friction law.

2007) and in the results obtained by the models that implement it. Recent modeling studies have shown that the VP model can represent with a certain level of accuracy the mean, global (> 100 km) drift of sea ice, but it fails at reproducing the observed properties of sea ice deformation, especially at the fine scales (Dansereau (2016); Lindsay et al. (2003), Kwok et al. (2008), and Girard et al. (2009)). VP-based models were also shown to capture the “linear kinematic features”, linear-like faults, or leads due to large velocity gradients in the cover (Kwok, 2001) only if run at high resolution, i.e. < 2 km, which is one order of magnitude higher than the observational data (Hutter and Losch, 2020).

It is not yet clear whether these shortcomings should be attributed to incorrect physics, problematic numerics or other factors (e.g. Bouchat et al., 2022; Hutter et al., 2022). In the meanwhile, research efforts have led to the development of new rheological frameworks with an alternative physical approach. Among those, Tremblay and Mysak (1997) developed a rheology based on granular mechanics using a Mohr-Coulomb failure envelope, Wilchinsky and Feltham (2006) proposed a continuum model where anisotropy was introduced at the scale of leads (which are oriented features) and Schreyer et al. (2006) proposed an elastic-decohesive constitutive model, with an explicit representation of leads.

However, this work will now focus on another branch of rheologies, with an innovative brittle-like approach, initiated with the works of Girard et al. (2011), Dansereau et al. (2016), and Ólason et al. (2022). Their rheological models are based on a progressive damaging mechanism, a concept borrowed from rock mechanics (e.g. Amitrano et al., 1999). These models have been shown to give a more faithful description of the deformation rates. These brittle rheologies are discussed in Chapter 4.

Chapter 4

Sea ice brittle modeling

This Chapter presents the novel solid-like sea ice modeling approach. Section 4.1 explains the new process of evaluation of a sea ice model, which motivates the recent state-of-the-art brittle-based rheological models described in later sections. A summarized timeline in sea ice brittle modeling is given at the end of the chapter.

4.1 A new modeling paradigm

Because of the growing importance of scaling analysis, hereafter we present the concepts used to investigate the scale-invariance of sea ice deformation. Then, we explain how these concepts have guided to a new sea ice modeling paradigm.

4.1.1 A quantitative approach to study scale-invariance

The degree of scale invariance in sea ice deformation can be measured quantitatively by examining the shape of the distributions of deformation rate invariants, $\dot{\epsilon}_I$, $\dot{\epsilon}_{II}$. These probability density functions (P) have been demonstrated to exhibit “heavy-tailed” characteristics, indicating a prevalence of extreme values. This heavy-tailed behavior follows a power-law decay of the form

$$P(\dot{\epsilon}_{\text{tot}}) = \dot{\epsilon}_{\text{tot}}^{-\gamma} \quad (4.1)$$

where $\dot{\epsilon}_{\text{tot}}$ indicates the magnitude of the total strain rate and $\gamma > 1$ is an exponent that depends on the spatial and timescale considered (Lindsay and Stern, 2003; Marsan et al., 2004). Nevertheless, from Equation 4.1 it is impossible to evaluate the scale at which a certain deformation is taking place, not even by comparing the relative number of deformation events of different sizes (Rampal et al., 2019).

The mean deformation rate has been shown to scale according to a power law (Lindsay and Stern, 2003; Marsan et al., 2004):

$$\langle \dot{\epsilon}_{\text{tot}} \rangle \sim L^{-\beta(1)} \quad (4.2a)$$

$$\langle \dot{\epsilon}_{\text{tot}} \rangle \sim T^{-\alpha(1)} \quad (4.2b)$$

where the scaling exponents $\beta, \alpha \geq 0$ quantify the degree of localization of the deformation. In the realm of space dynamics, a value of $\beta = 0$ signifies the uniform deformation of either an elastic solid or a viscous fluid. This type of deformation remains consistent across spatial scales. Conversely, when $\beta = 2$, representing the topological dimension applicable to a 2-D-like sea ice cover, it denotes a singular “point” where all deformation concentrates within an otherwise unaffected material, as discussed by Rampal et al. (2008). On the flip side, within the temporal domain, a value of $\alpha = 0$ signifies a uniform deformation, while a singular deformation event occurring in isolation over time aligns with the limit of $\alpha = 1$, as explained by Rampal et al. (2008).

In order to properly study how the scaling changes with the magnitude of the deformation events, one has to study the higher order moments of the distribution 4.1, e.g. the variance (order 2) and the skewness (order 3); in particular, one has to evaluate the change of β , α as the order changes. The proper way to do that is through so-called structure functions (in space and time, respectively):

$$\beta(q) = aq^2 + bq \quad (4.3a)$$

$$\alpha(q) = cq^2 + dq \quad (4.3b)$$

where q indicates the moment of the distribution and a, b, c, d are scalars. There are two notable cases:

- $a = 0$ or $c = 0$, i.e. the structure functions are linear;
- $a, c > 0$ or $b, d > 0$, i.e. the structure functions are convex.

In the first case, the amount of localization of large and small deformation events is the same, regardless of the scale. These systems are known as *monofractal*. The second instance implies that the higher-order moments of the distribution experience a notably greater rate of increase than the lower-order moments as the observational scale diminishes. Put differently, substantial deformation events manifest a more concentrated localization in both temporal and spatial dimensions compared to smaller events. The system is then said to exhibit *multifractal* scaling (Kolmogorov, 1962; Lovejoy and Schertzer, 2007). This multifractal scaling is referred to as *heterogeneity* in the spatial domain and *intermittency* in the temporal domain (Rampal et al., 2019).

4.1.2 The multifractal scaling properties of sea ice deformation

Spatial scaling analysis of sea ice deformation derived from radar or buoy drift data reveals a distinct multifractal scaling characterized by a power law relationship (of the form of Equation 4.2) encompassing the first, second, and third moments. This scaling phenomenon is discernible across a range extending from the resolution of the data to scales reaching hundreds of kilometers, as evidenced by studies conducted by Marsan et al. (2004), Rampal et al. (2008), Hutchings et al. (2011), and Bouillon and Rampal (2015a). Results from one of such studies are shown in Figure 4.1 and Figure 1.2. Figure 4.1 shows the dependence of the first three moments of the total deformation distribution on the spatial and temporal scales, respectively, as deduced from the Radarsat Geophysical Processor System (RGPS; Kwok 1998) data set and as simulated by neXtSIM model (Rampal et al., 2019).

From a qualitative point of view, deformation has been observed to be highly localized around long, narrow apertures distributed in the sea ice cover in “web-like arrays”, commonly known as linear kinematic features (LKFs; Kwok et al. 1998). Analyses of observations have shown that what originates and keeps “active” these high stress zones of the cover are very intense and intermittent events, i.e. events that are highly localized in the time domain. More specifically, intermittency has been shown to characterize sea ice deformation on a time window from 3 to 160 days Weiss and Dansereau (2017).

4.1.3 A new validation metric for sea ice models

A growing comprehension of the aforementioned properties of sea ice deformation is leading sea ice researchers to employ a new modeling paradigm to build rheology-based models. Indeed, the potentially crucial role of multifractal scaling in developing a sea ice rheological model that is able to statistically link the observed dynamics at the larger scales (\gtrsim

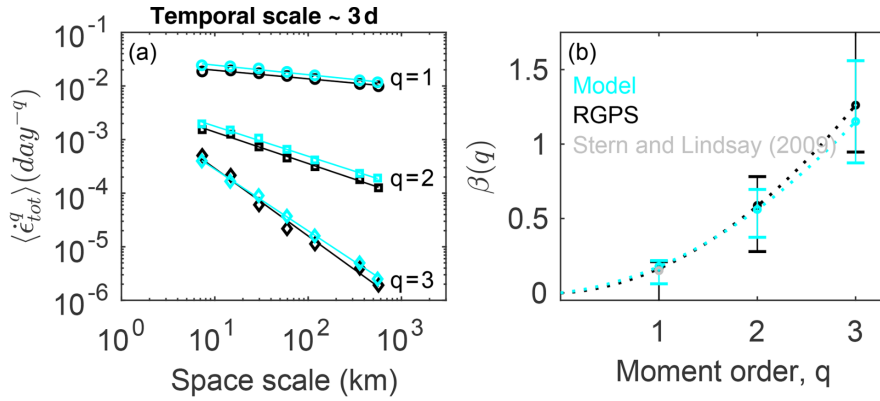


FIGURE 4.1: (a) Values of the first three moments of the rate of deformation distribution from (black) RGPS data and (light blue) neXtSIM simulations of $\langle \dot{\epsilon}_{tot}^q \rangle$ for $q = 1, 2, 3$, with space scales in the range 7.5 to 580 km; solid lines are the power-law scaling of Equation 4.2a. (b) Corresponding spatial structure function $\beta(q)$ of Equation 4.3a with the extrema of the bars indicating minimum and maximum power-law exponents obtained for two successive spatial scales. These effectively work as an estimation of the goodness of fit as in Bouillon and Rampal (2015a). Gray points represent the mean values for the considered time scales calculated by averaging over the period 1996–2008 (Stern and Lindsay, 2009).

Taken from Rampal et al. (2019)

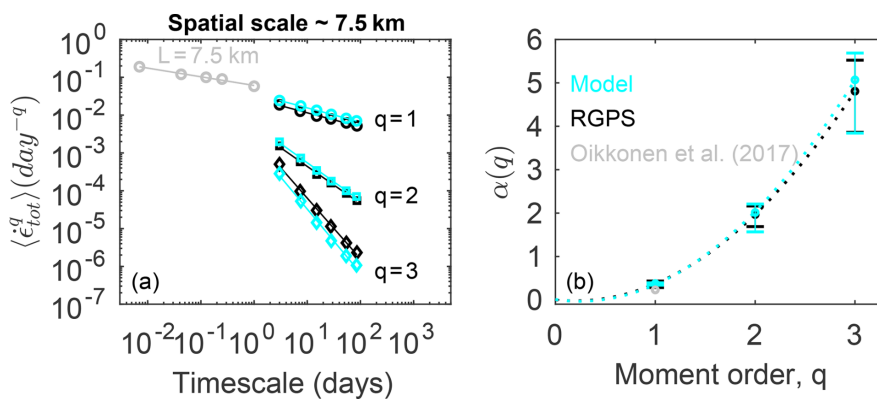


FIGURE 4.2: As Fig. 4.1 but as function of the temporal scales for a spatial scale of 7.5 km. The dotted gray points correspond to the mean rate of deformation values for a shorter timescale, 3 hours to 1 day with the same spatial scale (Oikkonen et al., 2017).

Taken from Rampal et al. (2019)

10 km) to the dynamics the smaller (unresolved) scales has been recognized (e.g. Weiss and Dansereau, 2017).

The self-similarity and multifractality observed in sea ice deformation pose great challenges for the continuum modeling framework (see Section 2.1) covered in this work. Its equations describe the progression of the mean quantities (see Section 2.5) in time. However, multifractality implies a lack of clear scale separation between mesoscale and larger-scale strain rates (Rampal et al., 2008) and no evident way of homogenizing field variables over different scales (Rampal et al., 2019) exists. In the absence of a defined spatial scale and temporal scale for sea ice deformation, the optimal approach within a continuum framework for sea ice modeling may involve accurately replicating the deformation statistics across scales. This encompasses capturing the statistics from the smallest resolved scales (nominal scale) to the largest scale. I.e. ranging from the spatial grid resolution (usually around 10 km) and model time step to the dimensions of the Arctic basin and the seasonal timescale. More quantitatively, that requires (Ólason, 2023)

- a) Power-law scaling of the first moments of the strain-rate distribution, i.e. $\langle \dot{\epsilon}_{\text{tot}}^q \rangle$, $q = 1, 2, 3$ should follow Equation 4.2;
- b) The correct scaling exponents and form for the structure functions $\alpha(q), \beta(q)$ and
- c) The moments should be of the correct magnitude.

The diagram in Figure 4.3 offers a graphical representation of the above requirements for the spatial scale of the deformation. The right hand side part (colored in red in the figure) represents the spatial scales resolved by the model, i.e. coarser than the model's resolution Δx , while the left-hand side (colored in blue) represents the unresolved scales. In order to fulfill requirements a) and b) the values of $\langle \dot{\epsilon}_{\text{tot}}^q \rangle$ should fall in a straight line whose slope is comparable to the one obtained by fitting observations (see Figure 4.1). Then, the points on the vertical red dashed line should be at the right (observed) height, i.e. $\langle \dot{\epsilon}_{\text{tot}}^q \rangle$ has the right magnitude, satisfying c). The deformation events happening at coarser scales than Δx are caused by grid scale interactions, while the ones in the drawn circles are the result of sub-grid scale physics. For these a different parametrization is needed. Had we adequate models with a high-enough resolution we would be able to resolve the lines colored in blue up to a certain scale χ , at which a new modeling approach would be needed¹. This unknown scale corresponds to the size of a stress concentrator. I.e. the typical length scale of features with higher stresses than those found in the areas surrounding them. This is the length scale at which the ‘‘multiplicative cascade’’ of deformation events (e.g. Marsan et al., 2004) starts.

The goal of the brittle rheological frameworks discussed later in this Chapter is precisely to fulfill the previous requirements and furnish a continuum-based approach that is apt at giving good results at all scales greater than the above-discussed stress concentrator scale.

4.2 The Elasto-Brittle rheology (EB)

4.2.1 Toward an elasto-brittle approach for sea ice rheology

Brittle-based rheology is based on the similarity between sea ice mechanical behavior and that of the Earth crust. For the latter, brittle fracturing, scaling properties and a Coulomb-like stress redistribution was already established (e.g. Kagan and Knopoff, 1980). For example, Tang (1997) and Amitrano et al. (1999) combined a linear elastic law

¹Discrete element modeling seems to be the answer, but this is an open research question.

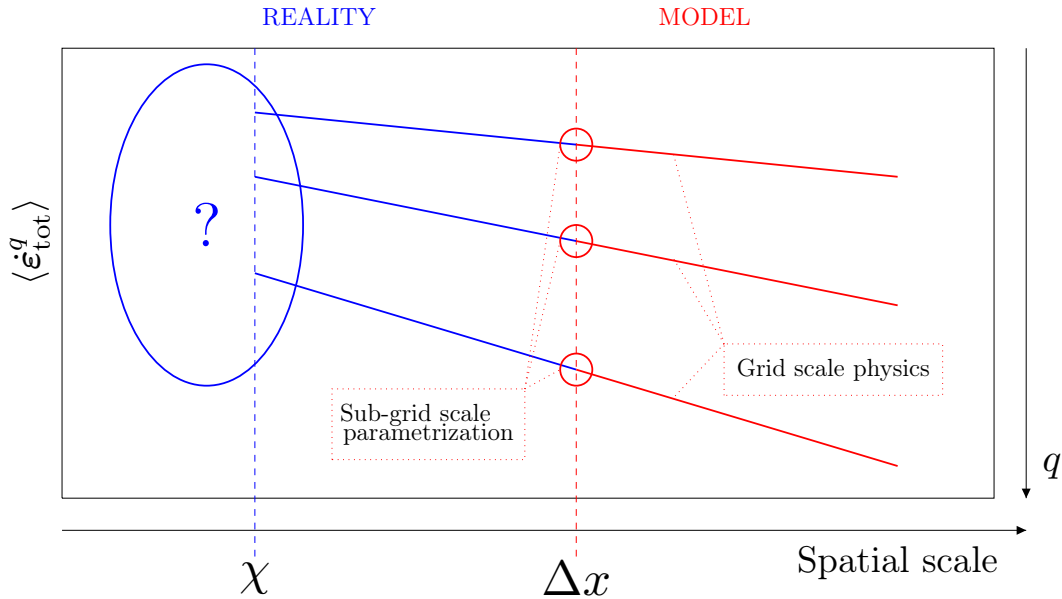


FIGURE 4.3: This diagram shows the spatial dependence of the first three moments of the deformation rate distribution on a typical timescale (see e.g. Figure 4.1), where q is the moment order and χ is the size at which single floes are resolved. See text for the explanation.

Taken from Ólason (2023)

with local threshold mechanics to obtain the desired nonlinear behavior of rocks at the macroscale. In particular, Amitrano et al. (1999) used a progressive damage mechanism based on a damage level affecting the elastic stiffness of the Earth crust and allowing stress redistribution triggering large-scale elastic deformation. Marsan and Weiss (2010) provided evidence for similarities between Earth crust and ice dynamics. They also showed that in both cases deformation is the result of a multiplicative cascade of local fracturing events (Marsan et al., 2004) with the influence of these events spanning longer time windows and larger spatial areas. Building upon these works, Girard et al. (2011) applied this “elasto-brittle” approach to the ice cover developing the so-called elasto-brittle (EB) rheology.

Development of the brittle-based rheological framework was motivated by the desire to reproduce the statistical and scaling properties that characterize sea ice deformation described in Section 4.1. It is based on continuum mechanics and is simple enough to be implemented in climate models (Girard et al., 2011).

In the EB rheology, ice is seen as a continuous elastic plate encountering progressive damage, simulating local fracturing events, i.e. the opening of leads and cracks. The internal stress is able to propagate over long distances as a result of a damage event, thanks to long-range elastic interactions.

The EB rheology was first implemented in the “neXt generation Sea Ice Model”, neXtSIM (Rampal et al., 2016). Since improvements were made from its initial introduction by Girard et al. (2011), we will present the improved version by Bouillon and Rampal (2015b) hereafter.

4.2.2 Constitutive law

The linear constitutive model was already introduced when discussing the (linear) elastic-plastic model (see Section 3.2.2):

$$\boldsymbol{\sigma} = E\mathbf{K} : \boldsymbol{\varepsilon} \quad (4.4)$$

where here E is an effective elastic modulus coupled to the spatially and temporally evolving level of damage of the material and \mathbf{K} is the dimensionless stiffness tensor given by Equation 3.15. By taking the time derivative of Equation 4.4 we can rewrite the constitutive law in terms of the rate of deformation tensor:

$$\frac{D\boldsymbol{\sigma}}{Dt} = E\mathbf{K} : \dot{\boldsymbol{\varepsilon}} + \dot{E}\mathbf{K} : \boldsymbol{\varepsilon} \quad (4.5)$$

where \dot{E} stands for the total time derivative of the effective elastic stiffness. In plane-stress hypothesis, valid in sea ice dynamics, \mathbf{K} assumes a simple form given by (e.g. Timoshenko and Goodier, 1951; Zienkiewicz and Taylor, 2000)²

$$\begin{bmatrix} (\mathbf{K} : \dot{\boldsymbol{\varepsilon}})_{11} \\ (\mathbf{K} : \dot{\boldsymbol{\varepsilon}})_{22} \\ (\mathbf{K} : \dot{\boldsymbol{\varepsilon}})_{12} \end{bmatrix} = \frac{1}{1-\nu^2} \begin{bmatrix} 1 & \nu & 0 \\ \nu & 1 & 0 \\ 0 & 0 & \frac{1-\nu}{2} \end{bmatrix} \begin{bmatrix} \dot{\varepsilon}_{11} \\ \dot{\varepsilon}_{22} \\ 2\dot{\varepsilon}_{12} \end{bmatrix}. \quad (4.6)$$

The effective stiffness changes with the level of damage and sea ice concentration as³:

$$E(A, d) = E_0 f(A)(1-d) \quad (4.7)$$

where E_0 is Young elastic modulus (intrinsic property), d is the damage level (e.g. Amirano et al., 1999), a dimensionless scalar variable, which is equal to 0 for undamaged ice and to 1 for “completely damaged ice” (see Section 4.2.4 for the details) and A is sea ice concentration (see Equation 2.18).

How the concentration impacts the elastic stiffness is not really known and thus has to be parametrized (Bouillon and Rampal, 2015b). The dependence of the compactness has a form inspired by the parametrization of the ice strength in VP models (see Equation 3.23)

$$f(A) = \exp[-c^*(1-A)] \quad (4.8)$$

where c^* is the compaction parameter in Hibler (1979) model, usually set to $c^* = 20$ (Rampal et al., 2019). This exponential factor can be interpreted as the local contact fraction between floes (as in Gray and Morland, 1994).

The dependence on the damage level in the constitutive equation can be made explicit by calculating \dot{E} from Equation 4.7:

$$\dot{E} = \frac{\partial f}{\partial A} \dot{A} - E \frac{\dot{d}}{1-d} \quad (4.9)$$

where \dot{d} is the mechanical time-change in damaging. As it does not impact significantly the results, we neglect the compactness change in time and write the constitutive law 4.5 as (see Bouillon and Rampal 2015b; Ólason et al. 2022)

$$\frac{D\boldsymbol{\sigma}}{Dt} = E\mathbf{K} : \dot{\boldsymbol{\varepsilon}} - \frac{\dot{d}}{1-d}\boldsymbol{\sigma}. \quad (4.10)$$

² $\dot{\varepsilon}_{21} = \dot{\varepsilon}_{12}$ by symmetry and as by definition of the plane-stress hypothesis all stresses perpendicular to plane are zero (Zienkiewicz and Taylor, 2000).

³In Girard et al. (2011)’s version the ice thickness h appears to the right-hand side of Equation 4.7. In this formulation, as in Bouillon and Rampal (2015b), h is explicitly present in the momentum equation 2.31 through explicit integration of $\boldsymbol{\sigma}$. included the ice thickness to the

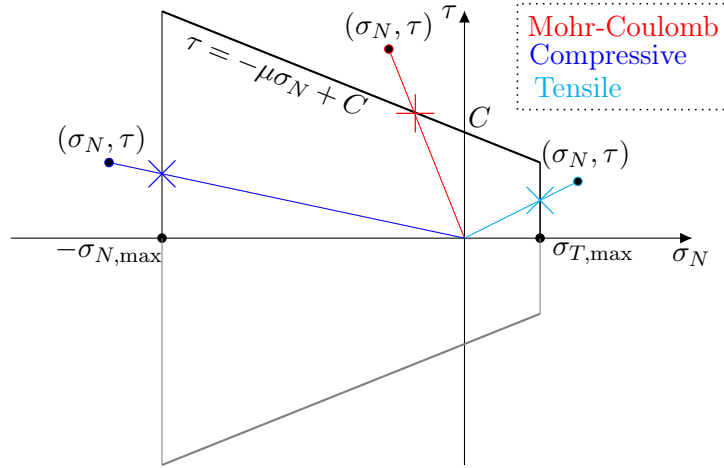


FIGURE 4.4: Failure envelope combining a Mohr-Coulomb criterion (thicker black line) with maximal compressive and tensile criteria. The lower symmetric branch has been coloured in gray. The three possible supercritical states on the upper branch have been represented. After the damaging process the states are brought back to the \times point on the yield curve.

4.2.3 Damage criterion

Study of fracture patterns has led sea ice scientists to hypothesize that failure occurs on many scales through highly localized deformation via scale-independent mechanisms (Schulson, 2004). On the basis of an analysis of in situ ice stresses and of satellite-derived ice strain rates as well as a comparison between field and laboratory behavior, a combination of the Mohr-Coulomb criterion with tensile and compressive criteria was found to best describe faulting within the sea ice cover (see Figure 3.11; Weiss et al. 2007; Richter-Menge et al. 2002).

Since the damaging process is isotropic (Amitrano, 2003), the damage criterion can be equally stated in any of the stress-invariant spaces. In the context of brittle rheologies, the damage criterion (Mohr-Coulomb; introduced at the end of Section 3.2.2) is often stated in terms of shear stress (e.g. Girard et al., 2011; Ólason et al., 2022) or in the principal stress space (e.g. Bouillon and Rampal, 2015b; Dansereau, 2016; Rampal et al., 2019) instead of the $\{\sigma_I, \sigma_{II}\}$ space (e.g. Plante et al., 2020). In sea ice models implementations, e.g. neXtSIMv1 (EB-,MEB-based) versus neXtSIMv2 (BMM-based), slightly different versions of the Mohr-Coulomb criterion have been used. However, the principles remain the same. Hereafter we will stick to the shear-normal stress representation of the envelopes, with the convention of negative compressive stress as elsewhere in this work.

For the EB model the following criterion is generally used (e.g. in neXtSIM, Bouillon and Rampal, 2015b):

$$|\tau| \leq -\mu\sigma_N + C \quad (\text{Mohr-Coulomb criterion}) \quad (4.11a)$$

$$\sigma_N \leq \sigma_{T,\max} \quad (\text{tensile stress criterion}) \quad (4.11b)$$

$$\sigma_N \geq -\sigma_{N,\max} \quad (\text{compressive stress criterion}) \quad (4.11c)$$

where μ is the internal friction coefficient, C is the cohesion (see Section 3.2.2) and $\sigma_{T,\max}, \sigma_{N,\max} > 0$ are the maximal tensile and compressive stress respectively. In order to constitute an additional effective constraint, $\sigma_{T,\max}$ must be smaller than C/μ . This failure envelope is represented in Figure 4.4.

In Girard et al. (2011) the friction coefficient μ was set to 0.7, a common value for geo-materials (Amitrano et al., 1999), seemingly scale-independent (Weiss and Schulson, 2009). On the contrary, the sea ice cohesion C strongly depends on the spatial scale (Weiss et al., 2007). Following Schulson (2004), Bouillon and Rampal (2015b) assumed the cohesion to scale with the model resolution as

$$C \approx C_{\text{ref}} \sqrt{\frac{l_{\text{ref}}}{\Delta x}} \quad (4.12)$$

where $l_{\text{ref}} = l_{\text{lab}}$ for which the cohesion is estimated to be around 1 MPa. In order to introduce natural heterogeneity, i.e. the presence of stress fractures, lead, shear zones (effectively, stress concentrators) at the model resolution scale the cohesion value at each model element is drawn randomly from a uniform distribution of values spanning estimates from in-situ stress measurements (Weiss et al., 2007). Typical ranges for C , guarantee a representation of stress concentrators in the 25 km – 10 km range (Bouillon and Rampal, 2015b). An important point is that Equation 4.12 implies that the compressive and tensile strength values also follow the same scaling law as C . From observations the following relationships are deduced (Bouillon and Rampal, 2015b): $\sigma_{T,\text{max}} = \frac{5}{4}C$, $\sigma_{N,\text{max}} = \frac{5}{2}C$.

4.2.4 Progressive damaging and healing

In the EB rheology, the mechanical parameter E is not constant, but coupled to the level of damage, described by d , $0 \leq d \leq 1$. This parameter is interpreted as a measure of the sub-grid cell defects or crack density (Kemeny and Cook, 1986). In other terms, the effect of sub-gridscale fracturing is represented by a parameter at the grid scale (Girard et al., 2011). Two competing mechanisms contribute to damage evolution. On the one hand we have *damaging*, representing fracturing and the opening of leads, occurring when the internal stress exceeds the mechanical resistance of the material, and which leads to its weakening (Dansereau, 2016). On the other, we have *healing*, representing the mechanical strength recovery through refreezing of open leads⁴.

When the stress exceeds the yield criterion presented in Equation 4.11, the level of damage of an element d increases and the elastic modulus E drops, leading to local strain softening (Amitrano et al., 1999). Since we are considering an elastic cover able to sustain long-range interactions, the decrease in E results in a stress redistribution around the damaged element, which mostly affects its nearest neighbors. Because of the stress redistribution, the strength threshold for damage can be exceeded in other elements and this can trigger an “avalanche” of damage events (Amitrano et al. 1999; Girard et al. 2011; see e.g. Fig. 2.4 in Dansereau 2016). This propagation mechanism is at the very root of the emergence of both spatial heterogeneity and anisotropy in the stress and strain fields, i.e. in the formation of linear-like features (Dansereau, 2016).

In the following, we will discuss the derivation of the evolution equation for the damage d in the EB model.

Damaging

Since the time scale of healing, T_h , is way larger than the characteristic time scale of damage propagation, T_d , the latter being comparable to the time of propagation of an elastic shear wave in the medium, we can treat damaging and healing separately.

⁴This has not to be confused with a thermodynamical healing process, e.g. the one taken into account by neXtSIMv1 (Rampal et al., 2016), or with the mechanical/thermal changes described in Section 2.5 because it applies only to damaged ice. The thermodynamical healing process in Rampal et al. (2016) is driven by a local temperature gradient between the bottom of the ice and the snow, reasoning that a cooler environment will cause faster freezing (healing).

The damaging mechanism of the EB model is based on the following assumptions:

- a) The model time step has to be smaller than the characteristic damaging time scale i.e. $T_d \gg \Delta t$. Furthermore, the damaging process is assumed to take place uniformly over T_d ;
- b) Stress states lying outside the failure envelope are unphysical (brittle failure would have occurred before). In order to bring them back to the yield curve, the damage has to change by a factor d_{crit} ;
- c) The strain of each model element is conserved during a damaging process, only the stress level is changed as a result.

We note that point c) is a fundamental assumption, which allows stress to be redistributed among neighbouring model elements, i.e. the avalanche process previously described takes place. We now discuss the damaging process.

The first step accounts for the elastic deformation without considering the damaging process, i.e. Equation 4.5 with a constant damage is employed rendering a potentially supercritical stress σ_i (Rampal et al., 2016). If the state σ_i happens to be supercritical, a damage factor d_{crit} is computed as the distance of σ_i to the yield curve moving on a line passing through the origin:

$$\sigma_f = d_{\text{crit}} \sigma_i. \quad (4.13)$$

furnishing a new physical state, σ_f , lying on the yield curve. The damage level of the material has therefore been increased. Clearly, the expression for d_{crit} changes based on which of the criteria in Equation 4.11 has been exceeded (see e.g. Plante et al. 2020, Rampal et al. 2016):

$$d_{\text{crit}} = \min \left[1, \frac{C}{(\tau + \mu \sigma_N)}, -\frac{\sigma_{N,\text{max}}}{\sigma_N}, \frac{\sigma_{T,\text{max}}}{\sigma_N} \right] \quad (4.14)$$

which ensures $0 < d_{\text{crit}} < 1$. We now want to derive the damage change in time, which will be then coupled to the healing process. Using the chain rule, the internal stress evolution may be written as

$$\frac{D\sigma}{Dt} = \frac{\partial \sigma}{\partial t} + \frac{\partial \sigma}{\partial \varepsilon} \dot{\varepsilon} + \frac{\partial \sigma}{\partial d} \dot{d}. \quad (4.15)$$

Combining this with Equation 4.10 gives

$$\frac{\partial \sigma}{\partial d} = \frac{-\sigma}{1-d}. \quad (4.16)$$

Rewriting Equation 4.13

$$\frac{\sigma_f - \sigma_i}{T_d} = -\sigma_i \frac{1 - d_{\text{crit}}}{T_d} \quad (4.17)$$

and observing that the left-hand side is an approximation of the time derivative gives

$$\frac{\partial \sigma_f}{\partial d} \dot{d} = \sigma_f \frac{1 - d_{\text{crit}}}{T_d}. \quad (4.18)$$

Combining Equations 4.16 (where $\sigma = \sigma_f$) and 4.18 we finally get the time-change in the level of damage:

$$\dot{d} = \frac{(1 - d_{\text{crit}})(1 - d)}{T_d}. \quad (4.19)$$

In the original EB formulation of Girard et al. (2011) a simpler version of the damaging mechanism was employed. Instead of employing a varying damage factor, they opted for a sub-iteration loop. In this loop, the elastic stiffness was consistently reduced by a constant damage factor at each iteration step until the stress state realigned with the yield curve. This was proved not to have significant impact on the simulated deformation fields, but required a much higher computational cost than the version of Bouillon and Rampal (2015b). However, they used the same form of the damage source term (right-hand side of Equation 4.19).

Healing

As introduced by Bouillon and Rampal (2015b), the mechanical healing process is handled by a simple restoring term

$$\dot{d} = -\frac{d}{T_d} \quad (4.20)$$

where the T_d is the damage relaxation time.

Damage level evolution

Coupling the damaging and the healing processes, the evolution equation for the damage level is established:

$$\dot{d} = \frac{(1 - d_{\text{crit}})(1 - d)}{T_d} - H(1 - d)\frac{d}{T_d} \quad (4.21)$$

where H is the Heaviside step function, ensuring that the damage level remains below the upper limit of 1..

Now, the coupling of the constitutive law Equation 4.10 is fully defined with E evolving according to Equation 4.7 and the damage level with Equation 4.21.

4.2.5 Results and known limitations of the EB rheology

In introducing the EB rheological framework, Girard et al. (2011) performed an idealized short timescale basin-scale simulation (three days) at the mid-coarse 10 km resolution neglecting advective effects on the dynamics. The simulated deformation rates and scaling laws were consistent with those expected based on RGPS observations (see Section 4.1.2). In addition to that, VP simulations with a similar setup were performed in order to make a comparison. The results for the shear rates of deformation are shown in Figure 4.5. It was also shown that the EB gives much better result in terms of statistical and scaling properties than the VP.

The EB rheology was also implemented in neXtSIM with a pan-Arctic simulation of one year (Rampal et al., 2016). The results showed that the model correctly reproduced the multi-scale statistics of the rate of deformation fields as well as the ice volume and extent of the ice cover.

A key limitation of the elasto-brittle framework lies in its ability to represent large, permanent deformation fields. Using a simple linear elastic law, the model will solve for the total strain ϵ without distinguishing between the elastic (recoverable) and the potentially permanent part of the deformation (Dansereau, 2016). An assumption on the strain partitioning of damaged ice thus have to be made.

Girard et al. (2011) assumed all the deformation of the damaged material to be elastic, which means the material will return to the original position after stress-unloading, but with a decreased elasticity. This approach might be suitable for short-term simulations, where advective processes are neglect, as in Girard et al. (2011). However, in order to run long-term simulations this assumption had to be revisited.

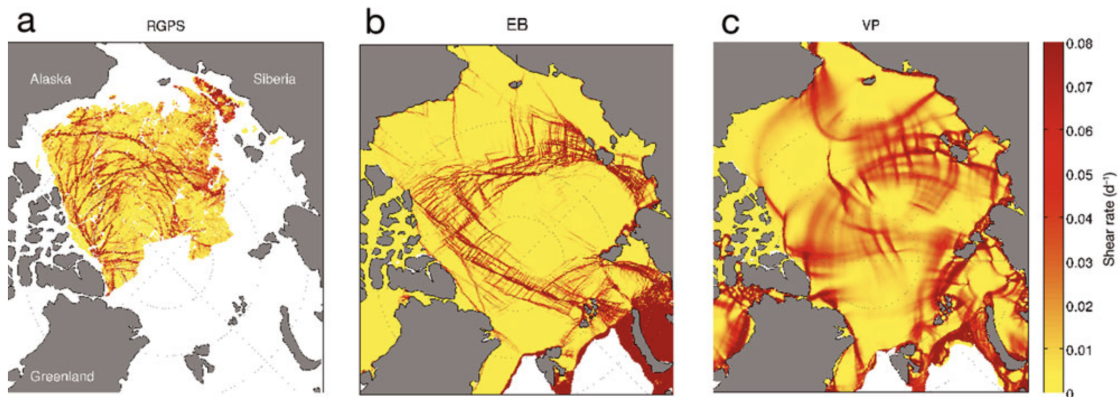


FIGURE 4.5: Shear rate from (a) RGPS observations, (b) EB simulation and (c) VP simulation. The RGPS observations represented were obtained between 27 March and 1 April 2007. Strain rates from EB and VP simulations were computed between 27 and 30 March 2007, for a temporal scale of 3 days.

Taken from Girard et al. (2011)

Strain rate estimates coming from RGPS observations suggested a dominant contribution of permanent deformations for a damaging elastic cover (Weiss et al., 2007; Marsan et al., 2004). This motivated Bouillon and Rampal (2015b) to assume damaged ice to only undergo permanent deformation in neXtSIM EB-based model with advection. Nevertheless, this all-permanent approach, opposite to the all-elastic one of Girard et al. (2011), is defective in that it implies an instantaneous dissipation of internal stress once the applied loading is removed or reset. This inability to “remember” the history of previous stresses strongly compromises EB-models to reproduce the intermittency, i.e. the multifractality in the time domain (see Section 4.1.1, intrinsic to sea ice (Dansereau, 2016)). The full dynamic-thermodynamic EB-based version of neXtSIM (Rampal et al., 2016) weakly reproduces this intermittency, which is instead well captured by the MEB-based version (Rampal et al., 2019).

In order to overcome these shortcomings, a suitable rheological model should discern between small/reversible and large/permanent deformations.

4.3 The Maxwell elasto-brittle rheology (MEB)

4.3.1 Motivation

In order to achieve a better representation of observed ice deformation rates, an extension to the EB rheology has been developed by Dansereau (2016). This Maxwell-Elasto-Brittle (MEB) rheology uses a linear-elastic constitutive model, like the EB, but with an additional viscous-like relaxation term. Thus effectively resulting in a Maxwell viscoelastic model. Nevertheless, the “apparent” viscosity, coupled to the damage level as the elastic modulus in the EB model, provides a way for highly damaged ice to dissipate stress into permanent deformations. That being said, an important difference with the Maxwell model (Maxwell, 1867) is that the fictitious viscosity is not meant to represent the viscoplastic creep of bulk ice (Duval et al., 1983).

Arguments in favor of a viscoelastic rheology with a pseudo-viscosity are (a) the already-presented similarity of sea ice with the lithosphere (see Section 4.2.1), where relaxation of elastic strains occurs in active faults (e.g. Çakir et al., 2012) and (b) the analogy

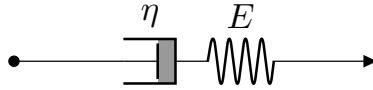


FIGURE 4.6: One-dimensional illustration of the Maxwell linear viscoelastic model. The mechanical model is given by a dashpot and a spring placed in series. In the MEB model both η and E evolve in space and time, being coupled to the compactness and damage level.

of ice with sheared granular media when it is highly packed. For flows in such media a high apparent viscosity is typical (Jop et al., 2006; Aranson and Tsimring, 2006).

Although not new in the context of rock-like materials modeling (e.g. Lyakhovsky et al., 1997), applied viscoelastic rheologies with an apparent viscosity term are fundamentally different from the MEB rheology. In those models, pseudo-viscous relaxation is meant to represent small brittle-failure deformations (Dansereau 2016; e.g. Lyakhovsky et al. 1997) not to link small to large deformations.

4.3.2 Constitutive model

In the MEB model, the ice sheet is modeled as an continuous, isotropic, compressible solid satisfying the Maxwell (linear viscoelastic) constitutive law (Maxwell, 1867). The one-dimensional representation of the Maxwell model is shown in Figure 4.6. It is composed of a linear elastic element, whose behavior is characterized through the elastic modulus E (see Figure 3.8), and of a viscous element, with a stress-independent viscosity η (see Figure 3.6).

Extending the one-dimensional Maxwell model concept to the solid ice sheet, the total deformation ε resulting from an applied stress σ reads

$$\varepsilon = \varepsilon_E + \varepsilon_v \quad (4.22)$$

i.e. it is effectively partitioned into an (instantaneous) elastic, reversible component, ε_E , and a (linearly increasing with time) viscous, permanent component, ε_v . The model assumes the viscous stress σ_v , i.e. the time-dependent part of the stress, to be linearly dependent on the strain rate

$$\sigma_v = \eta \mathbf{K} : \dot{\varepsilon}_v \quad (4.23)$$

where η is a stress-independent coefficient setting the rate of increase of permanent deformation with the time and has the dimensions of a viscosity (Dansereau, 2016). From the elastic constitutive law in terms of the rate of deformation tensor (Equation 4.5) follows

$$\begin{aligned} \frac{D\sigma_E}{Dt} &= E(\mathbf{K} : \dot{\varepsilon}_E) + \dot{E}(\mathbf{K} : \varepsilon_E) \\ &= E(\mathbf{K} : \dot{\varepsilon}) - E(\mathbf{K} : \dot{\varepsilon}_v) + \frac{\dot{E}}{E}\sigma_E \end{aligned} \quad (4.24)$$

$$= E(\mathbf{K} : \dot{\varepsilon}) - \frac{E}{\eta}\sigma_v + \frac{\dot{E}}{E}\sigma_E \quad (4.25)$$

Using that $\boldsymbol{\sigma} = \boldsymbol{\sigma}_E = \boldsymbol{\sigma}_v$ since the stress in each serially connected element must be equal to total stress (Ólason et al., 2022) the previous reads⁵

$$\frac{D\boldsymbol{\sigma}}{Dt} = E(\mathbf{K} : \dot{\boldsymbol{\varepsilon}}) - \frac{1}{\lambda}\boldsymbol{\sigma} + \frac{\dot{E}}{E}\boldsymbol{\sigma} \quad (4.26)$$

where we have introduced the viscous relaxation time $\lambda = \frac{\eta}{E}$.

The Maxwell model was originally designed to describe small deformations of viscoelastic materials (Maxwell, 1867). However, the MEB rheology aims at representing both small and large deformations. This means some non-linearity must enter the equations when transitioning from the small elastic to the large permanent deformations for which advective processes are non-negligible. Therefore, Dansereau (2016) stated the evolution of the internal stress in terms of the objective Gordon-Schowalter derivative (Saramito, 2016) rather than in terms of the usual material derivative:

$$\frac{D\boldsymbol{\sigma}}{Dt} = \frac{\partial\boldsymbol{\sigma}}{\partial t} + (\mathbf{u} \cdot \nabla)\boldsymbol{\sigma} + \beta_a(\nabla\mathbf{u}, \boldsymbol{\sigma}) \quad (4.27)$$

where the additional term β_a accounts for the effects of rotation and deformation on the evolution of $\boldsymbol{\sigma}$ and reads⁶

$$\beta_a(\nabla\mathbf{u}) = \boldsymbol{\sigma}\omega(\mathbf{u}) - \omega(\mathbf{u})\boldsymbol{\sigma} - a[\boldsymbol{\sigma}\boldsymbol{\varepsilon}(\mathbf{u}) + \boldsymbol{\varepsilon}(\mathbf{u})\boldsymbol{\sigma}] \quad (4.28)$$

with $\dot{\boldsymbol{\varepsilon}}(\mathbf{u})$, $\dot{\boldsymbol{\omega}}(\mathbf{u})$ the symmetric and antisymmetric part of the velocity gradient respectively (see Section 2.2.1).

4.3.3 Damage criterion

Referring to envelope used in the MEB implementation in neXtSIM model (Rampal et al., 2019), the same failure criterion was used (see Equation 4.11; Figure 4.4).

Originally, Dansereau (2016) used a Mohr-Coulomb criterion, stated in the principal stress plane combined with a tensile cut-off, which basically is the same as considering Equation 4.11 with $\sigma_{N,\max} \rightarrow \infty$. In this cutoff, the ultimate tensile strength is defined as the intersection of the Mohr-Coulomb criterion with the σ_2 axis (Paul, 1961).

As mentioned in Section 4.2.3, the way to introduce the material's natural heterogeneities in these models is by stochastically perturbing the spatial distribution of the cohesion.

4.3.4 Progressive damaging

In the following, we will keep with the notation already introduced in the EB model formulation. The mechanisms giving rise to the progressive damaging remain the same: one for the local degradation of the ice, i.e. damaging, and the other for its restrengthening, i.e. healing. As discussed in Section 4.3.2, the MEB model employs two mechanical parameters, the effective elastic stiffness E and the effective apparent viscosity η (both linked to the relaxation time λ). The sub-grid scale processes are parametrized with the

⁵We remark that in the original formulation by Dansereau (2016) the last term of Equation 4.26 was neglected.

⁶In their simulation Dansereau (2016) set $a = 1$, effectively using the so-called upper convected objective derivative (Saramito, 2016). Stating the constitutive law this way, frame-independence is guaranteed for both vector and tensor quantities.

dimensionless scalar parameter d at the grid scale, with the meaning already presented above⁷.

The assumptions outlined for the progressive damaging mechanism of the EB continue to hold in the MEB formulation. As for the newly added apparent viscous behavior we require the model time step to be very small compared to the viscous relaxation time and that a negligible part of the stress is dissipated in viscous deformations.

The damage source term in the MEB damage evolution equation is the same as in the EB (see Equation 4.19). In deriving the evolution equation, the time resolution was set to be the exact time of propagation of an elastic (shear) wave through the cover: $\Delta t = T_d = \frac{\Delta x}{c}$, with c the wave velocity. Average values for an heterogeneous ice pack indicate a value of c around 500 m s^{-1} (Marsan et al., 2011). Combined with the spatial resolution of current climate models, ranging from 1 km to 100 km, this implies a damaging time between $O(1)$ and $O(10^2)$ s.

As the assumption of a healing time inversely proportional to the damage level (see Section 4.2.4) possesses no real physical foundation, in the MEB model an even simpler parametrization is used:

$$\dot{d} = -\frac{1}{T_h} \quad (4.29)$$

where T_h is the characteristic time of healing, i.e. the time required for a completely damaged element ($d = 1$) to recover its initial stiffness ($d = 0$).

An order of magnitude for the healing time can be obtained by studies on leads re-freezing. For instance, in Petrich et al. (2007) it is shown that the time for 1 m of ice to grow within an opening of 10 cm with an air temperature of -15° is of $O(100)$ hours or $O(10^5)$ seconds.

Damage evolution equation

The difference, by several order of magnitudes, between T_h and T_d shows two decoupled competing mechanism, justifying the separate analysis. By putting them together, the continuous damage evolution equation for the MEB is obtained:

$$\dot{d} = \frac{(1 - d_{\text{crit}})(1 - d)}{T_d} - \frac{1}{T_h}. \quad (4.30)$$

4.3.5 Coupling of damage with mechanical parameters

The way in which the progressive damage mechanism couples with the MEB model's mechanical parameter constitutes one of the main advancements over the EB rheology. This coupling is based on the following ideas.

When in an undamaged state, sea ice is characterized by the (maximum) elastic modulus E_0 and very large apparent viscosity η_0 . In analogy to the usual behavior of solid undamaged media, in such a configuration sea ice is subject to small and reversible deformations, i.e. elastic. Under these conditions, the Maxwell constitutive law, Equation 4.26, is well approximated by a fully-elastic linear law.

On the other hand, large and permanent deformations are concentrated in highly damaged areas of the ice pack. The deformations at these locations are effectively modeled as the result of a large dissipation of internal stress in a relatively short amount of time. Consequently, the time scale over which dissipation occurs, i.e. the relaxation time $\lambda = \frac{\eta}{E}$, must be decrease in areas with high amounts of damage. As the completely damaged limit is approached ($d \rightarrow 1$), the cover begins to deform in a strictly irreversible manner with

⁷Originally, Dansereau (2016) used the opposite convention regarding the damage level, with $d = 0$ standing for completely damaged ice and $d = 1$ for undamaged ice.

$\lambda \rightarrow T_d$. In this limit the elastic memory is totally lost and the recovered behavior is the one of a soft viscous-plastic material. One such parametrization for E , η that renders the aforementioned behavior is (Dansereau, 2016):

$$E(d) = E_0 \exp[-c^*(1-A)](1-d) \quad (4.31)$$

$$\eta(d) = \eta_0 \exp[-c^*(1-A)](1-d)^\alpha \quad (4.32)$$

where $\alpha > 1$ is a constant damage parameter such that

$$\lambda(d) = \frac{\eta_0}{E_0}(1-d)^{\alpha-1} = \lambda_0(1-d)^{\alpha-1}. \quad (4.33)$$

We note that $d = d(t)$ and evolves according to Equation 4.30 and that sea ice concentration A is time-dependent as well. Typical values of the damage parameter and undamaged relaxation time used in a realistic setups are, respectively, $\alpha = 5$, $\lambda_0 = 10^7$ s (Rampal et al., 2019). In order to preserve the mathematical consistency of the constitutive law, either the limit $d = 1$ is never reached or the viscosity has to be constrained to an interval of allowed values.

4.3.6 Some results and known limitations of the MEB rheology

The MEB rheological framework has been successfully tested on both ideal and realistic setups and has furnished very promising results. The first test case was a simulation of ice flow through a narrow pathway in the Arctic (the Nares Strait; see Figure 1.1) in which the model was able to capture complex observed dynamical features like the spatial localization of thick ridges and the large discontinuity of the velocity field in correspondence of linear kinematic features (Dansereau et al., 2017).

In Rampal et al. (2019) the MEB was implemented into the neXtSIM model. Through a statistical analysis, this study showed that the neXtSIM model correctly reproduces the distribution of sea ice deformation rates, its scaling properties in both the space and time domains and its multi-fractal behavior (see Section 4.1.2). In particular, it was the first time that multi-fractality in the time domain is shown to be reproduced in a sea ice model (see Figure 4.2).

The main limitation of models implementing the MEB rheology was shown to be the excessive convergence of highly damaged ice, with unrealistic piling (Ólason et al., 2022). In fact, unlike rheologies based on the VP, the MEB (but also in the EB) rheology provides insufficient resistance to compression which leads to the just-mentioned excessive thickening of large amounts of ice in simulations longer than a year.

In addition to this, a dependence of the reproduced behavior on the time step arises when running longer simulations. For instance, in order to achieve a proper numerical performance, Rampal et al. (2019) had to use a much longer time step and could not use a fixed-point iteration scheme as in the original implementation (Dansereau, 2016; Ólason et al., 2022).

In the next section, a recently introduced rheological framework meant to address these issue is presented.

4.4 The brittle Bingham-Maxwell rheology (BBM)

4.4.1 Motivation

The brittle Bingham Maxwell (BBM) rheology (Ólason et al., 2022) is newly developed rheology meant to address the excessive thickening as well as the numerical issues discussed

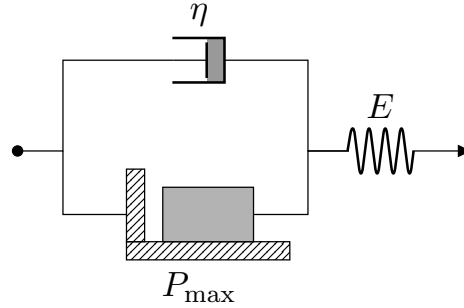


FIGURE 4.7: One-dimensional mechanical illustration of the Bingham-Maxwell model. It combines a spring in series with a dashpot and a parallel friction element.

in Section 4.3.6. The main addition is a new threshold for large, permanent deformations, implemented through a new Bingham-Maxwell constitutive model. As a consequence, this model is more apt to simulate ridging in high compression and to provide a resistance to ridging whenever the compressive stress is below a (newly introduced) threshold.

In their work, by analyzing the MEB-based solution of a Couette-flow problem, Dansereau (2016) suggested, as a possible subsequent improvement, the use of a more complex fluid model, e.g. Bingham or Oldroyd (Saramito, 2021; Cheddadi et al., 2008), of which the linear Maxwell model is a special case lacking a plastic threshold for the deformation or a solvent viscosity term. However, they suggested a different damaging criterion than the one used in the BBM.

In the BBM, the progressive damaging mechanism remains the same of the one presented in the MEB model (see Section 4.3.4).

4.4.2 Constitutive model

The constitutive model used in the BBM rheology is the Bingham-Maxwell model (Bingham, 1922; Saramito, 2021) with the elasticity and (apparent) viscosity on damage dependant on damage

The one-dimensional mechanical representation of Bingham-Maxwell model is shown in Figure 4.7. By adding a new friction element, with a characteristic critical stress P_{\max} , a new regime is defined (see Figure 4.8). In terms of normal stress, first we have a diverging regime, $\sigma_N > 0$, in which the friction element has no effect and the ice deforms with a total deformation ε partitioned in the elastic and viscous component $= \varepsilon_E + \varepsilon_v$. Then, when $-P_{\max} < \sigma_N < 0$, the friction element prevents any permanent deformation to occur and the linear elastic behavior is recovered: $\sigma_E = E\varepsilon_E$. Only when the compressive stress is sufficiently high, i.e. $\sigma_N < -P_{\max}$, the effect of the friction element ceases and permanent convergent deformation arises. In 1D the total stress σ is partitioned between the parallel viscous and friction element as $\sigma = \sigma_v - P_{\max}$, where P_{\max} is a constant quantity here. In terms of the viscous stress

$$\sigma_v = \sigma \left(1 + \frac{P_{\max}}{\sigma} \right). \quad (4.34)$$

We now apply Bingham-Maxwell model to the two dimensional ice sheet. By introducing a quantity

$$\tilde{P} = \begin{cases} \frac{P_{\max}}{\sigma_N} & \sigma_N < -P_{\max} \\ -1 & -P_{\max} < \sigma_N < 0 \\ 0 & \sigma_N > 0 \end{cases}, \quad (4.35)$$

Equation 4.34 generalizes into

$$\boldsymbol{\sigma}_v = (1 + \tilde{P})\boldsymbol{\sigma}. \quad (4.36)$$

which, contrary to Equation 4.34, is applicable under all conditions. In two dimensions, the ridging threshold P_{\max} is not constant and several parametrizations have been developed (Ólason et al., 2022). Following the results of the ridging model by Hopkins (1998), in neXtSIMv2 a VP ice strength-like dependence was assumed:

$$P_{\max} = P_0 \left(\frac{\hat{h}_{\text{thick}}}{h_0} \right)^{3/2} \exp[-c^*(1 - A)] \quad (4.37)$$

where \hat{h}_{thick} is the ice slab thickness (Equation 2.19), h_0 is a constant reference thickness, P_0 is a constant to parametrize P_{\max} , and c^* is a constant similar to the compaction parameter of Hibler (1979).

To obtain the constitutive equation of the BBM model, first substitute Equation 4.23 and the time derivative of Equation 4.22 into Equation 4.5 to get:

$$\begin{aligned} \frac{D\boldsymbol{\sigma}_E}{Dt} &= E(\mathbf{K} : \dot{\boldsymbol{\varepsilon}}_E) + \dot{E}(\mathbf{K} : \boldsymbol{\varepsilon}_E) \\ &= E(\mathbf{K} : \dot{\boldsymbol{\varepsilon}}) - E(\mathbf{K} : \dot{\boldsymbol{\varepsilon}}_v) + \boldsymbol{\sigma}_E \dot{E} \\ &= E(\mathbf{K} : \dot{\boldsymbol{\varepsilon}}) - \frac{E}{\eta} \boldsymbol{\sigma}_v + \boldsymbol{\sigma}_E \dot{E}. \end{aligned} \quad (4.38)$$

Now, by observing that $\boldsymbol{\sigma}_E = \boldsymbol{\sigma}$ and $\boldsymbol{\sigma}_v$ is given by Equation 4.36 we are able to write the constitutive law:

$$\frac{D\boldsymbol{\sigma}}{Dt} = E(\mathbf{K} : \dot{\boldsymbol{\varepsilon}}) - \frac{\boldsymbol{\sigma}}{\lambda} (1 + \tilde{P} - \lambda \dot{E}). \quad (4.39)$$

where $\lambda = \lambda(d)$ is the pseudo-viscous relaxation time defined above. Anticipating that the parametrization for E is the same as in the EB and MEB, we can explicit the dependence on the damage level change \dot{d} :

$$\frac{D\boldsymbol{\sigma}}{Dt} = E(\mathbf{K} : \dot{\boldsymbol{\varepsilon}}) - \frac{\boldsymbol{\sigma}}{\lambda} \left(1 + \tilde{P} + \lambda \frac{\dot{d}}{1-d} \right). \quad (4.40)$$

4.4.3 Damage criterion

The damage envelope used in BBM-based neXtSIM (Ólason et al., 2022) is based on the one used by Plante et al. (2020). They suggested adding a compressive cut-off to the usual Mohr-Coulomb criterion in order to avoid numerical instabilities when running simulations over longer periods. We note this upper compressive limit, to which we refer as N , is a numerical construct. It is chosen large enough as not to influence the results (Ólason et al., 2022). This parameter is let scale as the cohesion, according to Equation 4.12, with a chosen value at the lab scale $N_{\text{ref}} = 10$ GPa. This envelope is shown in Figure 4.8.

4.4.4 Damage propagation and coupling with mechanical parameters

The damage level in the BBM evolves in the same manner as in the MEB model. Therefore in the BBM, the damage level evolves according to Equation 4.30 with the damage factor being given by:

$$d_{\text{crit}} = \min \left[1, \frac{C}{(\tau + \mu\sigma_N)}, -\frac{N}{\sigma_N} \right] \quad (4.41)$$

which results in $0 < d_{\text{crit}} \leq 1$.

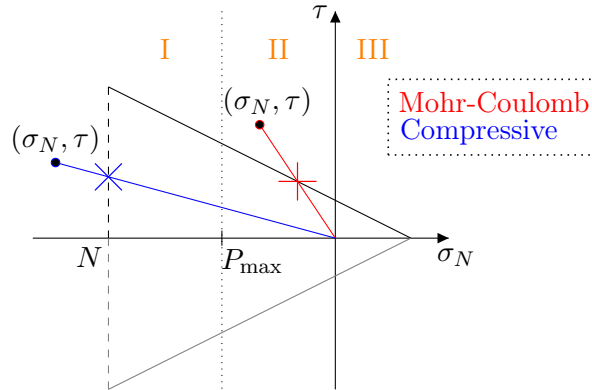


FIGURE 4.8: Failure envelope used in the BBM rheology by Ólason et al. (2022). Here, the compressive cut-off, N , is a numerical construct meant to avoid numerical instability and it is very large. The two points indicate the two possible supercritical states in the upper branch, which are brought back to the \times symbol (on the yield curve) following the damaging mechanism. The Roman numbers indicate the three main regimes of the BBM rheology: (I) is the ridging mode, (II) the purely elastic mode and (III) the diverging one.

However, there is a slight variation in the coupling of η with the damage level:

$$\eta = \eta_0(1 - d)^\alpha \exp[-\alpha c^*(1 - A)]. \quad (4.42)$$

This change compared to the MEB parametrization (Equation 4.32) is motivated by two reasons. First, the MEB formulation gave very high level of viscosity at low concentration, so the current formulation will give a more faithful viscous-like behavior at low-medium concentrations. Second, Equation 4.42 provides a relationship between damage and concentration. This is desirable as, e.g., waves are more likely to break the ice into small floes when moving traveling through low-packed areas.

4.4.5 Results

The BBM rheology was implemented in neXtSIM model neXtSIMv2. The model setup is very similar to that in Rampal et al. (2019) with oceanic and atmospheric forcing coming from realistic datasets (Ólason et al., 2022). For comparison, simulations a setup as close as possible to neXtSIMv2 with a mEVP rheology (Bouillon et al., 2009), a numerically more efficient version of the VP rheology (see Section 3.2.2), have been performed.

Results of a 20 years simulation in part of the Arctic showed a reasonable sea ice thickness magnitude and distribution when compared to observations. In particular, they did not suffer from the excessive thickening experienced by the MEB and EB in longer simulations. A spatial scaling analysis of the BBM and mEVP models, compared against RPGS-based observations was performed using the same method coarse-graining analysis method as in Marsan et al. (2004). The timescale used for the analysis was 3 days as in Rampal et al. (2019) (see Figure 4.1). The results are shown in Figure 4.9. We can see that the BBM-based model furnishes extremely good results on all the spatial scales, while the mEVP-based falls short at the shorter scales.

Determining the impact of sea-ice rheology on deformation statistics is complex, as factors like model configuration (e.g., numerical convergence, atmospheric representation,

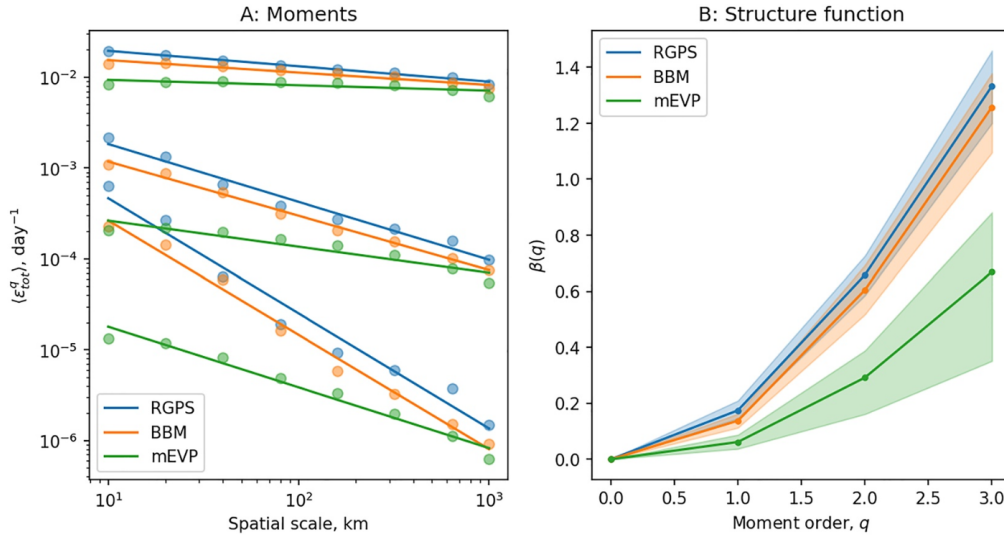


FIGURE 4.9: (a) Power-law fit (see Equation 4.2a) of the first three moments of the rate of the rate of deformation distribution over a 10 – 100 km range and (b) the corresponding fit of the spatial structure function β given by Equation 4.3a. Shown are the analyses based on (orange) neXtSIMv2 with the BBM, (green) mEVP and (blue) RGPS observations. The filled areas indicate the standard deviation from averaging moments from December 2006 to May 2007.

From Ólason et al. (2022).

spatial resolution) and physical parameterizations (e.g., ice strength parameters, ice thickness distribution) are equally influential. Therefore, attributing model performance exclusively to a particular rheological framework using current deformation metrics is not a straightforward task (Bouchat et al., 2022). However, the consistency of the above-mentioned deformation statistics obtained with the BBM rheology and the ones obtained with the mEVP rheology found in the Sea Ice Rheology Experiment (SIREx):1 (Bouchat et al., 2022) show that the source of heterogeneity (causing better statistics at the smaller scales) is physical and not due to these other factors (Ólason et al., 2022).

4.5 A timeline of sea ice brittle modeling

Building on the ideas in Marsan et al. (2004), Weiss and Marsan (2004), Schulson (2004), Schulson and Hibler (2004) and Weiss et al. (2007) Girard et al. (2011) proposed the elasto-brittle (EB) rheology. In this rheology, plasticity gave way to brittle behavior by introducing a damage propagation model. In this damage model, the sub-grid-scale is parametrized through a scalar variable, the damage level or fracture density, whose value changes whenever the local stress exceeds the Mohr-Coulomb failure criterion. These brittle rheologies are able to reproduce the observed properties of sea ice on both on the large-scale and at the finer scales including correct patterns of Linear Kinematic Features (LKFs).

The next step was taken by Dansereau (2016) with the development of the Maxwell-Elasto-Brittle model (MEB). In this approach ice is seen as a Maxwell (linear visco-elastic) medium fracturing in a brittle manner when a Mohr-Coulomb yield criterion is reached. This model differs from the previous EB model in that it is able to simulate the large and permanent deformations once the ice is fractured and fragmented (Ólason et al., 2022).

The EB and MEB rheologies have been tested on a broad range of spatial and temporal scales in the stand-alone large-scale sea ice model neXtSIM (Bouillon and Rampal, 2015b; Rampal et al., 2016; Rampal et al., 2019). Despite the generally satisfactory results obtained with the MEB rheology in the neXtSIM model, excessive convergence of highly damaged ice was observed (Rampal et al., 2019). To resolve this issue, Ólason et al. (2022) proposed the Bingham-Maxwell constitutive model (Bingham, 1922; Saramito, 2021) or BBM for short. Recently the BBM rheology has successfully been applied to a coupled ice-ocean sea ice model in a pan-Arctic simulation (Boutin et al., 2023). Figure 4.10 presents a timeline of the latest developments in the new brittle-based modeling approach.

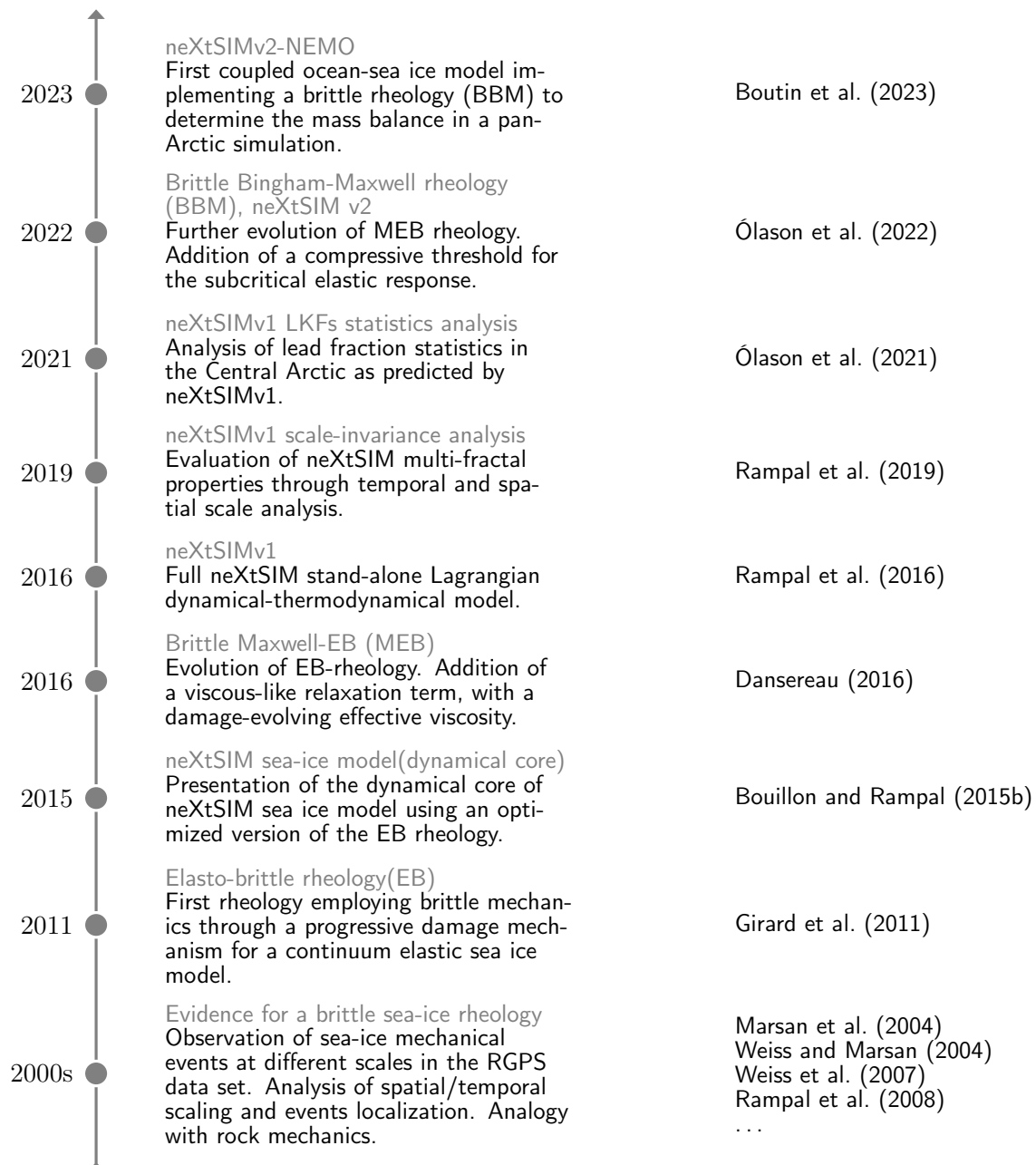


FIGURE 4.10: Timeline showing the ongoing research on Brittle rheologies and their implementation into the next generation sea-ice model (neXtSIM).

Chapter 5

Summary and concluding remarks

This thesis provides a review of the main approaches used to model sea ice mechanical behavior in a continuum framework, transitioning from traditional fluid-like models to state-of-the-art solid-like brittle models.

First, the physical components of sea-ice models, along with the underlying assumptions, were described. The variables used to describe the material state of the ice cover, e.g. thickness or concentration, follow a conservation equation taking into account their advection and the mechanical and thermodynamic (here not considered) changes to which they are subject. The chosen level of mechanical complexity determines also how ice is redistributed in the aftermath of deformation events. The atmosphere and the ocean force the ice causing it to drift and to deform. The key equation governing the kinematics of ice is the momentum equation. For the sea ice this equation contains terms for the external forces, i.e. air/water drags and the Coriolis force, as well as the internal forces, i.e. those stemming from the internal stress that has accumulated in the sea ice as a result of mechanical interactions throughout it. Figure 2.5 provides a graphical overview on how the physical components integrate inside a sea ice model.

After a review of the first historic efforts to model the drift of sea ice, the first rheological models were presented. The viscous rheologies schematize sea ice as a (linear) viscous fluid with a resistance to shear deformation given by the viscosity but without resistance to converging flow. These rheologies were found not to be very representative of ice mechanical behavior.

Plastic rheologies provide a more accurate description of sea ice mechanical behavior. The elastic-plastic (EP; Coon et al. 1974) and the viscous-plastic (VP; Hibler 1979) rheologies constitute two rheological models in which sea ice is assumed to deform in an elastic and viscous manner respectively, until a critical internal stress state is reached. In fact, the plastic rheologies are based on the concept of a yield curve. This is a curve in the stress space that defines which stress state a material can withstand before failing, i.e. before deforming plastically. How the ice state changes once such a stress state is reached is given by the prescription of a flow rule. The flow is normally chosen such that the plastic deformation is in the direction normal to the yield curve. Current climate models and operational modeling platforms are based on the VP rheology.

In the last two decades efforts have been made to correctly model the multifractal properties of sea ice in both space and time. These multifractal properties are known as heterogeneity and intermittency respectively. These requirements have been quantitatively evaluated by analyzing the spatial/temporal scale dependence of the statistical moments of the rate of deformation distribution as these are directly linked to the multifractality properties mentioned above.

Over the past two decades, there has been an acknowledgment of the similarity in the mechanical behavior between sea ice and the Earth's crust. The rocks in the Earth's crust deform in a manner closely resembling that described above. Additionally, the hypothesis of a cascading mechanism, in which local fracturing events propagate over extensive

distances through the ice cover, has been raised (e.g. Weiss and Marsan, 2004; Weiss et al., 2007; Schulson and Hibler, 2004). This recognition has prompted the implementation of elasto-brittle rheologies, a methodology already proven to be successful in rock mechanics (Amitrano et al., 1999), to the modeling of sea ice.

The Elasto-Brittle (EB; Girard et al. 2011) rheology considers the ice sheet as an elastic continuum with long-range interactions arising from a progressive damaging mechanism. The elastic stiffness evolves with the damage level accounted for in terms of a grid-scale dimensionless parameter that represents the concentration of fractures at the sub-grid scale. The neXtSIM model, based on the EB approach (Bouillon and Rampal, 2015b; Rampal et al., 2016), exhibits a greater ability to capture the spatial scaling of the deformation rate compared to the VP model.

The Maxwell-Elasto-Brittle (MEB; Dansereau 2016) extends the previous EB approach by adding an effective viscous behavior. Consequently, it can correctly represent large, permanent deformations, an aspect on which the EB model failed. The integration of MEB rheology in neXtSIM (Rampal et al., 2019) successfully managed to reproduce the observed intermittent nature of sea ice deformation. A behavior that was only weakly captured in the previous implementations using the EB rheology (Rampal et al., 2016).

The latest advancement in the realm of brittle rheology is the Brittle-Bingham-Maxwell rheology (BMM; Ólason et al. 2022). This model introduces a threshold for permanent deformations that prevents excessive thickening in extended simulations — a phenomenon observed in the MEB model.

The chronological evolution of the described sea ice brittle modeling advancements is illustrated in the timeline provided in Figure 4.10.

The field of sea ice modeling is still very much a work in progress. The most advanced sea-ice models based on brittle rheologies have shown to be successful of reproducing small-scale features. This raised the question of how the presence of these features impacts the ice-ocean and ice-atmosphere interactions in these models. Studies to answer this question have already been initiated using the neXtSIMv2 model (e.g. Boutin et al., 2023). Given the ability of sea ice to inhibit the heat transfer from atmosphere to the ocean and vice-versa, and the importance of this process for accurate climate forecasts, we expect the study of these interactions to be one of the major focus points for sea ice modeling research in the next years.

Another challenge in sea ice rheology research is the creation of parameterizations that accurately capture the relationship between the mechanical strength of large-scale ice cover (10–100 km) and its granular concentration and fracturing at the small scale (< 10 km; see Figure 4.3). Development of such parametrizations will allow the rheological framework to effectively represent the spatial and temporal mechanical transition between a densely packed, brittle ice pack and a loosely aggregated formation of ice floes, resembling the Marginal Ice Zone, i.e. the transitional zone between open sea and dense drift ice.

Appendix A

Discontinuous Galerkin solver in sea ice modeling

Solution to the partial differential equations discussed in this work are in operational practice approximated by numerical methods. A plethora of numerical schemes is available to find the approximation. For instructional purpose, we will present how approximations to the solutions of the conservation (see e.g. Equation 2.22) and advection equations (see Equation 2.21) can be found using one such scheme: the discontinuous Galerkin method.

A.1 Continuity equation

The continuity equation for sea ice thickness on domain $\Omega \subset \mathbb{R}^N$ with boundary $\partial\Omega$ is given by

$$\frac{\partial h}{\partial t} = -\nabla \cdot (\mathbf{u}h).$$

Let $\{\Omega_m : 1 \leq m \leq M\}$ be a grid mesh of open grid cells for Ω such that their closure $\bar{\Omega}_m$ satisfies $\bigcup_{m=1}^M \bar{\Omega}_m = \Omega$ and $\Omega_m \cap \Omega_l$ is negligible in \mathbb{R}^N if $m \neq l$. For the discontinuous Galerkin formulation we are seeking an approximation $h_V \in V \subset L(\Omega)$ such that $\forall \psi$ in some function vector space V of functions that are continuous on Ω_m for each $1 \leq m \leq M$ and for velocity $\mathbf{u} \in W \stackrel{def}{=} V^N$ the following holds

$$\int_{\Omega} \psi \frac{\partial h_V}{\partial t} \, d\mathbf{x} = - \int_{\Omega} \psi \nabla \cdot (\mathbf{u}_W h_V) \, d\mathbf{x} \quad (\text{A.1})$$

$$\frac{\partial}{\partial t} \int_{\Omega} \psi h_V \, d\mathbf{x} = - \int_{\Omega} \psi \nabla \cdot (\mathbf{u}_W h_V) \, d\mathbf{x} \quad (\text{A.2})$$

$$\frac{\partial}{\partial t} \sum_{m=1}^M \int_{\Omega_m} \psi h_V \, d\mathbf{x} = \sum_{m=1}^M - \int_{\Omega_m} \psi \nabla \cdot (\mathbf{u}_W h_V) \, d\mathbf{x} \quad (\text{A.3})$$

$$\frac{\partial}{\partial t} \sum_{m=1}^M \int_{\Omega_m} \psi h_V \, d\mathbf{x} = \sum_{m=1}^M \int_{\Omega_m} \nabla \psi \cdot \mathbf{u}_W h_V \, d\mathbf{x} - \sum_{m=1}^M \int_{\partial\Omega_m} \mathbf{n}|_{\partial\Omega_m} \cdot (\mathbf{u}_W h_V) \psi \, dS \quad (\text{A.4})$$

$$\begin{aligned} \frac{\partial}{\partial t} \sum_{m=1}^M \int_{\Omega_m} \psi h_V \, d\mathbf{x} &= \sum_{m=1}^M \int_{\Omega_m} \nabla \psi \cdot \mathbf{u}_W h_V \, d\mathbf{x} \\ &\quad - \sum_{m=1}^M \sum_{l=m+1}^M \int_{\partial\Omega_m \cap \partial\Omega_l} (\mathbf{u}_W h_V)|_{\partial\Omega_m \cap \partial\Omega_l} \cdot ((\mathbf{n}\psi)|_{\partial\Omega_m} + (\mathbf{n}\psi)|_{\partial\Omega_l}) \, dS \\ &\quad - \sum_{m=1}^M \int_{\partial\Omega_m \cap \partial\Omega} (\mathbf{u}_W h_V)|_{\partial\Omega} \cdot \mathbf{n}|_{\partial\Omega} \psi \, dS. \end{aligned} \quad (\text{A.5})$$

Here $(\mathbf{u}_W h_V)|_{\partial\Omega}$ is prescribed by the boundary conditions on the domain boundary $\partial\Omega$. $\mathbf{n}|_{\partial\Omega_m}$ is the outward pointing normal to the boundary of grid cell m and $\mathbf{n}_{\partial\Omega}$ the outward pointing normal to the domain. If $\partial\Omega_m \cap \partial\Omega_l \neq \emptyset$ the normal to the grid cell boundary satisfies $\mathbf{n}|_{\partial\Omega_m} = -\mathbf{n}|_{\partial\Omega_l}$ and so $(\mathbf{n}\psi)|_{\partial\Omega_m} + (\mathbf{n}\psi)|_{\partial\Omega_l} = \mathbf{n}|_{\Omega_m} (\psi|_{\partial\Omega_m} - \psi|_{\partial\Omega_l}) \stackrel{def}{=} \mathbf{n}|_{\Omega_m} \{\{\psi\}\}_{\partial\Omega_m}$. Since \mathbf{u}_W, h_V might contain discontinuities at the grid cell boundaries, $(\mathbf{u}_W h_V)|_{\partial\Omega_m \cap \partial\Omega_l}$ is not unambiguously defined. Here we decide to define it using the upwind flux, i.e.

$$(\mathbf{u}_W h_V)|_{\partial\Omega_m \cap \partial\Omega_l} = \begin{cases} (\mathbf{u}_W h_V)|_{\partial\Omega_m} & \text{if } \langle \mathbf{u}_W \rangle \cdot \mathbf{n}|_{\Omega_m} \geq 0 \\ (\mathbf{u}_W h_V)|_{\partial\Omega_l} & \text{if } \langle \mathbf{u}_W \rangle \cdot \mathbf{n}|_{\Omega_m} < 0 \end{cases} \quad (\text{A.6})$$

with $\langle \mathbf{u} \rangle = \frac{1}{2}(\mathbf{u}|_{\partial\Omega_m} + \mathbf{u}|_{\partial\Omega_l})$.

A.1.1 Finite dimensional approximation

If we assume V to be a finite dimensional space, we can choose a basis for it,

$$\{\psi_d\}_{d=1}^D \stackrel{def}{=} \{\psi_1, \dots, \psi_D\},$$

allowing us to expand the unknown thickness function in terms of its elements:

$$h_V = \sum_{k=1}^D c_k \psi_k$$

where the expansion coefficients $c_k = c_k(t)$ depend on time whereas the basis functions $\psi_d = \psi_d(\mathbf{x})$ depend on space. The formulation in Equation A.5 has to hold for any arbitrary function $\psi \in V$. As Equation A.5 is linear in ψ , this is equivalent to requiring it to hold for any basis function ψ_d with $1 \leq d \leq D$.

Inserting the expansion for h_V into the weak formulation of the conservation equation A.5 yields a system of ordinary differential equations for c_k :

$$\mathbf{M} \frac{d}{dt} \mathbf{c} = \mathbf{S} \mathbf{c} + \mathbf{f} \quad (\text{A.7})$$

with \mathbf{c} a vector consisting of the coefficients c_1, \dots, c_D and the elements of the matrices \mathbf{M}, \mathbf{S} and vector \mathbf{f} are given by

$$\begin{aligned} \mathbf{M}_{dk} &= \sum_{m=1}^M \int_{\Omega_m} \psi_d \psi_k \, d\mathbf{x} \\ \mathbf{S}_{dk} &= \sum_{m=1}^M \int_{\Omega_m} \nabla \psi_d \cdot (\mathbf{u}_W \psi_k) \, d\mathbf{x} \\ &\quad - \sum_{m=1}^M \sum_{l=m+1}^M \int_{\partial\Omega_m \cap \partial\Omega_l} (\psi_k \mathbf{u}_W)|_{\partial\Omega_m \cap \partial\Omega_l} \cdot \mathbf{n}|_{\partial\Omega_m} \{\{\psi_d\}\}_{\partial\Omega_m} \, dS \\ \mathbf{f}_d &= - \sum_{m=1}^M \int_{\partial\Omega} \psi_d (h \mathbf{u}_W)|_{\partial\Omega} \cdot \mathbf{n}|_{\partial\Omega} \, dS \end{aligned}$$

with $d = 1, \dots, D$ and $(\psi_k \mathbf{u}_W)|_{\partial\Omega_m \cap \partial\Omega_l}$ given by Equation A.6. Basis functions are usually selected to have their support within a single grid cells which simplifies the integrals above.

At this point a numerical approximation for $\frac{d}{dt}\mathbf{c}$ needs to be chosen. In this example we pick Euler forward $\frac{d}{dt}\mathbf{c}(t) \approx \frac{\mathbf{c}(t+\Delta t) - \mathbf{c}(t)}{\Delta t}$ with Δt the time step. In that case Equation A.7 becomes

$$\mathbf{M}\mathbf{c}(t + \Delta t) = \mathbf{M}\mathbf{c}(t) + \Delta t\mathbf{S}\mathbf{c}(t) + \Delta t\mathbf{f} \quad (\text{A.8})$$

which can be solved for $\mathbf{c}(t + \Delta t)$ given $\mathbf{c}(t)$ using conventional linear algebra methods. The linear system for other time-stepping methods can be derived in a similar way.

A.1.2 Advection equation

The advection equation for an arbitrary ice parameter $J \in \mathcal{J}$ is given by

$$S_J = \frac{DJ}{Dt} \stackrel{\text{def}}{=} \frac{\partial J}{\partial t} + \mathbf{u} \cdot \nabla J = \frac{\partial J}{\partial t} + \nabla \cdot (\mathbf{u}J) - (\nabla \cdot \mathbf{u})J$$

Again let $\Omega = \bigcup_{m=1}^M \bar{\Omega}_m$, $\Omega_m \cap \Omega_l = \emptyset$ if $m \neq l$ and let V, W be function spaces of functions (possibly different from those in the previous section) that are piecewise continuous on $\bar{\Omega}_m : \forall 1 \leq m \leq M$. Introduce the variable $q = \nabla \cdot \mathbf{u}$. For the discontinuous Galerkin approximation of the advection equation we search for $J_V \in V$, $q_W \in W$ such that $\forall \psi_V \in V$ and $\forall \psi_W \in W$

$$\int_{\Omega} \psi_V S_J \, d\mathbf{x} = \int_{\Omega} \psi_V \frac{\partial J_V}{\partial t} \, d\mathbf{x} + \int_{\Omega} \psi_V \nabla \cdot (\mathbf{u}J_V) \, d\mathbf{x} - \int_{\Omega} \psi_V q_W J_V \, d\mathbf{x} \quad (\text{A.9})$$

$$0 = \int_{\Omega} \psi_W q_W \, d\mathbf{x} - \int_{\Omega} \psi_W \nabla \cdot \mathbf{u} \, d\mathbf{x} \quad (\text{A.10})$$

Applying Gauss divergence theorem to Equation A.10 gives

$$\begin{aligned} 0 &= \sum_{m=1}^M \int_{\Omega_m} \psi_W q_W \, d\mathbf{x} - \sum_{m=1}^M \int_{\Omega_m} \psi_W \nabla \cdot \mathbf{u} \, d\mathbf{x} \\ &= \sum_{m=1}^M \int_{\Omega_m} (\psi_W q_W + \nabla \psi_W \cdot \mathbf{u}) \, d\mathbf{x} - \sum_{m=1}^M \int_{\partial\Omega_m} (\psi_W \mathbf{n} \cdot \mathbf{u})|_{\Omega_m} \, dS \\ &= \sum_{m=1}^M \int_{\Omega_m} (\psi_W q_W + \nabla \psi_W \cdot \mathbf{u}) \, d\mathbf{x} \\ &\quad - \sum_{m=1}^M \sum_{l=m+1}^M \int_{\partial\Omega_m \cup \partial\Omega_l} (\{\{\psi_W\}\} \mathbf{n})|_{\partial\Omega_m} \cdot \mathbf{u}|_{\partial\Omega_m \cap \partial\Omega_l} \, dS \\ &\quad - \sum_{m=1}^M \int_{\partial\Omega \cap \partial\Omega_m} \psi_W \mathbf{n}|_{\partial\Omega_m} \cdot \mathbf{u}|_{\partial\Omega} \, dS. \end{aligned} \quad (\text{A.11})$$

Here $\mathbf{u}|_{\partial\Omega}$ is given by the boundary conditions. Once again we use the upwind flux, but this time to define the velocity on the cell boundaries, i.e.

$$\mathbf{u}|_{\partial\Omega_m \cap \partial\Omega_l} \begin{cases} \mathbf{u}|_{\partial\Omega_m} & \text{if } \mathbf{n}|_{\partial\Omega_m} \cdot \langle \mathbf{u} \rangle|_{\partial\Omega_m} \geq 0 \\ \mathbf{u}|_{\partial\Omega_l} & \text{otherwise} \end{cases} \quad (\text{A.12})$$

The 1st and 2nd term in Equation A.9 are the same as those in Equation A.1 after substituting h_V with J_V . So, Equation A.9 can be rewritten as

$$\begin{aligned}
0 &= \frac{\partial}{\partial t} \sum_{m=1}^M \int_{\Omega_m} \psi_V J_V \, d\mathbf{x} - \sum_{m=1}^M \int_{\Omega_m} \nabla \psi_V \cdot \mathbf{u}_W J_V \, d\mathbf{x} \\
&+ \sum_{m=1}^M \sum_{l=m+1}^M \int_{\partial\Omega_m \cap \partial\Omega_l} (\mathbf{u} J_V)|_{\partial\Omega_m \cap \partial\Omega_l} \cdot (\{\{\psi_V\}\}\mathbf{n})|_{\partial\Omega_m} \, dS \\
&+ \sum_{m=1}^M \int_{\partial\Omega_m \cap \partial\Omega} (\mathbf{u} J_V)|_{\partial\Omega} \cdot \psi_V \mathbf{n}|_{\partial\Omega} \, dS \\
&- \sum_{m=1}^M \int_{\Omega_m} \psi_V [q_W J_V + S_J] \, d\mathbf{x}.
\end{aligned}$$

A.1.3 Finite dimensional approximation

Similar to what is done in A.1.1, we assume that $V = W$ and that V is a finite-dimensional function space with bases ψ_1, \dots, ψ_D . In that case, J_V and q_W can be expanded as $J_V = \sum_{d=1}^D c_d \psi_d$ and $q_W = \sum_{d=1}^D p_d \psi_d$. Inserting this into Equation A.10 gives

$$\begin{aligned}
\mathbf{S}^q \mathbf{p} &= \mathbf{f}^q \\
(\mathbf{S}^q)_{pk} &= \sum_{m=1}^M \int_{\Omega_m} \psi_p \psi_k \, d\mathbf{x} \\
(\mathbf{f}^q)_p &= \sum_{m=1}^M \sum_{l=m+1}^M \int_{\partial\Omega_m \cup \partial\Omega_l} (\{\{\psi_p\}\}\mathbf{n})|_{\partial\Omega_m} \cdot \mathbf{u}|_{\partial\Omega_m \cap \partial\Omega_l} \, dS \\
&+ \sum_{m=1}^M \int_{\partial\Omega \cap \partial\Omega_m} \psi_p \mathbf{n}|_{\partial\Omega_m} \cdot \mathbf{u}|_{\partial\Omega} \, dS - \sum_{m=1}^M \int_{\Omega_m} \nabla \psi_p \cdot \mathbf{u}
\end{aligned}$$

with \mathbf{p} the vector having p_1, \dots, p_D as its components.

Similarly, Equation A.13 becomes

$$\begin{aligned}
\mathbf{M}^J \frac{d}{dt} \mathbf{c} &= \mathbf{S}^J \mathbf{c} + \mathbf{p} \cdot \mathbf{T} \mathbf{c} + \mathbf{f}^J \\
(\mathbf{M}^J)_{dk} &= \sum_{m=1}^M \int_{\Omega_m} \psi_d \psi_k \, d\mathbf{x} \\
(\mathbf{S}^J)_{dk} &= \sum_{m=1}^M \int_{\Omega_m} \nabla \psi_d \cdot \mathbf{u}_W \psi_k \, d\mathbf{x} \\
&\quad - \sum_{m=1}^M \sum_{l=m+1}^M \int_{\partial\Omega_m \cap \partial\Omega_l} (\mathbf{u} \psi_k)|_{\partial\Omega_m \cap \partial\Omega_l} \cdot (\{\psi_d\} \mathbf{n})|_{\partial\Omega_m} \, dS \\
&\quad - \sum_{m=1}^M \int_{\partial\Omega_m \cap \partial\Omega} (\mathbf{u} \psi_k)|_{\partial\Omega} \cdot \psi_d \mathbf{n}|_{\partial\Omega} \, dS \\
(\mathbf{T}^J)_{bdk} &= \sum_{m=1}^M \int_{\Omega_m} \psi_d \psi_b \psi_k \, d\mathbf{x} \\
(\mathbf{f}^J)_d &= \sum_{m=1}^M \int_{\Omega_m} \psi_d S_J \, d\mathbf{x}
\end{aligned}$$

with \mathbf{c} the vector having c_1, \dots, c_D as components.

Inserting an approximation for the time-derivative e.g. the Euler forward $\frac{d}{dt} \mathbf{c}(t) \approx \frac{\mathbf{c}(t+\Delta t) - \mathbf{c}(t)}{\Delta t}$ gives

$$\begin{aligned}
\mathbf{S}^q \mathbf{p}(t) &= \mathbf{f}^q(t) \\
\mathbf{M}^J \mathbf{c}(t + \Delta t) &= \mathbf{M}^J \mathbf{c}(t) + \Delta t \mathbf{S}^J \mathbf{c}(t) + \Delta t \mathbf{p}(t) \cdot \mathbf{T}^J \mathbf{c}(t) + \Delta t \mathbf{f}^J(t). \quad (\text{A.13})
\end{aligned}$$

These equations can be solved one after another for $\mathbf{p}(t)$ and $\mathbf{c}(t + \Delta t)$ respectively using linear algebra methods. In case an implicit time-solver is used the 3rd term on the right-hand side of Equation A.13 becomes nonlinear $\mathbf{p}(t + \Delta t) \cdot \mathbf{T}^J \mathbf{c}(t + \Delta t)$. In this case a nonlinear solver, like a Gauss-Newton method, needs to be employed to solve for $\mathbf{p}(t + \Delta t)$ and $\mathbf{c}(t + \Delta t)$ complicating things somewhat.

Ringraziamenti

Desidero esprimere la mia sincera gratitudine al mio relatore, Alberto Carrassi, per avermi aperto le porte verso un tema così affascinante come quello della modellizzazione climatica e della Data Assimilation e per avermi permesso di entrare in contatto con una bellissima realtà di ricerca quale è SASIP. Difficile aspettarsi una tale fiducia riposta nei miei confronti dopo così poco tempo.

Allo stesso modo un sentito ringraziamento va al mio correlatore, Ivo Pasmans, per avermi costantemente seguito in questo lungo percorso, dedicandomi un enorme quantità del suo tempo e contribuendo in maniera decisiva nella realizzazione di questo lavoro. L'esperienza acquisita durante questi mesi grazie ai vostri consigli ed insegnamenti mi ha profondamente arricchito.

Ringrazio sentitamente i miei genitori per tutto quello che hanno fatto per me durante questi anni e per essere stati una costante fonte di supporto. Vi ringrazio per l'importanza che avete sempre dato al mio percorso di studi, permettendomi di raggiungere questo traguardo.

Ringrazio tanto le mie nonne, per il loro costante aiuto e per avere sempre tifato per me in ogni possibile occasione. Mi fate sentire davvero speciale, sono fortunato ad avervi. Ringrazio anche i miei zii, per avermi sempre supportato e creduto in me.

Ci tengo a ringraziare tutti i miei amici, che hanno rappresentato una componente fondamentale nella mia vita e, di conseguenza, nel raggiungimento di questo obiettivo. Un ringraziamento particolare va a

Daniele, per essere stato un amico vero, con cui parlare di tutto, da sempre;

Luca, per essere diventato un amico degno di questo nome, nonostante il poco tempo da cui ci conosciamo;

Filippo e Francesco, per l'inestimabile aiuto ricevuto durante questo percorso, a cui andrebbe dato un pezzo di questa Laurea;

Marco, per l'ultimo anno trascorso sotto lo stesso tetto, ricco di emozioni, ma soprattutto di risate, che hanno reso l'esperienza bolognese alquanto memorabile;

Arturo, per la sua bontà nell'aiutare nel momento del bisogno, dalla calcolatrice ad Elettromagnetismo all'aiuto per la realizzazione di molte immagini presenti in questa tesi.

Un ringraziamento speciale va a te Giu, con cui ho condiviso tantissimo in questi tre anni. Spero che questo sia solo il primo importante traguardo che raggiungeremo insieme. La tua importanza per me è difficilmente spiegabile a parole.

Grazie a tutti

Bibliography

- Amitrano, David (2003). “Brittle-ductile transition and associated seismicity: Experimental and numerical studies and relationship with the b value”. In: *Journal of Geophysical Research: Solid Earth* 108 (B1).
- Amitrano, David, Jean-Robert Grasso, and Didier Hantz (1999). “From diffuse to localised damage through elastic interaction”. In: *Geophysical Research Letters* 26.14, pp. 2109–2112.
- Aranson, Igor S. and Lev S. Tsimring (June 2006). “Patterns and collective behavior in granular media: Theoretical concepts”. In: *Rev. Mod. Phys.* 78.2, pp. 641–692.
- Barnes, H.A., J.F. Hutton, and K. Walters (1989). *An Introduction to Rheology*. Rheology Series. Elsevier Science.
- Bingham, E.C. (1922). *Fluidity and Plasticity*. McGraw-Hill.
- Bouchat, A. et al. (2022). “Sea Ice Rheology Experiment (SIREx): 1. Scaling and Statistical Properties of Sea-Ice Deformation Fields”. In: *Journal of Geophysical Research: Oceans* 127.4, e2021JC017667.
- Bouillon, S. and P. Rampal (2015a). “On producing sea ice deformation data sets from SAR-derived sea ice motion”. In: *The Cryosphere* 9.2, pp. 663–673.
- Bouillon, S. and P. Rampal (July 1, 2015b). “Presentation of the dynamical core of neXtSIM, a new sea ice model”. In: *Ocean Modelling* 91, pp. 23–37.
- Bouillon, S. et al. (2009). “An elastic–viscous–plastic sea ice model formulated on Arakawa B and C grids”. In: *Ocean Modelling* 27.3, pp. 174–184.
- Bouillon, S. et al. (2013). “The elastic–viscous–plastic method revisited”. In: *Ocean Modelling* 71, pp. 2–12.
- Boutin, G. et al. (2023). “Arctic sea ice mass balance in a new coupled ice–ocean model using a brittle rheology framework”. In: *The Cryosphere* 17.2, pp. 617–638.
- Brown, R.A. (1980). *Boundary-layer modeling for AIDJEX*. R.S. Pritchard. Sea Ice Processes and Models.
- Cabaniss, G.H., K.L. Hunkins, and N. Untersteiner (1965). “US-IGY Drifting Station Alpha, Arctic Ocean 1957-1958”. In: *Air Force Cambridge Research Laboratories, Special Reports* 38.
- Çakir, Ziyadin et al. (Dec. 2012). “Onset of aseismic creep on major strike slip faults”. In: *Geology* 40, pp. 1115–1118.
- Campbell, William J. (1965). “The wind-driven circulation of ice and water in a polar ocean”. In: *Journal of Geophysical Research (1896-1977)* 70.14, pp. 3279–3301.
- Campbell, William J. and L.A. Rasmussen (1972). “A numerical model for sea ice dynamics incorporating three alternative ice constitutive laws”. In: *Sea ice Proceedings*. Intern. Conf. Reykjavik. Iceland, pp. 176–87.
- Cheddadi, I. et al. (Oct. 1, 2008). “Numerical modelling of foam Couette flows”. In: *The European Physical Journal E* 27.2, pp. 123–133.
- Coon, M.D. (Apr. 1974). “Mechanical Behavior of Compacted Arctic Ice Floes”. In: *Journal of Petroleum Technology* 26.4, pp. 466–470.
- Coon, M.D. and R.S. Pritchard (1974). “Application of an elastic-plastic model of Arctic pack ice”. In: *The Coast and Shelf of the Beaufort Sea. Arctic Institute fo North America*, pp. 173–193.

- Coon, M.D. et al. (1974). "Modeling the pack ice as an elastic-plastic material". In: *AIDJEX Bulletin* 24, pp. 1–105.
- Coon, M.D. et al. (Nov. 2007). "Arctic Ice Dynamics Joint Experiment (AIDJEX) assumptions revisited and found inadequate". In: *J. Geophys. Res* 112.
- Coulomb, C.A. (1776). *Essai sur une application des regles de maximis & minimis a quelques problemes de statique: relatifs a l'architecture*. Vol. 7. Paris: Mémoires de Mathématique de l'Académie Royale des Sciences. 39 pp.
- Cushman-Roisin, Benoit (1994). *Introduction to geophysical fluid dynamics*. Englewood Cliffs, NJ, USA: Prentice Hall. 320 pp.
- Dansereau, V. (2016). "A Maxwell-Elasto-Brittle model for the drift and deformation of sea ice". PhD thesis. Grenoble, France: Université Grenoble Alpes.
- Dansereau, V. et al. (2016). "A Maxwell-elasto-brittle rheology for sea ice modelling". In: *The Cryosphere* 10, pp. 1339–1359.
- Dansereau, V. et al. (2017). "Ice bridges and ridges in the Maxwell-EB sea ice rheology". In: *The Cryosphere* 11.5, pp. 2033–2058.
- Doronin, Yu. P. (1970). "K Metodike Rascheta Splochennostii Dreifa L'dov.(On a method of calculating the compactness and drift of ice floes)." In: *AIDJEX Bulletin 3 (Originally In: Tr. Arkt. Antarkt. Nauch. Issled. Vol. 291, pp. 5-17.)*, pp. 22–39.
- Drucker, D.C. (1950). "Some implications of work hardening and ideal plasticity". In: 7, pp. 411–18.
- Duval, P., M. F. Ashby, and I. Anderman (Oct. 1, 1983). "Rate-controlling processes in the creep of polycrystalline ice". In: *J. Phys. Chem.* 87.21. Publisher: American Chemical Society, pp. 4066–4074.
- Ekman, V. W. (1902). "On the influence of the Earth's rotation on wind currents in the ocean (Om jordrotationens inverkan på vindströmmar i hafvet)". In: *Nyt Magazine for Naturvidenskab* 40.
- Ekman, V. W. (1905). "On the Influence of the Earth's Rotation on Ocean-Currents." In: *Arkiv. Matem., Astr. Fysik(Stockholm)*, p. 53.
- Erlingsson, Björn (Jan. 1988). "Two-Dimensional Deformation Patterns in Sea Ice". In: *Journal of Glaciology* 34, pp. 301–308.
- Feltham, D. (2008). "Sea Ice Rheology". In: *Annual Review of Fluid Mechanics* 40.1, pp. 91–112.
- Felzenbaum, A.I. (1958). "The theory of the steady drift of ice and the calculation of the long period mean drift in the central part of the Arctic basin". In: *Problems of the North* 2, pp. 5–15, 13–44.
- Gill, Adrian E. (1982). *Atmosphere-ocean dynamics*. Vol. 30. International geophysics series. Orlando, FL, USA: Academic Press. 662 pp.
- Girard, L. et al. (2009). "Evaluation of high-resolution sea ice models on the basis of statistical and scaling properties of Arctic sea ice drift and deformation". In: *Journal of Geophysical Research: Oceans* 114 (C8).
- Girard, L. et al. (2011). "A new modeling framework for sea-ice mechanics based on elasto-brittle rheology". In: *Annals of Glaciology* 52.57, pp. 123–132.
- Glen, J.W. (1970). "Thoughts on a Viscous Model for Sea Ice". In: *AIDJEX Bulletin* 2, pp. 18–27.
- Gray, J. M. N. T. and L. W. Morland (1994). "A two-dimensional model for the dynamics of sea ice". In: *Philosophical Transactions of the Royal Society of London. Series A: Physical and Engineering Sciences* 347.1682, pp. 219–290.
- Grobe, Amanda and Hannes Grobe (2007). *Section through an ice floe with parameters used in glaciological research to quantify and describe the coverage of sea ice*. URL: https://upload.wikimedia.org/wikipedia/commons/7/7c/Ice-floe_params_hg.png.

- Gudkovich, ZM and E.G. Nikiforov (1963). “Steady drift of a single ice floe”. In: *Tr. Arkt. Antarkt.* 253.
- Haapala, Jari (2000). “On the modelling of ice-thickness redistribution”. In: *Journal of Glaciology* 46.154. Publisher: Cambridge University Press, pp. 427–437.
- Hibler, W.D. (1974). “Differential sea-ice drift II. Comparison of mesoscale strain measurements to linear drift theory predictions”. In: *Journal of Glaciology* 13.69.
- Hibler, W.D. (1977). “A viscous sea ice law as a stochastic average of plasticity”. In: *Journal of Geophysical Research (1896-1977)* 82.27, pp. 3932–3938.
- Hibler, W.D. (1979). “A dynamic thermodynamic sea ice model”. In: *Journal of Physical Oceanography* 9.4, pp. 815–846.
- Hibler, W.D. (1980). “Modeling a Variable Thickness Sea Ice Cover”. In: *Monthly Weather Review. American Meteorological Society* 108.12, pp. 1943–1973.
- Hibler, W.D. and E.M. Schulson (2000). “On modeling the anisotropic failure and flow of flawed sea ice”. In: *Journal of Geophysical Research: Oceans* 105 (C7), pp. 17105–17120.
- Hopkins, Mark A. (1998). “Four stages of pressure ridging”. In: *Journal of Geophysical Research: Oceans* 103 (C10), pp. 21883–21891.
- Horvat, C. and E. Tziperman (2015). “A prognostic model of the sea-ice floe size and thickness distribution”. In: *The Cryosphere* 9.6, pp. 2119–2134.
- Hunke, E. and J. K. Dukowicz (Sept. 1, 1997). “An Elastic–Viscous–Plastic Model for Sea Ice Dynamics”. In: *Journal of Physical Oceanography* 27.9. Publisher: American Meteorological Society Section: Journal of Physical Oceanography, pp. 1849–1867.
- Hunke, E. et al. (2017). *CICE, The Los Alamos Sea Ice Model, Version 00*. URL: <https://www.osti.gov/biblio/1364126>.
- Hunter, S. C. (1983). *Mechanics of continuous media*. 2nd Edition. Chichester, Ellis Horwood Ltd.
- Hutchings, J. et al. (2011). “Spatial and temporal characterization of sea-ice deformation”. In: *Annals of Glaciology* 52.57, pp. 360–368.
- Hutter, N. and M. Losch (2020). “Feature-based comparison of sea ice deformation in lead-permitting sea ice simulations”. In: *The Cryosphere* 14.1, pp. 93–113.
- Hutter, N. et al. (2022). “Sea Ice Rheology Experiment (SIREx): 2. Evaluating Linear Kinematic Features in High-Resolution Sea Ice Simulations”. In: *Journal of Geophysical Research: Oceans* 127.4, e2021JC017666.
- Jop, Pierre, Yoël Forterre, and Olivier Pouliquen (June 1, 2006). “A constitutive law for dense granular flows”. In: *Nature* 441.7094, pp. 727–730.
- Kagan, Y. Y. and L. Knopoff (Aug. 1980). “Spatial distribution of earthquakes: the two-point correlation function”. In: *Geophysical Journal* 62.2, pp. 303–320.
- Kemeny, J. and N. G. W. Cook (Jan. 1986). “Effective moduli, non-linear deformation and strength of a cracked elastic solid”. In: *International Journal of Rock Mechanics and Mining Sciences and Geomechanics Abstracts* 23.2, pp. 107–118.
- Kheisin, D.Y. and V.O. Ivchenko (1973). “A numerical model of tidal ice drift with allowance for the interaction between floes”. In: *Izv. Atmos. Oceanic Phys.* 9.4, pp. 420–29.
- Kimmritz, M., S. Danilov, and M. Losch (May 1, 2016). “The adaptive EVP method for solving the sea ice momentum equation”. In: *Ocean Modelling* 101, pp. 59–67.
- Kolmogorov, A. N. (1962). “A refinement of previous hypotheses concerning the local structure of turbulence in a viscous incompressible fluid at high Reynolds number”. In: *Journal of Fluid Mechanics* 13.1, pp. 82–85.
- Kwok, R. (1998). “The RADARSAT Geophysical Processor System”. In: *Analysis of SAR Data of the Polar Oceans: Recent Advances*. Berlin, Heidelberg: Springer Berlin Heidelberg, pp. 235–257.

- Kwok, R. (2001). “Deformation of the Arctic Ocean Sea Ice Cover between November 1996 and April 1997: A Qualitative Survey”. In: *IUTAM Symposium on Scaling Laws in Ice Mechanics and Ice Dynamics*. Ed. by J. P. Dempsey and H. H. Shen. Dordrecht: Springer Netherlands, pp. 315–322.
- Kwok, R. et al. (1998). “Sea ice motion from satellite passive microwave imagery assessed with ERS SAR and buoy motions”. In: *Journal of Geophysical Research: Oceans* 103 (C4), pp. 8191–8214.
- Kwok, R. et al. (2008). “Variability of sea ice simulations assessed with RGPS kinematics”. In: *Journal of Geophysical Research: Oceans* 113 (C11).
- Laikhtman, D.L. (1958). “The drift of ice fields (O dreife ledianykh polei)”. In: *Gidrometeorologicheskii Institut, Trudy, Leningrad*.
- Lemieux, Jean-François et al. (2010). “Improving the numerical convergence of viscoplastic sea ice models with the Jacobian-free Newton–Krylov method”. In: *Journal of Computational Physics* 229.8, pp. 2840–2852.
- Lemieux, Jean-François et al. (2015). “A basal stress parameterization for modeling land-fast ice”. In: *Journal of Geophysical Research: Oceans* 120.4, pp. 3157–3173.
- Leppäranta, M. (2011). *The Drift of Sea Ice*. Second Edition. Springer-Praxis.
- Lindsay, R. and H. Stern (2003). “The RADARSAT Geophysical Processor System: Quality of Sea Ice Trajectory and Deformation Estimates”. In: *Journal of Atmospheric and Oceanic Technology* 20.9, pp. 1333–1347.
- Lindsay, R., J. Zhang, and D.A. Rothrock (2003). “Sea-ice deformation rates from satellite measurements and in a model”. In: *Atmosphere-Ocean* 41.1, pp. 35–47.
- Lovejoy, Shaun and Daniel Schertzer (2007). “Scale, Scaling and Multifractals in Geophysics: Twenty Years on”. In: *Nonlinear Dynamics in Geosciences*. New York, NY: Springer New York, pp. 311–337.
- Lubliner, J. (2008). *Plasticity Theory*. Dover books on engineering. Dover Publications.
- Lyakhovskiy, Vladimir, Yehuda Ben-Zion, and Amotz Agnon (1997). “Distributed damage, faulting, and friction”. In: *Journal of Geophysical Research: Solid Earth* 102 (B12), pp. 27635–27649.
- Marsan, D. and J. Weiss (Aug. 2010). “Space/time coupling in brittle deformation at geophysical scales”. In: *Earth and Planetary Science Letters* 296.3, pp. 353–359.
- Marsan, D. et al. (Oct. 2004). “Scale Dependence and Localization of the Deformation of Arctic Sea Ice”. In: *Phys. Rev. Lett.* 93.17, p. 178501.
- Marsan, D. et al. (2011). “Low-frequency bursts of horizontally polarized waves in the Arctic sea-ice cover”. In: *Journal of Glaciology* 57.202, pp. 231–237.
- Matsushita, Mitsugu (1985). “Fractal Viewpoint of Fracture and Accretion”. In: *Journal of the Physical Society of Japan* 54.3, pp. 857–860.
- Maxwell, James Clerk (1867). “IV. On the dynamical theory of gases”. In: *Philosophical Transactions of the Royal Society of London* 157, pp. 49–88.
- Maykut, G.A. (1982). “Large-scale heat exchange and ice production in the central Arctic”. In: *Journal of Geophysical Research: Oceans* 87 (C10), pp. 7971–7984.
- Maykut, G.A. and N. Untersteiner (1971). “Some results from a time-dependent thermodynamic model of sea ice”. In: *Journal of Geophysical Research (1896-1977)* 76.6, pp. 1550–1575.
- McPhee, Miles G. (2017). “The sea ice–ocean boundary layer”. In: *Sea Ice*. John Wiley & Sons, Ltd, pp. 138–159.
- Mellor, Malcolm (1986). “Mechanical Behavior of Sea Ice”. In: *The Geophysics of Sea Ice*. Ed. by N. Untersteiner. Boston, MA: Springer US, pp. 165–281.
- Nansen, F. (1897). *Farthest North*. Westminster: Archibald Constable.
- Nansen, F. (1902). “The oceanography of the north polar basin. The Norwegian Polar Expedition, 1893-1896”. In: *Scientific Results* 3, pp. 357–386.

- Nikiforov, E.G. (1957). "Changes in the compactness of the ice cover in relation to its dynamics." In: *Problemy Arktiki(Vyp2). Morskoi Transport Press. Leningrad.*
- Notz, D. and SIMIP Community (2020). "Arctic Sea Ice in CMIP6". In: *Geophysical Research Letters* 47.10, e2019GL086749.
- Notz, D. et al. (2016). "The CMIP6 Sea-Ice Model Intercomparison Project (SIMIP): understanding sea ice through climate-model simulations". In: *Geoscientific Model Development* 9.9, pp. 3427–3446.
- Nye, J. F. (1973). "The physical meaning of two-dimensional stresses in a floating ice cover". In: *AIDJEX Bulletin* 21, pp. 1–8.
- Oikkonen, A. et al. (2017). "Small-scale sea ice deformation during N-ICE2015: From compact pack ice to marginal ice zone". In: *Journal of Geophysical Research: Oceans* 122.6, pp. 5105–5120.
- Ólason, E. (2023). *How sea-ice rheology should be considered as a subgrid-scale parameterisation of stress relaxation within the ice*. August Cross-VESRI Monthly Journal Club. Institute of Computing for Climate Science, YouTube. URL: https://www.youtube.com/watch?v=NaSyZ_hdqqc (visited on 11/14/2023).
- Ólason, E., P. Rampal, and V. Dansereau (2021). "On the statistical properties of sea-ice lead fraction and heat fluxes in the Arctic". In: *The Cryosphere* 15.2, pp. 1053–1064.
- Ólason, E. et al. (2022). "A New Brittle Rheology and Numerical Framework for Large-Scale Sea-Ice Models". In: *Journal of Advances in Modeling Earth Systems* 14.8.
- Parmarter, R.R. and M.D. Coon (1973). "Mechanical models of ridging in the Arctic sea ice cover". In: *AIDJEX Bulletin* 19, pp. 59–112.
- Paul, Burton (June 1961). "A Modification of the Coulomb-Mohr Theory of Fracture". In: *Journal of Applied Mechanics* 28.2, pp. 259–268.
- Petrich, Chris, Pat J. Langhorne, and Tim G. Haskell (2007). "Formation and structure of refrozen cracks in land-fast first-year sea ice". In: *Journal of Geophysical Research: Oceans* 112 (C4).
- Phillips, A. and R. L. Sierakowski (Mar. 1, 1965). "On the concept of the yield surface". In: *Acta Mechanica* 1.1, pp. 29–35.
- Plante, M. et al. (2020). "Landfast sea ice material properties derived from ice bridge simulations using the Maxwell elasto-brittle rheology". In: *The Cryosphere* 14.6, pp. 2137–2157.
- Prandtl, L. (1905). "Über Flüssigkeitsbewegung bei sehr kleiner Reibung ("On the Motion of Fluids with Very Little Friction")". In: *Verhandlungen des III. Internationalen Mathematiker Kongresses, Heidelberg, 8-13 August 1904*, B. G. Teubner, Leipzig, pp. 485–491.
- Pritchard, R.S. (1974). "What?Strain?What Strain?" In: *AIDJEX Bulletin* 26, pp. 59–74.
- Pritchard, R.S. (June 1975). "An Elastic-Plastic Constitutive Law for Sea Ice". In: *Journal of Applied Mechanics* 42.2, pp. 379–384.
- Pritchard, R.S. (1977). "The effect of strength on simulations of sea ice dynamics". In: *Proceedings of the 4th International Conference on Port and Ocean Engineering under Arctic conditions*. Memorial University of Newfoundland, St. John's Canada, p. 12.
- Pritchard, R.S. (1980). "Sea ice processes and models proceedings of the Arctic Ice Dynamics Joint Experiment International Commission of Snow and Ice symposium". In: *Seattle University of Washington Press*.
- Rampal, P. et al. (2008). "Scaling properties of sea ice deformation from buoy dispersion analysis". In: *Journal of Geophysical Research: Oceans* 113 (C3).
- Rampal, P. et al. (May 20, 2016). "neXtSIM: a new Lagrangian sea ice model". In: *The Cryosphere* 10.3. Publisher: Copernicus GmbH, pp. 1055–1073.
- Rampal, P. et al. (2019). "On the multi-fractal scaling properties of sea ice deformation". In: *The Cryosphere* 13.9, pp. 2457–2474.

- Reed, Richard J. and William J. Campbell (1960). "Theory and observations of the drift of ice station Alpha". In: *ONR Final Rep., Task No. NR 307-250*.
- Richter, T. et al. (2023). "A dynamical core based on a discontinuous Galerkin method for higher-order finite-element sea ice modeling". In: *Geoscientific Model Development* 16.13, pp. 3907–3926.
- Richter-Menge, J.A. et al. (2002). "Relating arctic pack ice stress and deformation under winter conditions". In: *Journal of Geophysical Research: Oceans* 107 (C10), SHE–15.
- Ringeisen, Damien, Martin Losch, and L. Bruno Tremblay (2023). "Teardrop and Parabolic Lens Yield Curves for Viscous-Plastic Sea Ice Models: New Constitutive Equations and Failure Angles". In: *Journal of Advances in Modeling Earth Systems* 15.9, e2023MS003613.
- Rossby, C.G. and R.B. Montgomery (1935). "The layer of frictional influence in wind and ocean currents". In: 3.3, pp. 1–100.
- Rothrock, D.A. (1970). "The pressure term in the constitutive law of an ice pack". In: *AIDJEX Bulletin* 2, pp. 28–32.
- Rothrock, D.A. (1975a). "The energetics of the plastic deformation of pack ice by ridging". In: *Journal of Geophysical Research (1896-1977)* 80.33, pp. 4514–4519.
- Rothrock, D.A. (1975b). "The Mechanical Behavior of Pack Ice". In: *Annual Review of Earth and Planetary Sciences* 3.1, pp. 317–342.
- Rothrock, D.A. (1986). "Ice Thickness Distribution — Measurement and Theory". In: *The Geophysics of Sea Ice*. Ed. by N. Untersteiner. Boston, MA: Springer US, pp. 551–575.
- Rothrock, D.A. and A.S. Thorndike (1984). "Measuring the sea ice floe size distribution". In: *Journal of Geophysical Research: Oceans* 89 (C4), pp. 6477–6486.
- Ruzin, M.I. (1959). "The wind drift of ice in a heterogeneous pressure field (O vetrovom dreife l'dov v neodnorodnom pole davleniya)". In: *Tr. Arkt. i Antarkt. In-ta i Glavn. Geofiz. Observ. (Transactions of the Arctic and Antarctic Inst. and the Main Geophysical Observatory)* 226, pp. 123–135.
- Saramito, P. (Jan. 2016). *Complex fluids*. Vol. 79. Springer.
- Saramito, P. (2021). "A new brittle-elastoviscoplastic fluid based on the Drucker–Prager plasticity". In: *Journal of Non-Newtonian Fluid Mechanics* 294, p. 104584.
- Schofield, A.N. and P. Wroth (1968). *Critical State Soil Mechanics*. European civil engineering series. McGraw-Hill.
- Schreyer, H. L. et al. (2006). "Elastic-decohesive constitutive model for sea ice". In: *Journal of Geophysical Research: Oceans* 111 (C11).
- Schulson, E.M. (2004). "Compressive shear faults within arctic sea ice: Fracture on scales large and small". In: *Journal of Geophysical Research: Oceans* 109 (C7).
- Schulson, E.M. and W.D. Hibler (2004). "Fracture of the winter sea ice cover on the Arctic ocean". In: *Comptes Rendus Physique* 5.7, pp. 753–767.
- Shuleikin, V.V. (1938). "The drift of ice fields". In: 19, pp. 589–594.
- Solomon, H. (1970). "A study of ice dynamics relevant to AIDJEX". In: *AIDJEX Bulletin* 2, pp. 33–50.
- Stern, H. and R. Lindsay (2009). "Spatial scaling of Arctic sea ice deformation". In: *Journal of Geophysical Research: Oceans* 114 (C10).
- Sulsky, Deborah et al. (2007). "Using the material-point method to model sea ice dynamics". In: *Journal of Geophysical Research: Oceans* 112 (C2).
- Sverdrup, H.U. (1928). "The wind-drift of the ice on the North Siberian Shelf". In: *The Norwegian North Polar Expedition with the "Maud" 1918-1925, Scientific Results* 4, pp. 1–46.
- Tang, Chuman (1997). "Numerical simulation of progressive rock failure and associated seismicity". In: *International Journal of Rock Mechanics and Mining Sciences* 34.2, pp. 249–261.

- Thorndike, A.S. et al. (1975). "The thickness distribution of sea ice". In: *Journal of Geophysical Research (1896-1977)* 80.33, pp. 4501–4513.
- Timoshenko, S. and J.N. Goodier (1951). *Theory of Elasticity*. 2nd Edition. New York: McGraw-Hill.
- Tremblay, B. and L.A. Mysak (1997). "Modelling sea ice as a granular material, including the dilatancy effect". In: *Journal of Physical Oceanography* 27, pp. 2342–60.
- Truesdell, C. and W. Noll (2004). *The Non-Linear Field Theories of Mechanics*. 3rd ed. Springer Berlin, Heidelberg.
- Ukita, Jinro and Richard E. Moritz (1995). "Yield curves and flow rules of pack ice". In: *Journal of Geophysical Research: Oceans* 100 (C3), pp. 4545–4557.
- Untersteiner, N. et al. (2007). "AIDJEX Revisited: A Look Back at the U.S.-Canadian Arctic Ice Dynamics Joint Experiment 1970-78". In: *Arctic Institute of North America* 60.3, pp. 327–336.
- Weiss, J. and V. Dansereau (2017). "Linking scales in sea ice mechanics". In: *Philosophical Transactions of the Royal Society A: Mathematical, Physical and Engineering Sciences* 375.2086, p. 20150352.
- Weiss, J. and D. Marsan (2004). "Scale properties of sea ice deformation and fracturing". In: *Comptes Rendus Physique* 5.7, pp. 735–751.
- Weiss, J. and E.M. Schulson (Oct. 2009). "Coulombic faulting from the grain scale to the geophysical scale: lessons from ice". In: *Journal of Physics D: Applied Physics* 42.21, p. 214017.
- Weiss, J., E.M. Schulson, and Harry L. Stern (2007). "Sea ice rheology from in-situ, satellite and laboratory observations: Fracture and friction". In: *Earth and Planetary Science Letters* 255.1, pp. 1–8.
- Wilchinsky, Alexander and D. Feltham (June 2006). "Anisotropic model for granulated sea ice dynamics". In: *Journal of the Mechanics and Physics of Solids* 54, pp. 1147–1185.
- WMO (2014). "The WMO Sea ice nomenclature". In: 1- Terminology and Codes.259.
- Zhang, Jinlun and D.A. Rothrock (2005). "Effect of sea ice rheology in numerical investigations of climate". In: *Journal of Geophysical Research: Oceans* 110 (C8).
- Zienkiewicz, O. C. and R. L. Taylor (2000). *The Finite element method: the basis (Volume 1)*. Fifth Edition. Butterworth-Heinemann.
- Zubov, N.N (1945). "Arctic Ice (L'dy Arktiki)". In: *Izdatel'stvo Glavsermorputi, Moscow*.